uOttawa

L'Université canadienne
Canada's university

FACULTÉ DES ÉTUDES SUPÉRIEURES ET POSTOCTORALES

uOttawa

L'Université canadienne
Canada's university

FACULTY OF GRADUATE AND POSDOCTORAL STUDIES

Krystyna Anna Banas

AUTEUR DE LA THÈSE / AUTHOR OF THESIS

M.Cs. (Cellular and Molecular Medicine)

GRADE / DEGREE

Department of Cellular and Molecular Medicine

FACULTÉ, ÉCOLE, DÉPARTEMENT / FACULTY, SCHOOL, DEPARTMENT

K_{atp} Channel Kir6.2 Subunit Distribution Differs Between Muscles and Between Fiber Types in Skeletal Muscle

TITRE DE LA THÈSE / TITLE OF THESIS

Jean-Marc Renaud

DIRECTEUR (DIRECTRICE) DE LA THÈSE / THESIS SUPERVISOR

CO-DIRECTEUR (CO-DIRECTRICE) DE LA THÈSE / THESIS CO-SUPERVISOR

Rashmi Vothary

William Staines

Gary W. Slater

Le Doyen de la Faculté des études supérieures et postdoctorales / Dean of the Faculty of Graduate and Postdoctoral Studies

K_{ATP} CHANNEL Kir6.2 SUBUNIT DISTRIBUTION DIFFERS BETWEEN MUSCLES AND BETWEEN FIBER TYPES IN SKELETAL MUSCLE

By

Krystyna Anna Banas

Thesis submitted to the

Faculty of Graduate and Postdoctoral Studies

in partial fulfillment of the requirements for the degree of

Master of Science

Cellular and Molecular Medicine

Faculty of Medicine

University of Ottawa

Your file Votre référence
ISBN: 978-0-494-65505-4
Our file Notre référence
ISBN: 978-0-494-65505-4

ABSTRACT

The activity of the ATP-sensitive potassium (K_{ATP}) channel, whose sensitivity to ATP and ability to permit K^+ flux together allow the channel to couple the metabolic state of a cell to its membrane excitability, is important in several tissues for the maintenance of glucose homeostasis and cytoprotection. In skeletal muscle specifically, the channel has been shown to be involved in cell volume regulation, modulation of glucose uptake, and the prevention of fiber damage and contractile dysfunction during fatigue. The extent of the cytoprotective capabilities of the K_{ATP} channel vary tremendously between muscles with different muscle fiber type composition. Semi-quantitative measurement of Kir6.2 subunit content showed that variances exist in K_{ATP} channel content between fiber types and between different muscles. These differences may be related to the extent of importance of the channel's function in a specific muscle. The highest Kir6.2 content was observed in the most glycolytic fiber types and in the more glycolytic muscles studied, and it is these muscles and fiber types which appear to be most dependent on functional K_{ATP} channels for their cytoprotective role.

TABLE OF CONTENTS

LIST OF FIGURES

LIST OF TABLES

LIST OF ABBREVIATIONS

ABC: ATP-binding cassette

ADP: adenosine diphosphate

ANOVA: analysis of variance

AP: action potential

ATP: adenosine triphosphate

ATPase: adenosine triphosphatase

BAPTA-AM: (1,2-bis-(o-aminophenoxy)-ethane-N,N,N',N'-tetraacetic acid, tetraacetoxymethyl ester

BK_{Ca}: large conductance calcium-activated potassium channel

$[Ca^{2+}]_i$: intracellular calcium concentration

CFTR: cystic fibrosis transmembrane conductance regulator

ClC-1: voltage gated chloride channel

DAB: diaminobenzadine

DHPR: dihydropyridine receptor

EDL: extensor digitorum longus

E_K: K^+ equilibrium potential

ER: endoplasmic reticulum

FDB: flexor digitorum brevis

GLUT: glucose transporter

HRP: horse radish peroxidase

IF: immunofluorescence

IP3/DAG: inositol triphosphate/diacylglycerol

K_{ATP} channel: ATP-sensitive potassium channel

K_i[ATP]: ATP concentration required for half-maximum inhibition of channel activity

Kir: potassium inward rectifier

K_V: voltage gated potassium channel

M.C.T.: multiple comparisons test

MgADP: magnesium-adenosine-5'-diphosphate

MgATP: magnesium-adenosine-5'-triphosphate

mM: millimolar

Na_V: voltage gated sodium channel

NBF: nuclear binding fold

NKCC: Na^+-K^+-Cl^- cotransporter

PGY-1: P-glycoprotein 1

PIP_2: phosphatidylinositol 4,5-bisphosphate

PKA: protein kinase A

PLA: plantaris

RT-PCR: reverse transcription polymerase chain reaction

RyR: ryanodine receptor

SDS-PAGE: sodium dodecyl sulphate-polyacrylamide gel electrophoresis

S.E.M.: standard error of the mean

SERCA: sarco-endoplasmic reticulum calcium ATPase

SOL: soleus

SR: sarcoplasmic reticulum

SUR: sulfonylurea receptor

TA: tibialis anterior

TMD: transmembrane domain

VMH: ventromedial hypothalamus

ACKNOWLEDGEMENTS

Firstly, I would like to thank my supervisor, Dr Jean-Marc Renaud, for his enthusiasm, patience, scientific insight, technical assistance, humour, and especially for providing me with the privilege of working in his lab. Without this opportunity I could not have accomplished my goal of completing a Master's degree.

I would also like to thank my advisory committee, Dr. William Staines and Dr. Max Hincke for their excellent advice, suggestions, and guidance. I will in particular fondly remember your compliments on my "most elegant documentation and presentation of negative results". Also, I owe a special thank you to Charlene Clow for performing the MHC RT-PCRs and giving me that extra boost of confidence in my data.

I owe thanks to all my laboratory and CMM colleagues, both past and present: Kim, Rainy, Amalia, Louise, Patrick, Zhen, Tim, Andrew, Samir, Simon. The sense of humour of the Renaud lab crew is second to none! I've never shared so many great inside jokes with so many people. I am especially thankful to Astra and Maria for helping me through the frustrating moments, for providing emotional support and perspective when I most needed it, and for the camaraderie. You guys helped make my grad school experience a memorable one.

A huge thank you to my wonderful family for putting up with me and my (sometimes unusual) work and study schedule, and for providing me with much needed distractions, lots of laughs, and copious amounts of coffee and Nestea Zero.

Finally, I wish to thank my parents, Andrzej and Theresa Banas. Tata and Mom: if it weren't for your unending encouragement, support, and love, I cannot fathom how I would have made it through this crazy chapter of my life called graduate school. To you I dedicate this thesis.

Vitality shows in not only the ability to persist but the ability to start over.

F. Scott Fitzgerald

CHAPTER 1

INTRODUCTION

Ion channels play an important role in numerous tissues, including skeletal muscle. Specific channels facilitate diffusion of potassium, sodium, chloride, and calcium across cell membranes down their concentration gradient, resulting in such actions as transmitting nervous impulses, facilitating insulin exocytosis, or altering membrane excitability to cause muscle contraction.

A channel may also have multiple roles within a cell. One such channel is the ATP-sensitive potassium (K_{ATP}) channel which is found in skeletal muscle. The K_{ATP} channel is thus named because it is both sensitive to ATP and can permit K^+ flux which permits it to couple the energy state of a cell to its membrane excitability. The channel is formed from protein tetramers of the pore-forming Kir6.2 and the regulatory SUR2A subunits. It is closed by increases in intracellular ATP and opened by increases in MgADP, PIP_2, and H^+. Apart from its localization in skeletal muscle, K_{ATP} channels have also been identified in numerous tissues including the hypothalamus, cardiac muscle, and smooth muscle.

In skeletal muscle specifically, the channel has been shown to be involved in regulation of cell volume [1], modulation of glucose uptake [2], and most importantly, in regards to this thesis, the prevention of contractile dysfunction and fiber damage during exercise and fatigue [3, 4]. The extent of the cytoprotective capabilities of the K_{ATP} channel vary tremendously between muscles with different muscle fiber type composition. These differences in the K_{ATP} channel's cytoprotective effects may arise from differential regulation of channel activity between fiber types and different muscles, and/or variances in channel content between fiber types and different muscles.

The overall objective of this study was to determine whether the content of K_{ATP} channels varies between muscles and between muscle fiber types in soleus (SOL), extensor digitorum longus (EDL), and flexor digitorum brevis (FDB). The hypothesis was that

"K_{ATP} channel content in the t-tubules varies between muscles in the order of EDL>FDB>SOL, within fiber types in the order of IIB>IIX>IIA>I, and varies independently of t-tubular content."

To meet the objective of this study and to test the above hypothesis, the following aims were undertaken:

Aim 1: Develop a technique to study fiber type and Kir6.2 content in single mouse muscle fibers;

Aim 2: Identify single and multiple MHC types expressed within fibers to assess if fibers composed of multiple myosins form a large proportion of unexercised muscle and need to be accounted for when considering relative K_{ATP} channel content;

Aim 3: Quantify relative Kir6.2 content in the transverse tubules of different fiber types in different muscles, since the absence of this K_{ATP} subunit is directly related to loss of cytoprotection in skeletal muscles, and;

Aim 4: Determine the dependence of Kir6.2 content on fiber t-tubule volume by using the α_1 DHPR subunit content as an index of t-tubular content.

ION CHANNELS OF SKELETAL MUSCLE

A number of integral membrane proteins exist to allow passage or transport of ions and large molecules through the cell membrane and through the surface of intracellular compartments. These proteins, known as channels and transporters, can respond to alterations in a cell's physical and chemical environment and intracellular milieu. All ion channels and some transporters permit ions and other molecules to move across the cell membrane via facilitated diffusion down their concentration gradients [5]. Other transporters actively transport molecules against their concentration gradients using ATP or other sources of energy. In skeletal muscle, ion channels and transporters play an integral role in membrane excitation and the contraction cycle of skeletal muscle.

Membrane Excitation and Contraction of Skeletal Muscle

The contraction of skeletal muscle is initiated when a motor neuron stimulates the generation of action potentials (APs) at the neuromuscular junction. The APs then

propagate along the cell membrane as well as deep into muscle fiber interior via the transverse or t-tubules [6]. The t-tubules are located in close proximity to the sarcoplasmic reticulum (SR) that stores Ca^{2+}. The cell membrane is depolarized due to an influx of Na^+ via voltage-gated Na^+ channels and subsequently repolarized by K^+ efflux through voltage gated potassium channels. As the depolarization signal is transferred via interaction between channels in the t-tubular membrane and the SR, it activates the release of Ca^{2+} into the cytoplasm. This free Ca^{2+} binds troponin located along the actin-containing thin filaments and causes a conformational change in the troponin protein complex. This change permits tropomyosin to move to reveal actin's myosin-binding sites. In a process dependent on ATP hydrolysis, the myosins of the thick filaments then bind and pull the thin filaments toward the center of the sarcomere to generate force in the muscle. The muscle relaxes when an AP is no longer generated. Ca^{2+} detaches from troponin and is actively transported into the SR via Ca^{2+} ATPases in the SR membrane. Removal of Ca^{2+} from the cytoplasm into the SR lumen at the end of contraction permits the muscle to relax and the activity of Na^+/K^+ ATPases in the cell membrane help to restore the Na^+ and K^+ gradients across the cell membrane for excitability. These processes also occur at the expense of ATP hydrolysis.

Channels and transporters involved in contraction

Voltage-gated sodium (Na_V) and voltage-gated potassium (K_V) channels permit ion fluxes necessary for initiation of the contraction cycle [7]. Both Na_V and K_V channels are formed of pore-forming, voltage-sensitive α subunits and modulatory β subunits [8, 9]. They are present in both the cell membrane and t-tubules of skeletal muscle. Na_V channels rapidly activate and inactivate in response to changes in membrane potential, when opening to permit Na^+ influx which causes the quick depolarization of the cell membrane [10]. K_V channels open during the membrane depolarization phase of the AP, acting to repolarize the cell membrane via K^+ efflux.

During the action potential depolarization phase, the voltage-sensitive Ca^{2+} channels in the t-tubular membrane or dihydropyridine receptors (DHPR), and the intracellular Ca^{2+} release channels or ryanodine receptors (RyR), work in concert to lead to the release of

Ca^{2+} required for contraction. The DHPR is also known as the L-type calcium channel. It is formed by α1, γ, and δ/α2 membrane spanning subunits and a cytosolic β subunit [11]. The skeletal DHPR α1 subunit is responsible for Ca^{2+} selectivity, voltage-dependent gating, and dihydropyridine sensitivity. The β subunit is involved in channel assembly as well as modulating channel kinetics by increasing current activation [12, 13]. The γ subunit may also modify channel activity by increasing channel inactivation through hyperpolarization [14]. The role of the δ/α2 complex is not known in E-C coupling, though it has been speculated to couple gating current with channel opening [15]. Unlike the cardiac DHPR, the skeletal DHPR does not behave as an ion-conducting channel but is a voltage sensor for the RyR [16, 17]. The RyR is composed of four identical, large protein subunits that form a square around a Ca^{2+} release channel. RyR channels are present on the SR membrane and localize such that one tetrad of DHPRs on the t-tubular membrane opposes every other RyR channel (a ratio of 1:2 for DHPR:RyR channels) [18, 19]. During excitation-contraction coupling, the DHPR α1 subunit undergoes a conformational change and through its physical interaction with RyR causes the opening of this SR Ca^{2+} channel, thus releasing Ca^{2+} necessary for contraction into the cytoplasm [20].

The sarco-endoplasmic reticulum Ca^{2+} ATPase (SERCA) pump is a transporter consisting of a single polypeptide and is found in the sarcoplasmic reticulum membrane. It is responsible for causing muscle relaxation by lowering cytosolic Ca^{2+}. For every ATP molecule hydrolyzed, two Ca^{2+} ions are transported back into the SR [21]. Two different SERCA isoforms are found in adult skeletal muscle: SERCA1 in fast-twitch and SERCA2 in slow twitch skeletal muscle [22]. By returning Ca^{2+} to the SR, the SERCA pump ensures the SR Ca^{2+} store is replenished for future muscle contraction.

Transporters involved in modulation of action potential

In skeletal muscle, two transporters that are commonly found amongst a variety of cell types are specifically involved in modulating action potentials in muscle. The Na^+-K^+-ATPase, or Na^+/K^+ pump, is formed from 2 main subunits: the α subunit that possesses Na^+, K^+, and ATP binding sites, and the β subunit that confers the pump's localization to

the cell membrane as well as α subunit activation [23-25]. By hydrolyzing ATP, it can pump 3 Na^+ out of the cell while taking in 2 K^+, permitting the restoration of sodium and potassium gradients across the membrane. Since intracellular Na^+ and extracellular K^+ accumulation will lead to a reduction in AP amplitude, the activity of Na^+/K^+ pumps aid in maintenance of membrane excitability during muscle contraction [24]. The other transporter, the Na^+-K^+-Cl^- cotransporter or NKCC, is a large protein with 12 transmembrane domains. It permits the movement of 1 Na^+, 1 K^+, and 2 Cl^- across the cell membrane [26]. The NKCC provides an electroneutral, inwardly directed flux of these three ions in muscle [27]. During muscle contraction, it is thought to help reduce the accumulation of extracellular K^+ and intracellular K^+ depletion but without hyperpolarization [28].

The large conductance calcium-activated potassium channel, or BK_{Ca} channel, is present in both sarcolemma and t-tubules and similar to K_V channels consists of four pore-forming α subunits and four regulatory β subunits [29, 30]. BK_{Ca} channels are highly selective for K^+, and again like the K_V channel are activated by membrane depolarization. BK_{Ca} channels also exhibit voltage sensitivity to increased intracellular Ca^{2+}, for instance when Ca^{2+} is released from the SR during contraction [31]. As $[Ca^{2+}]_i$ increases, more channels will open as the membrane becomes further depolarized. The activation of these channels permits a K^+ efflux that can help speed up the rate of membrane repolarization when intracellular calcium is released chronically [32].

Ion channels involved in resting membrane potential

There are two major channels activated at rest in the muscle cell membrane: the voltage gated chloride channel ClC-1 and the strong inward rectifier K^+ channel Kir2.1. The ClC-1 channel is a homodimeric channel possessing two ion conducting pores, two selectivity filters, and two voltage sensors [33, 34]. Although it has very low single channel conductance, it is present in the cell membrane (particularly in the t-tubules) at high density, allowing large populations of ClC-1 channels to be responsible for about 80% of total resting membrane conductance [35, 36]. It is thought that activity of ClC-1 channels help to stabilize resting membrane potential as well as contribute to the AP

repolarizing current [37].

Strong inward rectifier K^+ channels, such as Kir2.1, are also present at high density in the t-tubules [38]. The Kir2.1 channel consists of a tetramer of pore-forming subunits, similar to the channel pore of another inwardly-rectifying channel, the weak inward rectifier ATP-sensitive potassium channel, or K_{ATP} channel. Like the ClC-1 channels, the Kir2.1 channels also represent a significant conductance in skeletal muscle, and are thought to facilitate K^+ re-uptake after each action potential [39]. K_{ATP} channels consist of Kir6.2 pore-forming subunits and SUR regulatory subunits and have also been implicated in maintenance of resting potential as they have been shown to be active *in vivo* at rest [29].

The importance of ion channels in muscle is not limited to muscle contraction and membrane potential alone. One specific example is the K_{ATP} channel. This channel is named because ATP was the first metabolite found to regulate the channel by closing it when bound to its intracellular side [40]. The channel is found in numerous tissues and has several functions. Because ATP generally regulates its activity, the K_{ATP} channel can act as an energy sensor connecting the energy state of a cell to the electrical activity of its cell membrane.

K_{ATP} CHANNEL

Structure

The K_{ATP} channel is an octameric complex formed by four Kir protein subunits and four SUR protein subunits [41] (Figure 1-1). The Kir protein subunit is a member of the superfamily of potassium inwardly rectifying (Kir) channels and a tetramer of Kir subunits forms the channel pore [42]. The associated SUR protein subunit is named for its affinity for sulfonylureas (a class of anti-diabetic drugs), is a member of the ATP-binding cassette (ABC) superfamily, and plays a regulatory role in channel function [43, 44].

Kir Subunit

Seven subfamilies exist in the Kir family of inwardly rectifying K^+ channels that includes

FIGURE 1-1

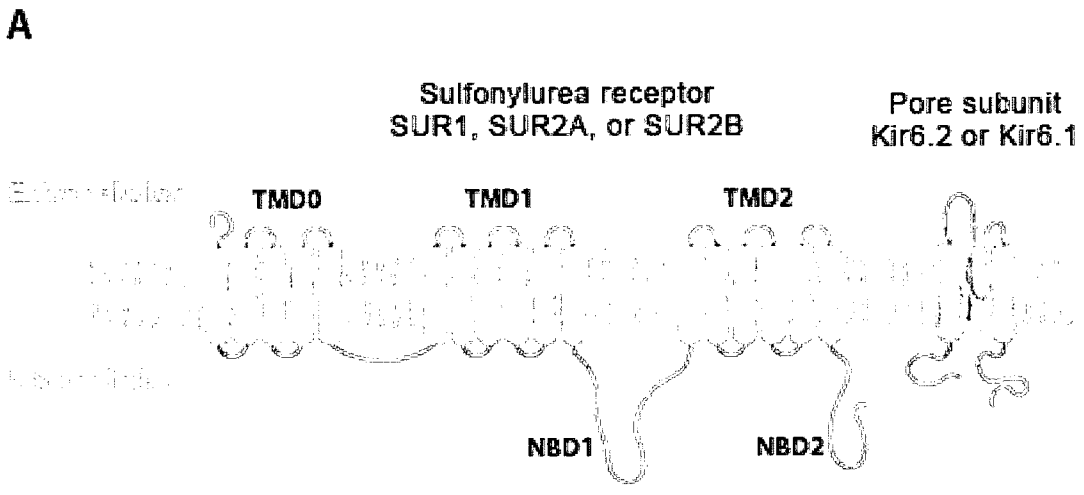

Figure 1-1: Molecular structure of the K_{ATP} channel. (a) Membrane topology of SUR and Kir6.x proteins: The SUR subunit (blue) is thought to have three transmembrane domains, TMD0, TMD1 and TMD2 consisting of five, six and six membrane spanning regions respectively, and two intracellular NBFs. Kir6.x (pink) has two transmembrane domains, M1 and M2. (b) Assembly of K_{ATP} channel: The K_{ATP} channel is a hetero-octameric channel composed of 8 subunits, with four pore-forming Kir6.x subunits (Kir6.1 or Kir6.2) and four regulatory SUR subunits (SUR1 or SUR2A or SUR2B) (*Adapted from Ashcroft 2005[46]*).

Kir1 to Kir7. The term "inward rectifier" refers to the ability of Kir channels to conduct larger inward currents at membrane potentials more negative than the K^+ equilibrium potential (E_K), than outward currents at membrane potentials more positive than E_K [45]. The inward rectification of the different subfamilies varies, with Kir2 and Kir3 being strong rectifiers, meaning that they allow virtually no outward current. The other Kir channel subfamilies are weakly rectifying proteins, indicating that they primarily conduct inward currents but small amounts of outward current as well.

The Kir6.x family forms the Kir subunits of the K_{ATP} channel and consists of three members: Kir6.1 and Kir6.2 that are found in several mammalian tissues, and Kir6.3 found in the embryonic brain of zebrafish [47-49]. Of interest to this study are Kir6.1 and Kir6.2, which have both been cloned. Located on chromosome 12, the human Kir6.1 gene is about 9.7 kb in length, contains three exons, and translates into a 424 amino acid protein [42], while the human Kir6.2 subunit is transcribed from an intronless gene on chromosome 11 of about 4.3 kb in length and gives rise to a 390 amino acid protein [42]. Despite arising from different genes, Kir6.1 and Kir6.2 share approximately 70% amino acid similarity [50]. Like other Kir channels, both Kir6.1 and 6.2 subunits possess two transmembrane domains (M1 and M2) separated by an H5 loop [51] (Figure 1-1A). This loop is common to all K^+ channels and confers its potassium selectivity [52]. The Kir subunit also confers the closing of the channel by ATP, with the binding of as little as one molecule of ATP causing the channel to remain closed [53]. Further details regarding the regulation of the channel via the Kir subunit will be described in a later section.

SUR Subunit

The second K_{ATP} channel subunit is the SUR protein. SURs are members of the ABC protein superfamily, which also includes the cystic fibrosis transmembrane conductance regulator (CFTR), and multi-drug resistance proteins such as P-glycoprotein (PGY-1) [43]. Two different SUR genes encode the SUR isoforms. The human SUR1 gene has 39 exons spread over 100 kb and translates a protein of 1582 amino acids [42]. The human SUR2 gene is located on chromosome 12 and consists of 39 exons spread over 100 kb

[54]. Interestingly, the gene of the SUR1 subunit is clustered together with another K_{ATP} channel subunit gene, Kir6.2, on chromosome 11 at position 11p15.1 [42]. Two major isoforms of SUR2 exist and are a result of alternative splicing of the 3' region of SUR2. The SUR2A transcript variant includes exon 38A while the SUR2B transcript variant includes exon 38B [50, 55, 56]. The resulting SUR2A and 2B proteins are 1545 and 1546 amino acids in length respectively and differ by only 42 amino acids in their C-terminal regions [50, 55].

The proposed topology of the SUR subunit matches that of other ABC protein family members. The SUR protein consists of 17 transmembrane spans consisting of an N-terminal transmembrane domain (TMD0) that connects to the rest of the protein via a linker domain, two cytoplasmic nucleotide binding fold (NBF) domains, and two additional transmembrane domains (TMD1 and TMD2) [57, 58] (Figure 1-1A). Unlike the ABC family members CFTR (a Cl^- channel responsible for secretion of Cl^- into lung epithelia) and PGY-1 (an ATP-dependent efflux pump responsible for decreasing intracellular drug accumulation), the SUR protein is not involved in transport of substrate across a membrane but instead modifies the Kir subunit's nucleotide sensitivity and determines its pharmacology [59]. However, like other ABC proteins, the SUR protein structure has ABCs or NBFs on the cytoplasmic side of the membrane that contain highly conserved motifs. Within the SUR protein's NBF1 and NBF2 are Walker A and B regions and the ABC signature link sequence, a Q loop and an H loop [60]. These motifs are implicated in ADP and ATP binding [61].

Channel Formation and Membrane Targeting

Both Kir6.2 and SUR subunits possess endoplasmic reticulum (ER) retention sequences that prevent the trafficking of one subunit type independently of the other to the cell membrane surface. The ER retention signal is located between TMD1 and NBF1 in the SUR protein and within the last 26-36 amino acid residues of the Kir protein's C-terminal region [62]. These retrograde signals become blocked when the proteins dimerize, thus permitting translocation and cell surface channel expression. There is also an antegrade signal in the C-terminus of the SUR protein that permits the exit of this subunit from the ER and Golgi apparatus [63].

REGULATION OF K_{ATP} CHANNEL ACTIVITY

The K_{ATP} channel is a voltage insensitive but ligand sensitive channel. The ligands known to activate the channel can act via the Kir or SUR subunit. A number of pharmacological compounds can also act on the SUR subunit to open or close the K_{ATP} channel and some of these compounds and their actions are summarized in Table 1-1. Intracellular ligands regulating K_{ATP} channel activity, including ATP, H^+, ADP, PIP_2, and Mg^{2+} nucleotides can fluctuate during metabolic activity, further emphasizing the channel's coupling of metabolic sensitivity with electrical activity.

Kir Subunit Channel Regulation

ATP binds to the intracellular side of the Kir subunit to regulate the K_{ATP} channel. *In vitro,* the K_{ATP} channel has been shown to have a K_i[ATP] between 20 to 100 μM [40, 159]. The α and β phosphate groups of ATP interact with Lys185 and Arg201 residues at the C-terminal of one Kir subunit [64]. The ATP γ phosphate group interacts with Arg50 residue at the N-terminal of an adjacent Kir subunit [65]. The ATP adenine ring also interacts with residues Glu179 to Ile182 of one Kir subunit and the Arg301 of a second subunit. Together, the residues of two adjacent subunits form a single ATP binding site on Kir6.2 [64, 66]. Since each channel pore is formed of four Kir subunits, one K_{ATP} channel contains a total of four ATP binding sites. Interestingly, ATP binding to even a single site is thought to cause a global conformational change in all four cytosolic ATP binding domains, making a single ATP molecule sufficient for pore closure [67]. Unlike binding sites on ATPases, ATP binding to the K_{ATP} channel is Mg^{2+} independent [68]. K_{ATP} channel sensitivity to ATP can vary based on what other channel regulators are present, and can range from 10 to 300 μM [42, 50]. Magnesium-free ADP can also bind the Kir6 subunit to prevent channel opening, but has much lower affinity than ATP [69, 70].

In contrast to ATP, some cellular molecules have been shown to act on the Kir subunit to open the channel. Even with the presence of intracellular ATP in the millimolar range, decreasing intracellular pH by application of NH_2Cl or CO_2 affects ATP's ability to inhibit the K_{ATP} channel [71, 72]. It has been determined via mutation studies that Thr71,

TABLE 1-1

Drug	Effect on Channel	Subunit Specificity
Diazoxide	opener	SUR1, SUR2B >>> SUR2A
Cromakalim	opener	SUR2A, SUR2B >> SUR1
Pinacidil	opener	SUR2A, SUR2B>>SUR1
Tolbutamide	blocker	SUR1 >>> SUR2A, SUR2B
Glibenclamide	blocker	SUR1 > SUR2A≈SUR2B

Table 1-1: Differential Specificities of K_{ATP} Channel Openers and Blockers. Pharmacological compounds can bind to the SUR subunit to either close or open K_{ATP} channels with efficacy varying depending on the SUR subunit expressed within the channel.

Cys166, and His175 residues on the Kir subunit are required for H^+-induced activation of the K_{ATP} channel [72-74]. PIP_2, a phospholipid found in the cell membrane that forms part of the IP3/DAG signaling pathway, has also been shown to activate the K_{ATP} channel. It is thought to reduce the channel's ATP sensitivity by interfering with ATP binding to the Kir subunit [75]. Several residues along the Kir subunit Lys39, Glu179 and Arg301 appear to be shared by both PIP_2 and ATP as part of their respective binding sites, suggesting that binding of PIP_2 displaces bound ATP [76].

SUR Subunit Channel Regulation

The binding of ATP and Mg^{2+} nucleotides (i.e. MgATP, MgADP) with the SUR subunits can open the K_{ATP} channel [77-79]. However, these NBFs differ from those of other ABC proteins because they do not transport substrates across a gradient [60]. Also, unlike many other ABC proteins, only one of the two NBFs (NBF2) possesses ATPase activity [80]. NBF1 has high affinity for ATP and ADP, with nucleotide binding occurring independently of Mg^{2+} [81]. In contrast, NBF2 has low affinity for ATP and ADP, and nucleotide binding is Mg^{2+} dependent [81]. Photoaffinity labeling studies using radioactively labeled 8-azido-ATP illustrate that the magnitude of Mg^{2+} dependency for binding NBFs varies between subunit isoforms. SUR1 is more dependent on Mg^{2+} at both NBF sites while the NBF on SUR2A/B sites are less dependent [80]. Point mutation studies have isolated the Walker A and B motifs as key for Mg^{2+} nucleotide activity because mutations within these motifs abolish the MgADP-mediated channel activation [82, 83].

MgATP acts to enhance channel activity indirectly. MgATP is hydrolyzed to MgADP at NBF2. The subsequent binding of MgADP is thought to open the K_{ATP} channel by reducing the sensitivity of the Kir subunits for ATP [83, 84]. Differences in the ATP/ADP ratio present within a cell will also affect Mg^{2+} nucleotide binding and channel activity. At a low ATP/ADP ratio, Mg^{2+} free ATP will bind NBF1 of SUR1 while MgADP will bind NBF2 [79, 84]. In turn, this reduces ATP binding on the Kir subunit and opens the channel. However, if the ATP/ADP ratio increases, the reduction in MgADP induces the dissociation of MgADP from NBF2 and ATP from NBF1, which

consequently allows ATP to bind to Kir6.2 and close the channel [84].

K_{ATP} CHANNEL DISTRIBUTION IN DIFFERENT TISSUES

The K_{ATP} channel is found amongst several tissues and is formed of different subunit isoforms, which results in differential sensitivity to channel modulating compounds depending on the role of the channel. A summary of the common subunit combinations found in tissues expressing K_{ATP} channels is found in Table 1-2.

K_{ATP} Channel Subunit Expression outside of Skeletal and Cardiac Muscle

Nervous System

In the nervous system, isoform composition varies with regional localization. The glucose-responsive neurons in the hypothalamus express Kir6.2, as established by electrophysiological experiments illustrating that no K_{ATP} channel membrane current was present in the hypothalamus of Kir6.2$^{-/-}$ mice but that membrane current was detected in wild type mice [85]. The presence of the SUR1 subunits was determined by sensitivity of channel activity to SUR-1 specific tolbutamide [86, 87]. The subunit compositions were also confirmed by RT-PCR analysis that showed the presence of only Kir6.2 and SUR1 in the VMH neurons [85]. Other brain regions, such as the substantia nigra, contain dopaminergic neurons possessing a mixture of K_{ATP} channels. Kir6.2/SUR1, Kir6.2/SUR2B, as well as Kir6.2/SUR1+2B channels containing SUR heterogeneity within a single channel were distinguished from one another by their differences in tolbutamide sensitivity and again subunit identities were confirmed with RT-PCR [88, 89]. Similarly, electrophysiological experiments coupled with single cell RT-PCR showed that interneurons in the striatum of the basal ganglia contain K_{ATP} channels composed of Kir6.1/SUR1 subunits based on their tolbutamide and glibenclamide inhibition [90].

Pancreas

Both pancreatic alpha and β-cells, responsible for glucagon and insulin release respectively, express the Kir6.2/SUR1 channel combination. This subunit combination was determined by a combination of presence of the specific mRNAs in the pancreas as

TABLE 1-2

Kir Isoform	SUR Isoform	Tissue Expression
Kir6.1	SUR1	Basal Ganglia
Kir6.1	SUR2B	Aorta
Kir6.2	SUR1	Pancreas Hypothalamus Cardiac Muscle (atria)
Kir6.2	SUR2A	Skeletal Muscle Cardiac Muscle (atria and ventricles)
Kir6.2	SUR2B	Non-Vascular Smooth Muscle (bladder, stomach, colon)
Kir6.2	SUR1 SUR2B SUR1+2B	Substantia Nigra
Kir6.1 Kir6.2	SUR2B	Vascular Smooth Muscle

Table 1-2: Common combinations of K_{ATP} channel subunits observed in various tissues.

well as tolbutamide and diazoxide sensitivities seen through patch clamp studies [42, 48, 91].

Vasculature

In vascular smooth muscle, the K_{ATP} channels can be composed of Kir6.1 or Kir6.2/SUR2B subunits, with the SUR identities established by virtue that these channels are activated by both diazoxide and pinacidil [50, 92]. Small and intermediate arteries, as well as capillaries and arterioles in the brain and skeletal muscle, and capillaries were shown to contain Kir6.1/SUR2B channels by in situ hybridization, while immunohistochemistry also demonstrated Kir6.2 localization in addition to Kir6.1 and SUR2B expression [93, 94]. The aorta, however, appears to possess only Kir6.1/SUR2B channels and at much lower density that in other vessels, as shown by immunohistochemical and pharmacological studies [93-95]. Non-vascular smooth muscles expressing functional K_{ATP} channels include the bladder, colon, and stomach, and these channels have been identified by a combination of RT-PCR, electrophysiological, and/or pharmacological experiments as having Kir6.2/SUR2B channel composition [96, 97]. K_{ATP} channels are not limited to smooth muscle but have been identified and studied extensively in both cardiac and skeletal muscle.

<u>K_{ATP} Channel Subunit Expression in Cardiac and Skeletal Muscle</u>

Two K_{ATP} channel populations exist in cardiac and skeletal muscle: the sarcolemmal K_{ATP} channels that are typically composed of Kir6.2/SUR2A subunits localizing to the muscle cell membrane [29, 54, 98], and the putative mitochondrial K_{ATP} channel (mitoK_{ATP}) localizing to the inner mitochondrial membrane [99]. Although the presence of the mitoK_{ATP} channel has been validated repeatedly via single channel conductance studies, the molecular identity of the channel is still unknown [100]. For the remainder of this thesis, any reference to skeletal and cardiac muscle K_{ATP} channels will focus on the sarcolemmal channel whose identity has been confirmed.

The finding that Kir6.2/SUR2A together form the cardiac and skeletal muscle K_{ATP} channel is based on numerous mRNA expression and electrophysiological experiments [42, 50, 101]. More recent studies, however, have provided molecular, pharmacological,

and histological evidence for the expression of other K_{ATP} channel subunits in both types of muscle. Most channel localization studies have been performed on cardiac muscle alone, and show that while all known K_{ATP} channel subunits are expressed in cardiac muscle the subunits demonstrate differential localization within cardiomyocytes.

Cardiac Muscle

Like skeletal muscle, cardiac muscle is considered to primarily express channels composed of Kir6.2 and SUR2A subunits. In concordance with earlier mRNA studies [55, 101] different anti-Kir6.2 antibodies showed that Kir6.2 is universally distributed over the sarcolemmal and t-tubular surface of isolated rat ventricular myocytes [94, 102]. Similarly, the SUR2A subunit also showed strong sarcolemmal expression when identified by both pan-SUR2 (identifying both SUR2 isoforms) and SUR2A-specific antibodies [94, 102]. Furthermore, using double immunofluorescence (IF) and by overlapping fluorescence intensity profiles of a cross section of labeled muscle cells, it was shown that Kir6.2 and SUR2A co-localize in isolated cardiac muscle cells [102]. However, the pattern observed was not completely identical between the two studies, and may be a result of differences in the primary antibodies used or may be an artifact of different fixation protocols that prevent clear visualization of the staining pattern. Though the Kir6.1 subunit was detected in cardiomyocytes, it stained inconsistently across different cells. In some instances it showed a longitudinal streaked pattern (suggesting that it may be associated with myofibrillar structures) and in others it had occasional punctate immunofluorescence localized at or just below the sarcolemma [94]. However, RT-PCR has indicated the presence of Kir6.1 mRNA in the heart [49, 103]. Coupling the immunohistochemical observations with the mRNA data, it is possible but not certain that Kir6.1-containing K_{ATP} channels are expressed in cardiac muscle.

Cardiac muscle was further probed with antibodies against SUR1 and SUR2B. Conflicting data exists for the cardiac localization of SUR1. One study suggested that SUR1 protein is expressed in or just below the sarcolemma [94], but there was no attempt to test its co-localization with a sarcolemmal marker. In another study, SUR1 protein was not detected at all [102]. However, a recent study combining immunohistochemical

and electrophysiological data has thoroughly illustrated that SUR1 forms the regulatory subunit of atrial but not ventricular K_{ATP} channels [104]. Using their own anti-SUR1 antibody, strong membrane-localized SUR1 staining was shown in atrial cardiomyocytes of both wild type and SUR1-overexpressing mice, while little to no SUR1 staining was visible in wild type or $SUR1^{-/-}$ ventricular cardiomyocytes nor atrial cardiomyocytes of $SUR1^{-/-}$ mice [104]. Activity of SUR1-containing K_{ATP} channels was confirmed by inside-out patch clamp and whole cell electrophysiological experiments of atrial cardiomyocytes: SUR-1 specific diazoxide activation occurred in wild type but not $SUR1^{-/-}$ myocytes, and large ATP-sensitive currents was observed in wild type inside-out atrial patches while essentially no current was seen in $SUR1^{-/-}$ patches [104]. SUR2B was specifically detected by immunofluorescence (IF) in the cell membrane of cardiac muscle in two studies, while an additional study alluded to its presence using a pan-SUR2 antibody that detects both SUR2A and 2B isoforms [94, 102, 105]. SUR2B has been shown to co-localize with the t-tubular marker $IXE11_2$ and appeared to localize in a transverse striated pattern consistent with the Z-lines of the muscle cell [102]. Finally, in two different studies Western blotting detected SUR2B in the microsomal (t-tubular) membrane fraction [102, 105]. Electrophysiological data has confirmed the presence of SUR2A in cardiomyocytes; however, these studies may not have detected SUR2B expression as they likely were unable to isolate a membrane patch from the cardiac cell t-tubules.

Skeletal Muscle

Though extensively investigated in cardiac muscle, K_{ATP} channel subunit composition in different muscles using subunit-specific antibodies has surprisingly not yet been reported for skeletal muscle. One study exists which thoroughly characterized SUR isoform expression in skeletal muscle by RT-PCR and pharmacological means, while another study looked superficially at Kir6.2 localization in skeletal muscle immunohistochemically and by Western blotting.

Tricarico and colleagues [106] recently showed that both Kir6.1 and Kir6.2 mRNA are expressed in skeletal muscle, but that Kir6.2 mRNA is the most abundant transcript in the

skeletal muscles studied (SOL, EDL, FDB, TA), and is in concordance with previous mRNA data [55, 101]. Kir6.1 mRNA was also detected in the same muscles. As the mRNA content was similar across all muscles, its presence is likely attributed to the Kir6.1 subunits of vascular smooth muscle K_{ATP} channels [106]. On the other hand, contrary to Kir6.1, Kir6.2 mRNA content varied significantly between muscles, being in the order of FDB≈TA>>EDL>SOL [106]. SUR2A mRNA was also expressed in relatively high amounts in skeletal muscle, but in a different order compared to Kir6.2 mRNA. The level of expression of SUR2A was greatest in FDB, with the overall mRNA content in the order of FDB >SOL>>EDL≈TA [106]. SUR2B and SUR1 mRNA were also detected in some muscles, with SUR2B exhibiting no statistically significant differences in expression across the muscles, albeit a trend was observed where TA>FDB>SOL≈EDL [106]. In comparison, SUR1 mRNA was present at very low levels in all muscles except the FDB, which had five times greater expression of SUR1 mRNA than the other muscles [106]. While the presence of the SUR2B transcript was not completely surprising since it is co-expressed with Kir6.1 in vascular smooth muscle [92], the presence of SUR1 mRNA was highly unusual because it had not previously been detected in skeletal muscle [101].

By exploiting the differential sensitivity of the SUR subunits to various channel openers and blockers (Table 1-1), the mean channel currents were measured from SOL, EDL, TA, and FDB membrane patches via an inside out membrane configuration standard patch-clamp technique. Based on channel sensitivity to cromakalim/glibenclamide combined with diazoxide/tolbutamide insensitivity, the majority of patches tested in tibialis (83%), soleus (80%), EDL (83%) and FDB (42%) expressed the SUR2A subunit [106]. Sensitivity to diazoxide and cromakalim indicated that the remaining patches in TA (17%), SOL (20%), and EDL (17%) appear to be composed of the SUR2B subunit [106], suggesting that this subunit is also expressed in skeletal muscle K_{ATP} channels. In comparison, the FDB showed differing SUR composition in its K_{ATP} channels: in the FDB alone, 33% of patches tested demonstrated diazoxide/tolbutamide/glibenclamide sensitivity coupled with cromakalim insensitivity, which corresponds to a SUR1-specific channel response [106]. The presence of SUR1-containing channels concurs with the

very high SUR1 mRNA levels observed in FDB, making it plausible that Kir6.2/SUR1 channels which have been identified in atrial cardiac muscle may also natively exist within this specific skeletal muscle.

In comparison to the SUR subunit's expression across muscles, the specific cellular localization of K_{ATP} channels within skeletal muscle is poorly characterized. It has been shown through Western blotting comparing co-localization of a Kir6.2 antibody with a sarcolemmal marker (Na^+/K^+ ATPase) or t-tubule marker (L-type Ca^{2+} channel) that the Kir6.2 protein localizes primarily in the sarcolemmal fraction of rat and human muscle cell membranes [29]. Immunofluorescence of muscle cross sections using the same commercial anti-Kir6.2 antibody that identified Kir6.2 via Western blotting showed that all muscle fiber peripheries stain for Kir6.2 [29]. Unfortunately, this study does not account for fluorescence visible diffusing into some fibers that alludes to a potential t-tubular K_{ATP} channel population. Additionally, it does not confirm histologically the co-localization of Kir6.2 expression with the sarcolemmal marker, nor does it assess fiber type differences or expression of other K_{ATP} channel subunits that may be present based upon evidence from variable K_{ATP} channel subunit localization in cardiac muscle.

FUNCTIONS OF THE K_{ATP} CHANNEL

The K_{ATP} channel plays different roles in the various tissues in which it is expressed. The channel's three major roles are maintenance of glucose homeostasis, cell volume regulation, and cytoprotection. In keeping with the objective of this thesis, the specific focus of this section will be the role of the K_{ATP} channel in cytoprotection of skeletal muscle.

Glucose homeostasis in different tissues

The channel is involved in modulating glucose homeostasis in several tissues including the pancreas, hypothalamus, and skeletal muscle.

Pancreas

Under normal conditions in wild type mice, glucose is transported into pancreatic β-cells via the GLUT2 transporter. Cell metabolism increases and ATP is produced, and in

conjunction with this process the cell membrane depolarizes leading to an Ca^{2+} influx and increase of intracellular calcium that stimulates insulin secretion [107, 108]. In physiological experiments performed on Kir6.2$^{-/-}$ mice, the presence of either low or high glucose did not lead to any changes in β-cell membrane potential [109]. Further, although basal intracellular Ca^{2+} was higher in Kir6.2$^{-/-}$ pancreatic islets than in wild type islets, basal insulin secretion did not differ from that of wild type islets [109]. Even perfusing Kir6.2$^{-/-}$ islets with high glucose did not significantly increase insulin secretion compared to the increase observed for wild type islets [109]. These findings suggested that K_{ATP} channel closure induced the membrane depolarization and the rapid rise of intracellular Ca^{2+} that is critical for glucose-stimulated insulin secretion. It appears that to stimulate insulin secretion, the increased intracellular ATP leads to binding and closure of β-cell K_{ATP} channels which then lead to depolarization of the cell membrane. In turn, the depolarization triggers activation of voltage-gated Ca^{2+} channel to cause Ca^{2+} influx, and the rise in intracellular calcium leads to exocytosis of insulin granules [108].

The K_{ATP} channel works in a slightly different fashion in pancreatic α-cells to result in glucagon release. It was noted that when K_{ATP} channel activity was blocked genetically or pharmacologically in pancreatic α-cells, action potential firing stopped and glucagon secretion was suppressed. This effect was also observed when voltage-gated Na^{+} and N-type Ca^{2+} channels were blocked [85, 110]. Moderate membrane depolarization in α-cells, however, appeared to lead to reduced but not entirely suppressed electrical activity of the membrane, permitting glucagon secretion [110]. Based in part on these findings, it is thought that at high glucose levels, increased metabolism leads to increases in the intracellular ATP/ADP ratios, which in turn cause α-cell K_{ATP} channels to close. This channel closure consequently causes a strong membrane depolarization that inactivates voltage-gated Ca^{2+} channels as well as voltage gated Na^{+} channels. The subsequent reduction in Ca^{2+} influx then suppresses glucagon secretion from α-cells. K_{ATP} channels in α-cells thus control glucagon secretion using a similar pathway as that for insulin secretion in β-cells, but employ a different set of membrane channels in this pathway. An increase in glucose in pancreatic α-cells has effects similar to those observed in β-cells with respect to K_{ATP} channel activity and resting membrane potential. However, the

secretion of glucagon also depends on modulation of the sodium action potential. The depolarization due to inactivation of K_{ATP} channels is not only greater than that observed for β- cells but also causes the inactivation of both Na^+ and Ca^{2+} channels. The end result is that K_{ATP} channel closure prevents, rather than activates, the release of glucagon in α-cells [110].

Hypothalamus

As mentioned previously, the hypothalamus also contains K_{ATP} channels which can play a role outside the pancreas in mediating glucagon secretion. The hypothalamus contains glucose responsive neurons possessing K_{ATP} channels in the ventromedial hypothalamic (VMH) region and glucose sensitive neurons in the lateral hypothalamus [85]. Similar to pancreatic cells, in the hypothalamus an increase in glucose results in a rise of ATP levels. The increase in ATP then causes the closure of K_{ATP} channels, which in turn leads to membrane depolarization [111]. However, unlike in the pancreas, under normal conditions K_{ATP} channel closure increases action potential firing. Typically, under hypoglycemic conditions, activation of autonomic neurons stimulates glucagon secretion [112]. However, VMH neurons of Kir6.2$^{-/-}$ mice do not demonstrate increased neuronal firing with high glucose whereas wild type neurons show a significant increase in firing rate in response to high glucose, [85, 87]. Further, the response to pharmacologically-induced hypoglycemia in Kir6.2$^{-/-}$ mice is not increased glucagon secretion from α-cells as is seen in wild type mice, even though glucagon secretion remains normal at the level of the pancreas [85]. Though the entire mechanism behind it is not fully understood, together these data indicate that a hypothalamic glucose-sensing and glucagon secretion mechanism is dependent on functional K_{ATP} channels.

Skeletal muscle

The K_{ATP} channel is also involved in modulating glucose uptake into skeletal muscle. *In vivo*, basal glucose uptake has been shown to be about two times greater in Kir6.2$^{-/-}$ EDL and gastrocnemius than in wild type. In comparison, the *in vivo* basal glucose uptake in Kir6.2$^{-/-}$ soleus is similar to that observed in Kir6.2$^{-/-}$ EDL and red gastrocnemius, and does not differ significantly from wild type soleus [2]. These findings were further confirmed *in vitro*, where K_{ATP} channel deficiency significantly increased basal glucose

uptake in EDL but not in soleus. Insulin stimulated glucose uptake is also enhanced in all Kir6.2$^{-/-}$ muscles. This effect is significantly greater (2 to 2.5x greater than wild type) both *in vivo* and *in vitro* for soleus and red gastrocnemius [2]. The same effect of increased insulin-stimulated glucose uptake was observed with K_{ATP} channel-deficient SUR2$^{-/-}$ mice [113]. *In vivo* insulin-stimulated glucose uptake was also shown to be significantly greater for Kir6.2$^{-/-}$ EDL compared to wild type; however, glucose uptake occurs to a much lower extent than for soleus [2], and in fact, no significant difference exists *in vitro* in the glucose uptake of Kir6.2$^{-/-}$ and wild type EDL [2]. Similar differences in glucose uptake were also observed when K_{ATP} channels were blocked pharmacologically using glibenclamide, thus illustrating that the responses observed in Kir6.2$^{-/-}$ muscles are directly related to the loss of channel function and not to indirect or compensatory effects due to changes in other tissues. Together, these observations suggest that the K_{ATP} channel's function when it comes to glucose uptake is differentially mediated between muscles with different fiber types. The K_{ATP} channel modulates insulin-stimulated glucose uptake to a greater extent in muscles primarily of type I and IIA fibers (soleus, red gastrocnemius) while it affects basal glucose uptake to a greater extent in muscles primarily composed of type IIX and IIB fibers (white gastrocnemius, EDL). The mechanism by which glucose uptake is modulated by K_{ATP} channels is still not understood.

Volume regulation in skeletal muscle

In concert with the sodium-potassium-chloride (NKCC) co-transporter, it has been proposed that the K_{ATP} channel helps maintain cell volume under hyperosmotic conditions [1]. Hyperosmolarity induced by incubation with a mannitol solution significantly increased the rate of Na^+, K^+, and Cl^- uptake by NKCC by approximately 20x in both soleus and plantaris (PLA) compared to the basal uptake rate [1]. However, pharmacological inhibition of ATP production significantly increased NKCC's activity in soleus, while in plantaris, metabolic inhibition did not increase in NKCC activity [1]. The addition of K_{ATP} channel blocker glibenclamide significantly reduced both metabolic inhibition- and hyperosmolarity-induced NKCC activity in soleus. In comparison, the addition of high concentrations of glibenclamide (25 μM) increased NKCC activity in

plantaris and EDL, but glibenclamide coupled with hyperosmotic conditions did not diminish NKCC activity like it did in soleus [1]. Since previously it was shown that PKA activity is known to activate glyconeogenesis and stimulate glycolysis, which both lead to increased ATP production [114, 115], it was proposed that K_{ATP} channel activity is stimulated when hyperosmolarity depresses PKA activity that subsequently decreases ATP production [1]. The opening of K_{ATP} channels and resultant K^+ efflux then activates the NKCC as a mechanism to counter osmotic changes and potassium fluctuations [1]. As for the effect on glucose uptake illustrated above, the role of the K_{ATP} channel in cell volume regulation is greater for the soleus muscle (primarily type I and IIA fibers) but not as important in EDL or PLA muscles (both primarily type IIX and IIB fibers) [1].

Cytoprotection in skeletal muscle

A major function of the K_{ATP} channel is to provide cytoprotection from metabolic stress for tissues such as the brain, heart, and skeletal muscle. Types of stresses include pathophysiological stresses, such as ischemia in the brain and in muscle, or physiological stresses, such as fatigue due to strenuous exercise in skeletal muscle. Fatigue is a significant metabolic stress on muscles, and has been shown to diminish force generation upwards of 70% in soleus, 80% in FDB, and 90% in EDL [4, 116]. Experimental evidence suggests that the channel can protect tissues via the vasculature by increasing oxygen delivery to the vascular bed, and it can also protect tissues from cell damage and contractile dysfunction by reducing ATP depletion, minimizing damaging increases in intracellular calcium, and regulating membrane excitability. As this thesis centers on the importance of K_{ATP} channels in skeletal muscle, this section will focus on current knowledge of the K_{ATP} channel's role in cytoprotection particularly within and between skeletal muscles of varied fiber type composition.

Vasodilation

It has been shown that under ischemia, the body's response is a rapid increase in blood flow by vessel dilatation, also known as reactive hyperemia [117, 118]. An experiment performed in pigs showed that as blood flow was decreased to the hind limb, those animals infused with K_{ATP} channel blocker glibenclamide had significant increases in

vascular resistance and lowered ability to extract O_2 compared to control animals possessing functional K_{ATP} channels, hence suggesting that K_{ATP} channels are important in mediating regional control of blood flow [119]. Similarly, administration of the K_{ATP} channel blocker tolbutamide to humans who were experiencing a localized ischemia in the arm (due to tightening of a blood pressure cuff) had significantly reduced total reactive hyperemic blood flow to the forearm as compared to control, suggesting again K_{ATP} channel involvement in vascular smooth muscle tone regulation [120]. Since the reduction of blood flow from an occlusion or constriction (i.e. due to contraction of large muscle groups during intense exercise or due to inflation of a blood pressure cuff) can result in decreased perfusion of skeletal muscle, it in turn reduces tissue access to oxygen, glucose, and free fatty acids [118, 119]. The vasodilation mediated by K_{ATP} channels, therefore, may indirectly protect skeletal muscle from damage by attempting to assure that tissue needs for O_2 and other nutrients are met quickly after the tissue has faced a period of reduced blood flow or ischemic stress [119, 120].

Contractile Dysfunction

Although K_{ATP} channels are inactive at rest in skeletal muscle [121, 122], their presence and activity are crucial for preventing fiber damage in muscle during exercise and fatigue. Two studies emphasizing the channel's importance in skeletal muscle *in vivo* involved Kir6.2$^{-/-}$ mice that were elicited to swim daily for 28 days or to run on a treadmill daily over a 4-5 week period [3, 123]. The swimming regimen resulted in fiber damage in both the hamstrings and cardiomyocytes of Kir6.2$^{-/-}$ mice [123]. Both tissues showed necrosis; further histological investigation of the hind limb revealed increased numbers of internal nuclei, prominent nucleoli, and basophilic cytoplasm, all of which indicate fiber regeneration by satellite cells [123, 124]. Similarly, the diaphragm muscles of several treadmill-run Kir6.2$^{-/-}$ mice showed mild to severe fiber damage by infiltration of connective tissue and/or mononucleated cells, while some of the Kir6.2$^{-/-}$ hind limb muscles contained internal nuclei [3].

In vitro evidence also suggests that the presence of the channel is important for preventing contractile dysfunction. Unstimulated force, a contractile dysfunction that develops when muscles fail to relax between contractions, arises at a faster rate and is

present to a greater extent in isolated K_{ATP} channel-deficient muscles [116, 121]. Similarly in isolated FDB fibers, greater than 60% of fibers lacking K_{ATP} channel activity through either genetic or pharmacological means (glibenclamide) become partially or fully supercontracted when stimulated under a fatigue protocol [4]. Excessive depolarization is yet another contractile dysfunction. Glibenclamide-treated fibers have also been shown to experience fast and large membrane depolarizations during fatigue (from -80 mV to -30 mV over a 60 s period) that lead to fiber supercontraction [125].

In both whole muscles and single fibers, it was shown that increases in intracellular Ca^{2+} were responsible for the contractile dysfunctions that occurred in the absence of K_{ATP} channel activity [4, 125]. The reduction of Ca^{2+} influx into K_{ATP}-deficient muscle during fatigue, either by blocking DHPR channels with verapamil or by lowering extracellular $[Ca^{2+}]$, was able to reduce unstimulated force during fatigue, eliminate unstimulated force during recovery, and permit nearly complete force recovery to pre-fatigue levels after 30 min [125]. Similarly, the addition of verapamil was able to minimize the extent of membrane depolarization in a number of glibenclamide-treated fibers [125].

The addition of pinacidil, a channel opener, to either EDL or soleus muscles stimulated to fatigue illustrated that activation of K_{ATP} channels can reduce force by causing a reduction in action potential amplitude [126]. Coupling this finding with the observations regarding calcium and membrane depolarization, it appears that K_{ATP} channels act to prevent contractile dysfunction and resultant fiber damage by reducing the possibility of large membrane depolarization that may lead to a Ca^{2+} overload. Excessive depolarization can lead to activation of DHPR channels that can permit excessive increases in intracellular Ca^{2+} (and unstimulated force). Large increases in $[Ca^{2+}]_i$ are a known cause of fiber damage, and they can cause inactivation of other membrane channels to affect overall membrane excitability as well as increase production of cell-damaging reactive oxygen species and Ca^{2+}-dependent proteases [125, 127-129].

A number of differences have been observed between the responses of various muscles and fiber types to the lack of K_{ATP} channel activity during fatigue. Unstimulated force arises at a faster rate and is present to a greater extent in K_{ATP} channel-deficient FDB and

EDL than in soleus type muscles [116, 121]. Force recovery after fatigue is diminished in K_{ATP} channel-deficient muscles, but to a greater extent in the EDL and FDB than in soleus [121]. While treatment with pinacidil can significantly improve force recovery in EDL, it has no effect on soleus force recovery [121, 126]. Looking across different muscles, it appears that the K_{ATP} channel plays a more important role for EDL and FDB than for soleus in response to fatigue.

Studies using single fibers further demonstrate differences between fiber types within a single muscle. Most K_{ATP}-deficient FDB fibers became partially or fully supercontracted during fatigue [4]. These fibers demonstrated large increases in unstimulated intracellular Ca^{2+}, faster decreases in tetanic Ca^{2+}, and the majority of supercontracted fibers ceased contracting within 60 to 120 ms and did not recover [4]. However, not all intact fibers were similarly affected. Interestingly, three of the 28 partially or fully supercontracted fibers exhibited sporadic contractions during fatigue. Every wild type fiber tested as well as a few K_{ATP}-deficient fibers actually recovered within 10 min post-fatigue to pre-fatigue calcium levels. None of the K_{ATP}-deficient fibers that supercontracted recovered [4]. In a membrane depolarization study, many but not all glibenclamide-treated fibers supercontracted, and those which did not supercontract experienced only small membrane depolarizations (20 mV increase) comparable to those observed in wild type or verapamil/glibenclamide-treated FDB fibers, while a different subset of verapamil/glibenclamide treated FDB fibers that did not supercontract experienced large membrane depolarizations comparable to that experienced by fibers treated with glibenclamide alone [125]. The subtle differences in fatigue responses could be attributed to the various fiber types present in the FDB.

Although *in vivo* the fiber damage observed in treadmill-run Kir6.2$^{-/-}$ mice was limited to 25% of EDL fibers, 12% of PLA fibers, and 13% of TA fibers, there was essentially no damage evident in the soleus (<1% of fibers affected). This supports the earlier observation that force recovery is affected to a greater extent in EDL than in soleus. The damaged fibers identified in the treadmill-run Kir6.2$^{-/-}$ mice were almost exclusively (99%) type IIB [3]. While this finding supports the greater importance for K_{ATP} channel function in cytoprotection of EDL (a muscle containing high type IIB content) as

compared to soleus (a muscle containing almost no IIB fibers), it does not explain the observations of fiber damage *in vitro* during fatigue in FDB.

The FDB is primarily composed of IIA and IIX fibers and has less than 1% IIB fiber composition, thus strongly indicating that the K_{ATP} channel's cytoprotective effect is not limited to IIB fibers, as was suggested by *in vivo* data. Furthermore, the findings from single FDB fiber studies allude to differences in the role of the channel amongst fiber types. It still remains unclear why a discrepancy exists between the types of fibers damaged during fatigue *in vivo* and *in vitro*. One possibility is that treadmill running leads to recruitment of primarily IIB fibers *in vivo*. Another possibility is that type IIB fibers may experience greater metabolic stress as they are highly glycolytic, whereas type I, IIA, or IIX fibers can better cope with metabolic stress since they are more oxidative fibers. On the other hand, the isolated single fibers *in vitro* were forced to face greater stress than they would experience *in vivo* because of an imposed fatigue protocol.

Overall, the importance of the K_{ATP} channel in glucose uptake, cell volume, and cytoprotection varies between muscles and/or fiber types. It appears from recent studies that cytoprotection is the most important role of the K_{ATP} channel in skeletal muscle, particularly with respect to the K_{ATP} channel population present in the t-tubules where the majority of ion and metabolite fluxes occur during contraction and fatigue. To better understand the nature of these differences, it is necessary to investigate if K_{ATP} channel content and/or activity varies within the t-tubules across different muscles and fiber types.

HYPOTHESIS AND AIMS OF THIS THESIS

The objective of this study was to determine if differences in t-tubular K_{ATP} channel content between soleus, EDL, and FDB exist that may account for differential cytoprotective effects between muscles. The hypothesis was that "K_{ATP} channel content in the t-tubules varies between muscles in the order of EDL>FDB>SOL, within fiber types in the order of IIB>IIX>IIA>I, and varies independently of t-tubular content."

To meet the objective of this study and to test the above hypothesis, the following aims were undertaken:

Aim 1: Development of a technique to study fiber type and Kir6.2 content in single mouse muscle fibers;

Aim 2: Identification of single and multiple MHC types expressed within fibers to assess if fibers composed of multiple myosins form a large proportion of unexercised muscle and need to be accounted for when considering relative K_{ATP} channel content;

Aim 3: Relative quantification of Kir6.2 content in the transverse tubules of different fiber types in different muscles, since the absence of this K_{ATP} subunit is directly related to loss of cytoprotection in skeletal muscles, and;

Aim 4: Determination of dependence of Kir6.2 content on fiber t-tubule volume, by using the α_1 DHPR subunit content as an index of t-tubular content.

CHAPTER 2

MATERIALS AND METHODS

MATERIALS

Chemicals and materials employed in this study are summarized in Appendix 1.

METHODS

Animals

Two-to-four month old mice (Charles River Laboratories, Canada) were fed *ad libitum* and housed according to the guidelines of the Canadian Council for Animal Care. The Animal Care Committee of the University of Ottawa approved all experimental procedures used in this study. Prior to muscle excision, mice were anaesthetized with a single intraperitoneal injection of 2.2 mg ketamine/0.4 mg xylazine/0.22 mg acepromazine per 10 g of animal body weight. The final volume of anaesthetic injected was never greater than 0.06 mL.

Single Fiber Preparation

Single muscle fibers were isolated as per Cifelli *et al.* [4] and were then stained using a standard immunofluorescence protocol. Briefly, mouse FDB muscles were dissected in the presence of physiological solution (bubbled with 5% CO_2/95% O_2 to maintain pH 7.4) and cleared of outer connective tissues to facilitate muscle digestion by 0.3% collagenase. After 2.5 hours of 37°C incubation with intermittent swirling, fibers were gently triturated with a plastic Pasteur pipette, diluted in fresh pre-warmed DMEM and dispersed onto freshly prepared Matrigel-coated glass coverslips. Separated fibers were left for 90 min at 37°C to promote attachment to coverslips.

Isolated muscle fibers plated on Matrigel- or laminin-coated coverslips were acclimated from 37°C to 25°C within a chamber with constant flow through of 5% O_2/95% CO_2. While in the chamber, fibers were treated with Ca^{2+} buffering treatment (10 μM BAPTA-AM; ionomycin (5 μM) + EGTA (10 mM)) or control solution (Ca^{2+} free Tyrode) for 30 min. After treatment, cells were briefly rinsed in Ca^{2+} free Tyrode (2 x 5 min) and then

TABLE 2-1

Fixative	Composition	Reference
Paraformaldehyde	2 or 4% (w/v) PFA in 1X PBS	[130]
Zinc Paraformaldehyde (ZnPF)	10% ethanol 30% acetone 4% (w/v) PFA 8 mM $ZnCl_2$ Tyrode solution (pH 7.4) consisting of: 140 mM NaCl 5 mM KCl, 10 mM HEPES, 2 mM BAPTA, 10 mM glucose, 10 mM sodium pyruvate	[131]
Lana's Fixative (modified DeMartino-Zamboni fixative)	4% (w/v) PFA 3% (v/v) picric acid in 10 mM phosphate buffer	[132-134, 157]

Table 2-1. Fixatives tested for single skeletal muscle fiber protocol.

acclimated to 4°C for 30 min in Ca^{2+} free Tyrode solution in preparation for fixation. Fibers were fixed with one of three fixatives (Table 2-1) at 4°C for 20 min. Immunofluorescence protocol was as described for cross sections.

Immunofluorescence localization of K_{ATP} and DHPR Channel Subunits

Muscle Preparation

The FDB, EDL, and soleus muscles were dissected, gently dried on Whatman paper, embedded in a small amount of 4°C-cooled OCT compound and frozen in isopentane precooled in liquid nitrogen. Muscles were stored at -80°C until immunofluorescence and RT-PCR analysis. For immunohistochemistry, consecutive cross sections of 10 μm thickness were cut from the mid-belly of the muscle on a cryostat (Leica Microtome, HM 500M) cooled to -18°C, mounted on Superfrost Plus slides, and stored at -80°C until use.

Fiber type, Kir6.2 and DHPR Immunofluorescence

To determine fiber type and to quantify Kir6.2 and DHPR protein content, six consecutive cross sections (10 μm) were obtained from each muscle tested and mounted on positively-charged glass slides. Each slide contained a cross section of EDL, SOL, and FDB from the same animal.

Several slides containing muscle cross sections were thawed for 15 minutes at 35°C on a slide dryer (Fisher Scientific, Canada). Cross sections were blocked for one hour at room temperature with 0.5% BSA in PBS. Sections were then exposed to primary antibody for 2.5 h at room temperature in a humid chamber. Cross sections used for fiber typing were double labeled with anti-laminin and one of anti-type I, IIA, IIX, or IIB MHC antibodies to permit identification of individual fiber boundaries. For the quantification of Kir6.2 or DHPRα_1, separate cross sections were single labeled with antibodies against either of these proteins (Table 2-2). Excess primary antibody was removed by three PBS washes (5 minutes per wash). Cross sections were then incubated 45 minutes at 37°C with fluorescence-conjugated secondary antibodies (Table 2-2) in a humid chamber. After rinsing three times with PBS, sections were mounted using antifade reagent and stored at -80°C until image acquisition. Control cross sections were also stained concurrently to

TABLE 2-2

Primary Antibody	Isotype	Dilution	Source
A4.840 (anti-type I MHC)	Mouse IgM	None	Mouse hybridoma (DSHB, U Iowa)
SC71 (anti-type IIA MHC)	Mouse IgG	None	Mouse hybridoma (DSMZ, Germany)
6A1 (anti-type IIX MHC)	Mouse IgM	None	Mouse hybridoma (L. Leinwand)
BFF3 (anti-type IIB MHC)	Mouse IgM	None	Mouse hybridoma (DSMZ, Germany)
Anti Laminin	Rabbit IgG	1:1000	Sigma Cat. # L-9393
Anti DHPR (α_1 subunit)	Mouse IgG	1:500	Chemicon Cat. # MAB427
Anti Kir6.2 (C terminus)	Rabbit IgG	1:100	Alomone Cat. # APC-020
Secondary Antibody	**Isotype**	**Dilution**	**Source**
FITC-conjugated Goat anti-Mouse IgM	Goat IgG	1:200	Chemicon Cat. # AP128F
FITC-conjugated Goat anti-Mouse IgG	Goat IgG	1:200	Sigma Cat. # F-4143
Rhodamine-conjugated Goat anti-Rabbit IgG	Goat IgG	1:200	Jackson Laboratories Cat. # 111-025-144

Table 2-2. Antibodies employed for immunofluorescence. All commercially supplied primary and secondary antibodies were diluted with 0.3% Triton-X 100 in 1X PBS solution. The fiber type-specific antibodies were used as undiluted supernatants collected from hybridoma cultures, with addition of 0.3% Triton-X 100 to enhance antibody penetration into tissue.

test for autofluorescence and non-specific secondary antibody binding. The controls included cross sections incubated without any antibody or without primary antibody but with secondary antibody. These controls consistently did not exhibit autofluorescence or non-specific secondary antibody binding. The specificity of the anti-Kir6.2 antibody could not be tested using muscles from Kir6.2$^{-/-}$ mice because a portion of a non-functional Kir6.2 protein is expressed in these animals (personal communication, T. Miki and S. Seino).

Image Acquisition and Analysis

Fluorescence images were obtained using a Sony digital camera (model DXC-950, Canada) attached to an Axiophot-2 fluorescence microscope (Zeiss, Canada). For all images captured of anti-Kir6.2-labeled cross sections, acquisition settings (exposure time, gain, intensity, offset, and binning) were initially set to maximize the imaging of the antibody and then preserved to facilitate comparison of fluorescence intensity/quantification across experiments. Images of all muscles from a single animal were obtained all at once. This process was then repeated for anti-DHPR-labeled cross sections. For fiber type determination, variations in anti-MHC staining between SOL, EDL, and FDB required that image acquisition settings were optimized for each muscle to ensure that all positive fibers were visible in each sample and that background was minimized.

Fluorescence intensity was then determined using the Northern Eclipse (EMPIX Inc., USA) drawing/mask tool as shown in Figure 2-1. Briefly, each fiber in a Kir6.2 image was encircled within its inner perimeter (enclosing the fiber's t-tubular network). The master mask file was then transposed onto images of the same muscle region in consecutive cross sections stained with other antibodies. Colour fluorescence images were converted to 16-bit grayscale for analysis. The average fluorescence intensity per unit area (average grey/μm^2) of identical intra-fiber regions was obtained via Northern Eclipse software. Intensity data from all antibodies was sorted for each muscle based on the cross sectional areas measured. In the event that Northern Eclipse identified multiple regions with equal cross-sectional areas, fiber identities were verified manually.

Immunohistochemical and immunofluorescence quantification has been performed previously on various tissues, including pituitary adenoma, lung, and muscle, to detect differences in the expression of hormones, free radicals, and basal lamina proteins respectively [160-162]. Several important parameters were considered when designing these experiments to quantify staining intensity, such as section thickness, primary antibody incubation period, and reproducibility of the immunohistochemical or immunofluorescence protocol [163, 164].

RT-PCR

RT-PCR analysis was performed to verify that MHC transcripts were present for each MHC detected by immunofluorescence. RT-PCR analysis was performed on DNAse I-treated RNA isolated from two-to-four month old CD1 mice. Myosin heavy chain expression profiles were examined using primers flanking each of the MHC isoforms (MHC I, IIA, IIB, and IIX). Table 2-3 outlines primers employed in this study.

FIGURE 2-1

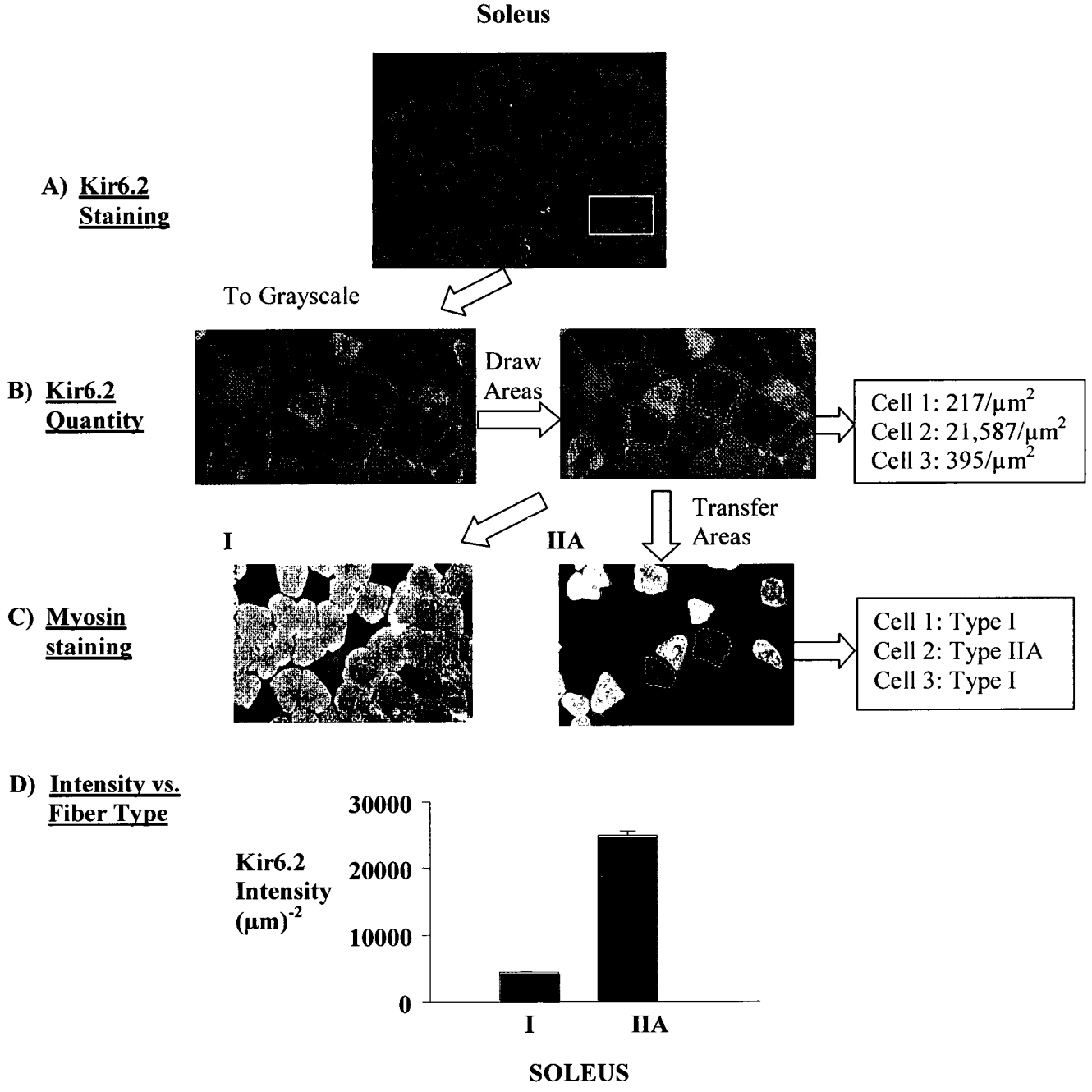

Figure 2-1. Process of quantification of t-tubular content of Kir6.2 protein. A) Ten μm cross-sections containing 4-6 layers of t-tubules are stained with anti-Kir6.2 (red). B) After converting the fluorescent image to gray scale, areas are traced inside fibers to determine the fluorescence intensity/μm^2. C) Traces (or masks) are transferred to cross-sections stained for different antibodies. D) Fluorescence intensity of Kir6.2 is plotted for different fiber types.

TABLE 2-3

Primer	Sequence
MHC I-fwd	AGTTCCGCAAGGTGCAGCAC
MHC I-rev	CCACCTAAAGGGATGTTGCAA
MHC IIA-fwd	CGGGTGAAGAGCCGGGAGGT
MHC IIA-rev	GAAGATGGTTGCAAACGTGAC
MHC IIB-fwd	ACAGACTAAAGTGAAAGCCTA
MHC IIB-rev	CACATTTTGTGATTTCTCCTGT
MHC IIX-fwd	CGGGTGAAGAGCCGGGAGTT
MHC IIX-rev	CTCTCCTGATGTACAAATGAT

Table 2-3. RT-PCR primers for myosin heavy chain mRNA transcript amplification.

CHAPTER 3

RESULTS

DEVELOPMENT OF SINGLE SKELETAL MUSCLE FIBER PROTOCOL FOR IMMUNOHISTOCHEMISTRY

The original approach to study the K_{ATP} channel subunit distribution involved labeling single muscle fibers using immunofluorescence. Similar analysis by immunohistochemistry and immunofluorescence has been performed on isolated cardiomyocytes but no protocol existed for single skeletal muscle fibers. The aim of this study was to optimize experimental conditions for immunohistochemical study of single muscle fibers. The main issues addressed were the type of fiber adherence substrate used for coverslips, the necessity for buffering of free calcium, and fixation. Optimization of these factors would minimize fiber loss from coverslips through the numerous washes during immunohistochemical processing and help maintain a high proportion of straight, quality fibers for immunofluorescence analysis.

Fiber Adherence to Coverslip and Calcium Buffering

For fiber adherence, two different substrates were tested: mouse laminin (a basement membrane and extracellular matrix protein) and Matrigel (a commercial preparation of extracellular matrix proteins collagen V, laminin, and entactin) [135]. Both laminin and Matrigel have been used successfully to promote substrate adherence of C2C12 and single cardiac muscle cell preparations [136, 137].

For immunohistochemistry of intracellular proteins, cell membranes must become permeable to antibodies. However, the process of dissolving cell membranes via fixation can lead to fiber contraction and subsequent morphological changes because it increases Ca^{2+} permeability. For each of the two cell adherence substrates tested, three different approaches were used to buffer Ca^{2+} present in the bathing solution or released from the sarcoplasmic reticulum: i) BAPTA-AM (1,2-bis-(o-aminophenoxy)-ethane-N,N,N',N'-tetraacetic acid, tetraacetoxymethyl ester), ii) ionomycin/EGTA, and iii) zero

Ca^{2+}solution. Exposing fibers to 10 μM BAPTA-AM allows for the buffering of Ca^{2+} once BAPTA is freed from AM by esterases. The second Ca^{2+} buffer involved ionomycin/EGTA, where EGTA acts as a high affinity Ca^{2+} buffer while ionomycin is a Ca^{2+} ionophore to increase membrane permeability to Ca^{2+}. In this case, Ca^{2+} is buffered on the extracellular side of the membrane and intracellular Ca^{2+} decreases as it leaves the fibers through pores created by ionomycin. The third solution tested does not constitute a buffer, but is a zero Ca^{2+}solution.

After separating individual fibers by trituration, fibers were added in excess to both laminin-coated and Matrigel-coated coverslips (Figure 3-1 A, B) and incubated for 90 min at 37°C. Prior to addition of a calcium buffer, both laminin- and Matrigel-coated coverslips contained a number of fibers exhibiting similar morphology.

Fibers were then incubated 30 min in one of the three solutions to buffer calcium as described above. After the incubation, fibers had three major appearances: straight, rippled, or bent/contracted. To be categorized as straight, fibers had to have smooth appearance along the fiber periphery/cell membrane and be aligned approximately 180° (examples: green arrows in Figure 3-1). Bent/contracted fibers had one or more breaks in their linear morphology (135° or greater) and/or had sections where 50% of more of the fiber had rippled appearance along the cell membrane, such that it was partially to fully supercontracted (red arrows-panels C, E, F). Rippled fibers are fibers intermediate to "straight" and "bent" fibers. These fibers were characterized by small, localized rippled disruptions to an otherwise smooth cell membrane, and although the fiber may have slight deviation from 180° the rest of the fiber looks like a "straight" fiber (yellow arrow-panel H).

Fibers exhibiting straight, rippled and bent/contracted appearance after each Ca^{2+} buffering treatment and after fixation were enumerated to assess the success of various treatment combinations. The proportion of fibers remaining straight after each treatment step is shown in Figure 3-2.

FIGURE 3-1

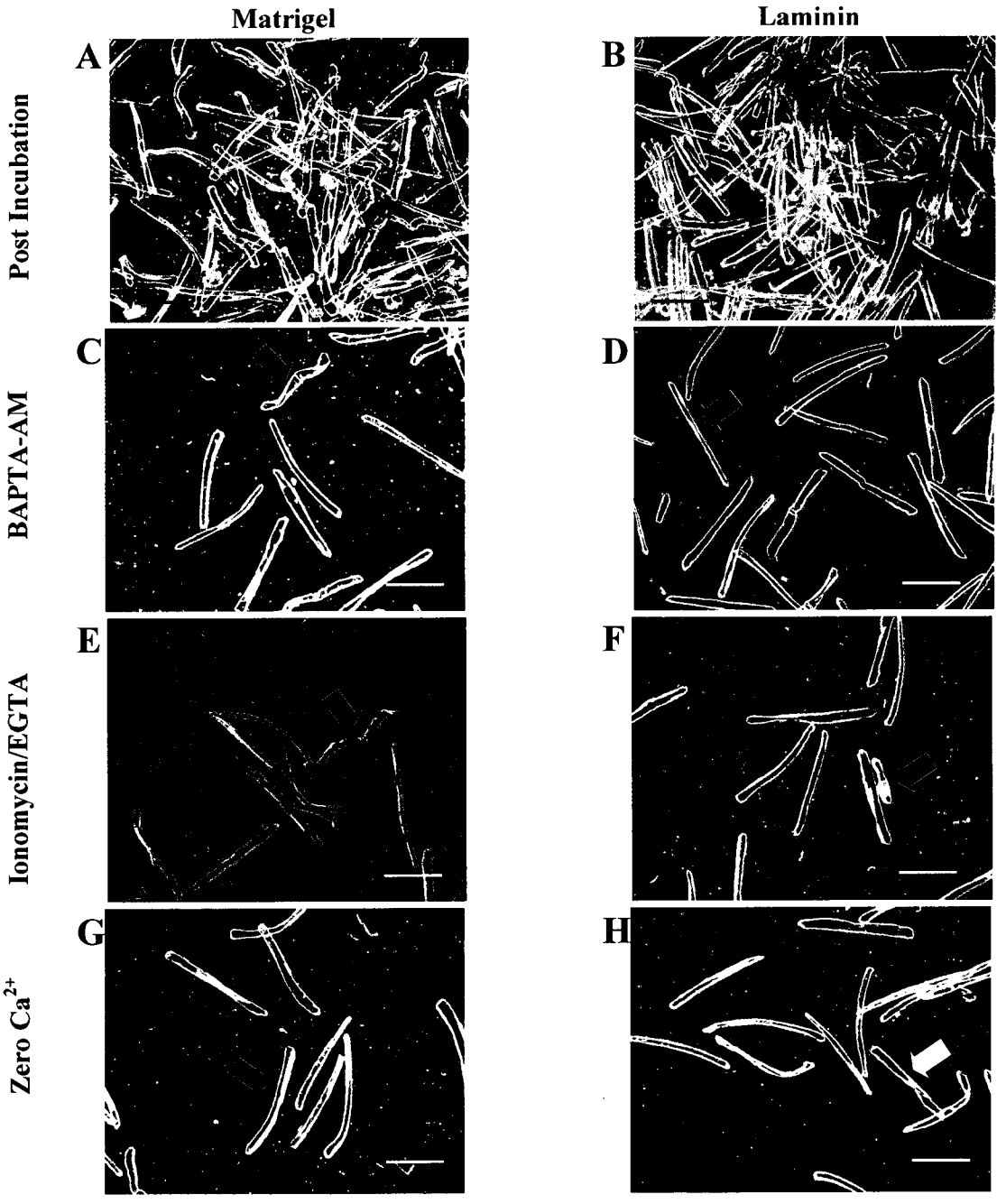

Figure 3-1: Matrigel- and laminin-plated fibers after Ca^{2+} buffering share morphology similar to freshly plated fibers. A/B: Fiber appearance after plating. C/D: After 30 min BAPTA-AM incubation. E/F: After 30 min ionomycin/EGTA incubation. G/H: After 30 min zero Ca^{2+} incubation. Arrows: green = straight, red = bent, yellow = rippled fibers. Bar = 250 μm

FIGURE 3-2

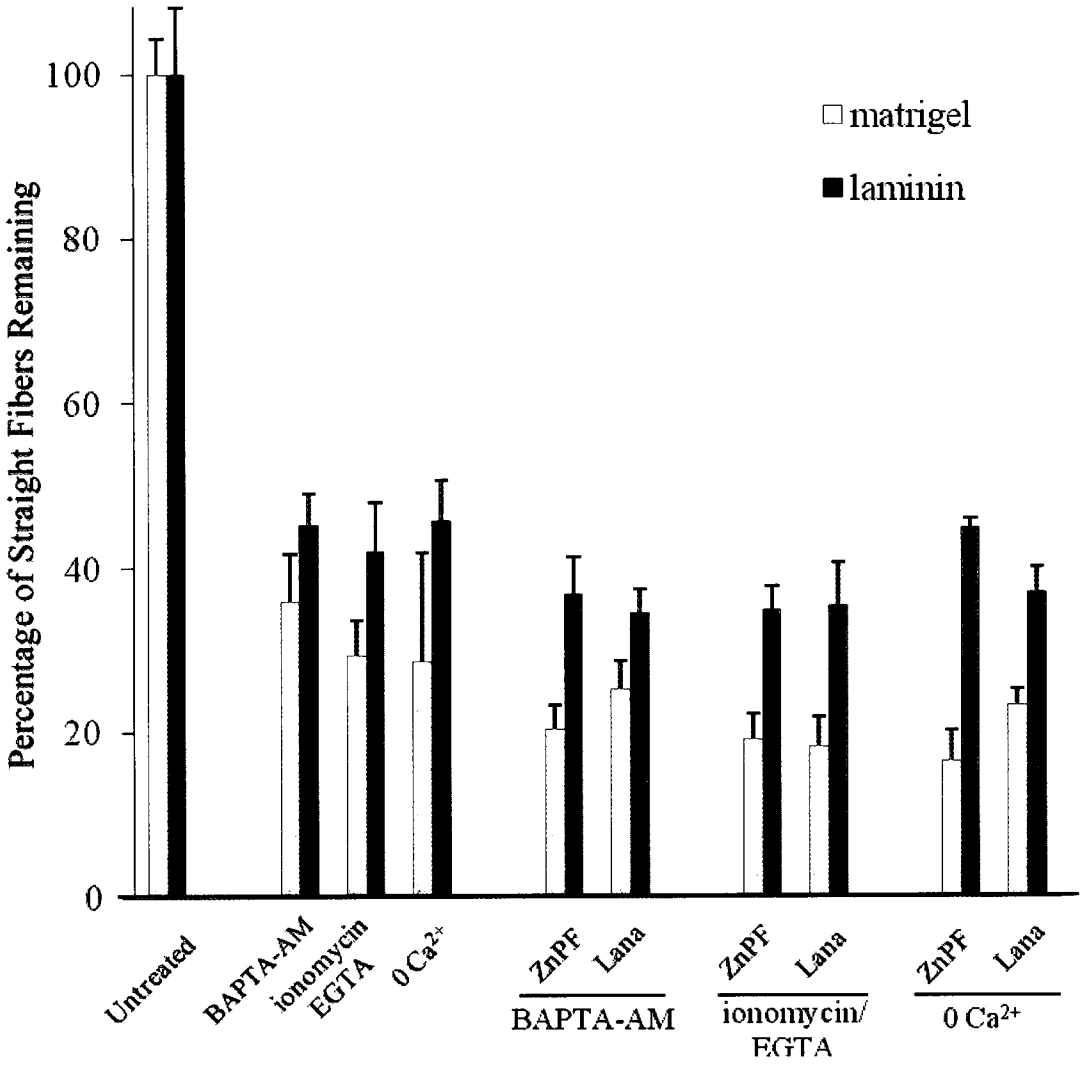

Figure 3-2: Comparison of different cell adherence substrates, calcium buffering treatments, and fixatives on maintenance of straight fiber morphology. Laminin-plated fibers remain straighter during processing than Matrigel-plated fibers. Untreated refers to fibers enumerated after 90 min incubation at 37°C. (n = 3 - 6 coverslips per treatment)

With all three treatments (Ca^{2+} buffering and zero Ca^{2+}), there was a loss of straight fibers compared to the number present after the 90 min incubation period. With Matrigel-coated coverslips, the number of straight fibers decreased by 65%, 70%, and 71% depending on the treatment (Figure 3-2). When laminin-coated coverslips were used, the number of straight fibers was reduced by 56%, 60%, and 65%--this loss was to a slightly lesser extent than that observed for Matrigel-coated coverslips (Figure 3-2). Between the various treatments, there was no significant difference between the numbers of straight fibers remaining (Figure 3-2).

Fixation Protocol

A fixative was added following the Ca^{2+} buffer or control solution treatment. Three fixatives were tested: paraformaldehyde (PFA), zinc-paraformaldehyde fixative (ZnPF), and Lana's (a modified DeMartino-Zamboni) fixative (Table 2-1).

Many fibers did not remain on the coverslips following the addition of 2 or 4% paraformaldehyde fixative for 5 min. Regardless of the Ca^{2+} buffering conditions, less than 50% of the fibers remained on the coverslips: 40% ± 7.4% fibers at 2% PFA and 13% ± 3.4% fibers at 4% PFA remained following exposure to paraformaldehyde. Furthermore, most of the fibers remaining were not suitable for further immunohistochemical analyses because they were rippled, bent, or supercontracted (Figure 3-3). Thus, paraformaldehyde was excluded as a candidate fixative for further testing.

After 20 min of Lana and ZnPF fixation, fiber morphology was assessed. The most striking difference between the appearance of fibers fixed with Lana versus ZnPF occurred independent of the substrate/Ca^{2+} buffering treatment combination used. After fixing with ZnPF, a streaked pattern arose within the fibers (Figure 3-4 A, Figure 3-5) and in many cases the A-I bands were not visible. In comparison, the Lana-fixed fibers retained a clear, see-through appearance with A-I banding visible (Figure 3-4, panel B). The proportion of straight fibers was further reduced with both ZnPF and Lana fixation, with fewer straight fibers remaining on Matrigel-coated coverslips. The remaining proportion of straight fibers was similar for both Ca^{2+} buffering treatments (35 - 37 % on

FIGURE 3-3

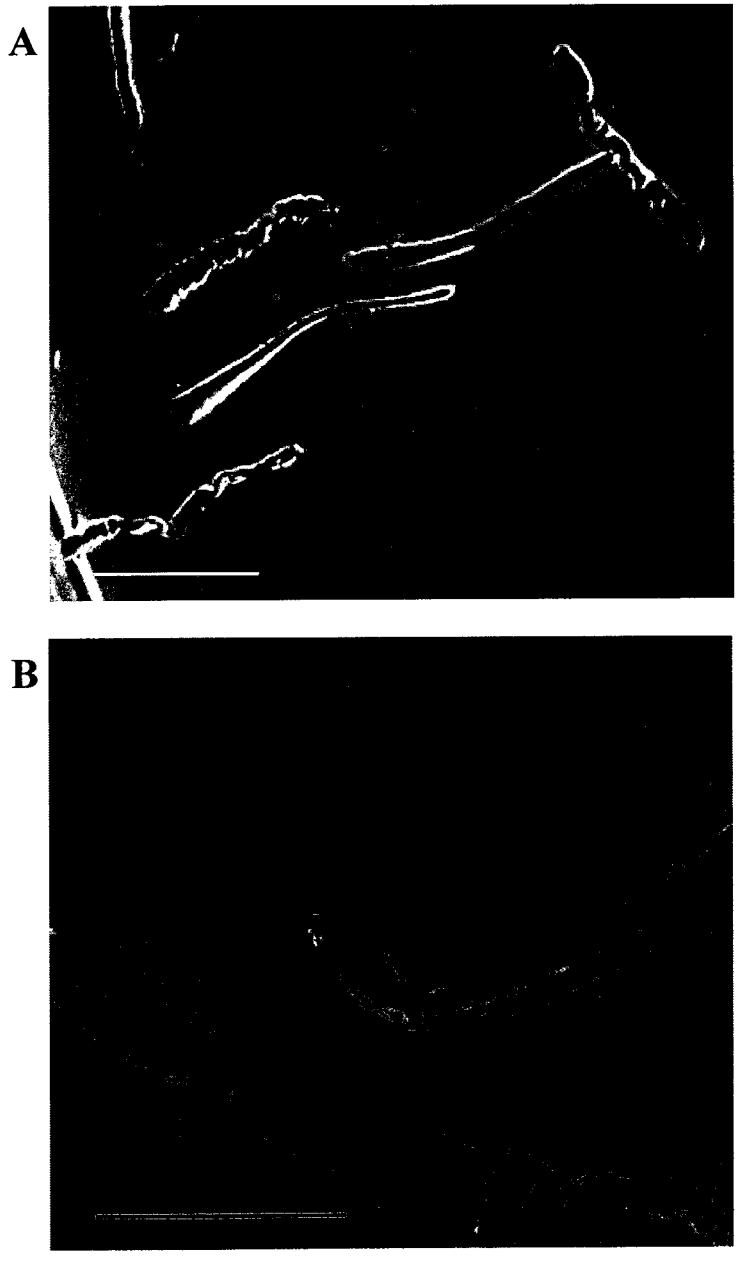

Figure 3-3: Paraformaldehyde fixation results in poor morphology and few fibers after treatment. Fibers were laminin-plated, treated with BAPTA-AM, and fixed with 2% (A) and 4% (B) paraformaldehyde (white bar=250 μm, black bar =100 μm)

FIGURE 3-4

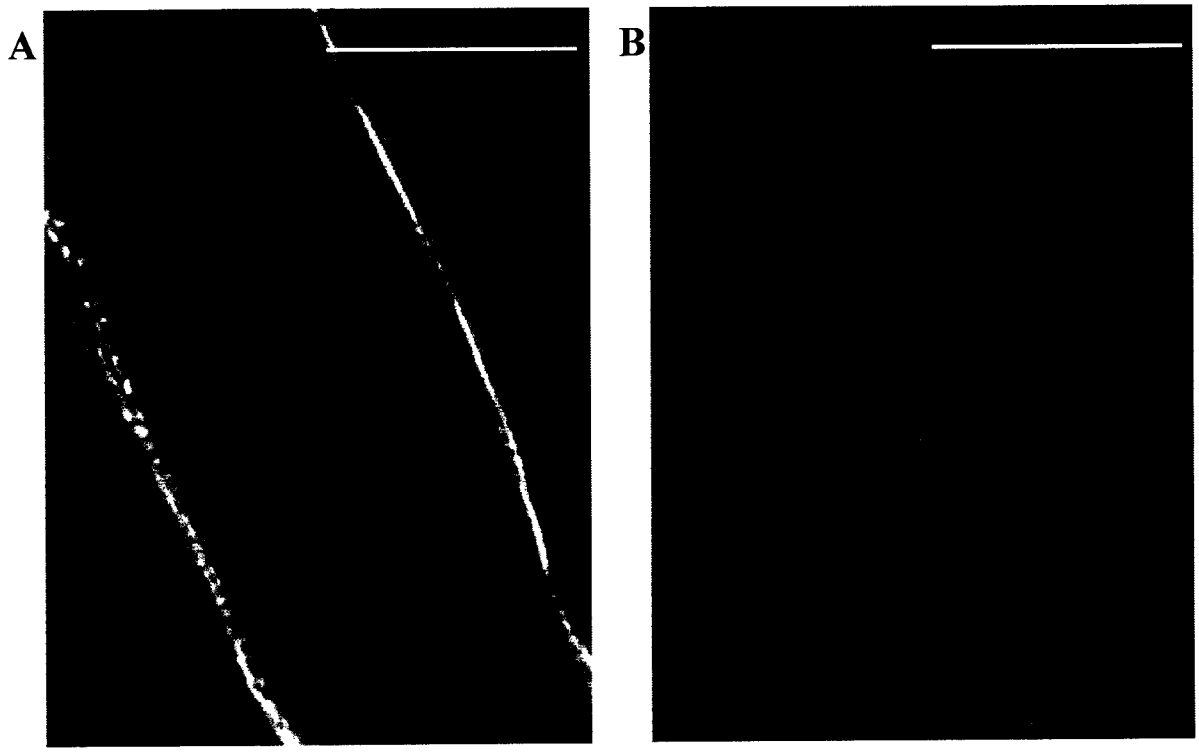

Figure 3-4: Loss of A-I bands in fibers in ZnPF fixative (A) but not in Lana's fixative (B) is dependent on the fixative used. Fibers were plated on laminin-coated coverslips, treated with ionomycin and EGTA for 30 min, and fixed with either ZnPF (A) or Lana's (B) fixative for 20 min. (Bar=25 μm).

FIGURE 3-5

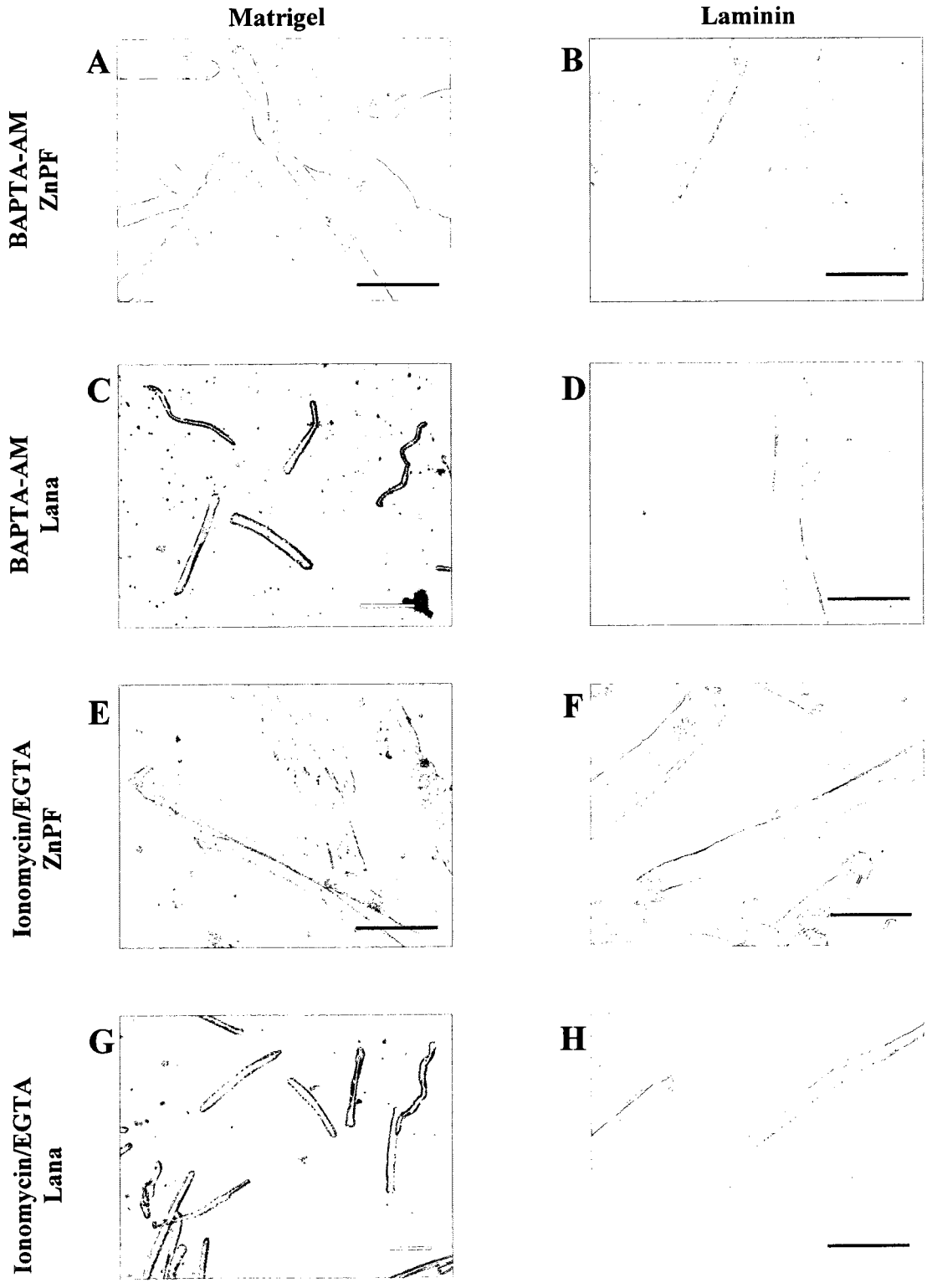
Matrigel
Laminin
A
B
C
D
E
F
G
H
BAPTA-AM ZnPF
BAPTA-AM Lana
Ionomycin/EGTA ZnPF
Ionomycin/EGTA Lana

FIGURE 3-5 continued

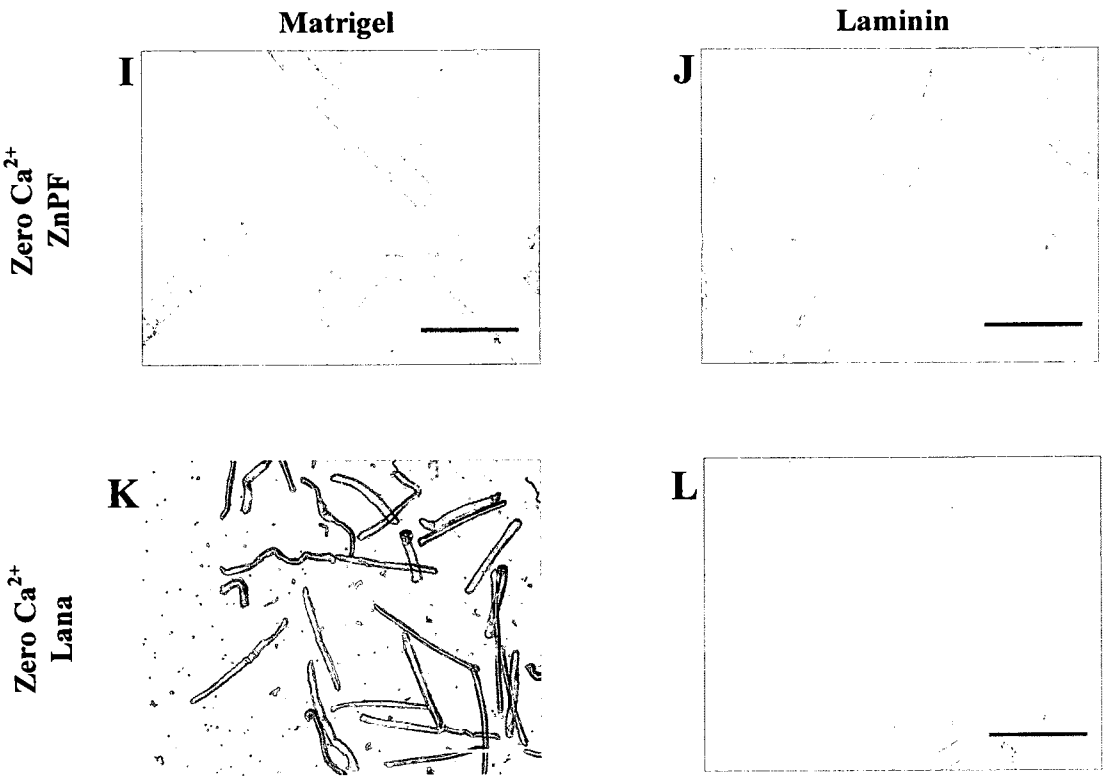

Figure 3-5: Laminin-plated fibers after Ca^{2+} buffering/fixation show better overall morphology compared to Matrigel-plated fibers, but fibers treated with zero Ca^{2+} solution retain the best overall morphology. A/B: Fibers after 30 min of BAPTA-AM + ZnPF fixative. C/D: Fibers after 30 min of BAPTA-AM + Lana's fixative. E/ F: Fibers after 30 min of ionomycin/EGTA + ZnPF fixative. G/H: Fibers after 30 min of ionomycin/EGTA + Lana's fixative. I/J: Fibers after 30 min of zero Ca^{2+} solution + ZnPF fixative. K/L: Fibers after 30 min of zero Ca^{2+} solution + Lana's fixative. (white bar=250 μm, black bar=100 μm)

laminin-coated coverslips and 20-25% of fibers remaining on Matrigel- coated coverslips). The greatest proportion of straight fibers remained on laminin-coated coverslips that received zero Ca^{2+} solution treatment (Figure 3-2).

Based on these results, it appeared that to obtain the largest number of straight fibers, the optimal conditions were laminin-coated coverslips, zero Ca^{2+} solution treatment, and Lana's fixative. These were conditions employed when optimizing the single fiber immunofluorescence protocol.

Immunofluorescence Protocol Optimization

Four antibodies were tested: anti-type I and anti-type IIA MHC antibodies, anti-Kir6.2 antibody, and anti-DHPR antibody. Confocal microscopy was used to determine an antibody's staining pattern through the thickness of a single fiber. By obtaining 0.5 μm-thick image slices from the top (cell membrane surface) to the bottom (opposing cell membrane surface) of a fiber, it was clear that the anti-DHPR antibody stained fibers thoroughly. A paired banding pattern appeared as expected, where the paired green bands correspond to pairs of t-tubules located at the junction of the A and I bands of two adjacent sarcomeres while the darker lines correspond to the A and I bands (Figure 3-6 A, B). Anti-Kir6.2 antibody staining pattern matched that observed for anti-DHPR antibody staining at the cell membrane surface (Figure 3-6 C). However, the anti-Kir6.2 antibody was only visible near the cell surface, while images of optical sections at mid-fiber illustrated limited immunofluorescence within the fiber (Figure 3-6 D). The same limited immunofluorescence within fibers was observed for anti-MHC I and IIA (data not shown).

In an attempt to improve antibody penetration, two methods were tested: 10% sucrose incubation followed by freeze cracking, and -20°C methanol treatment after fixation [94]. The aim was to create large pores or cracks in the cell membrane after fixation, thus improving the access of antibody molecules to the antigenic sites within the fiber. Separately, fibers were also agitated on an automatic shaker during antibody incubation to try and facilitate penetration. Unfortunately, these treatments did not improve the diffusion of the antibodies into single muscle fibers and were stopped (data not shown).

FIGURE 3-6

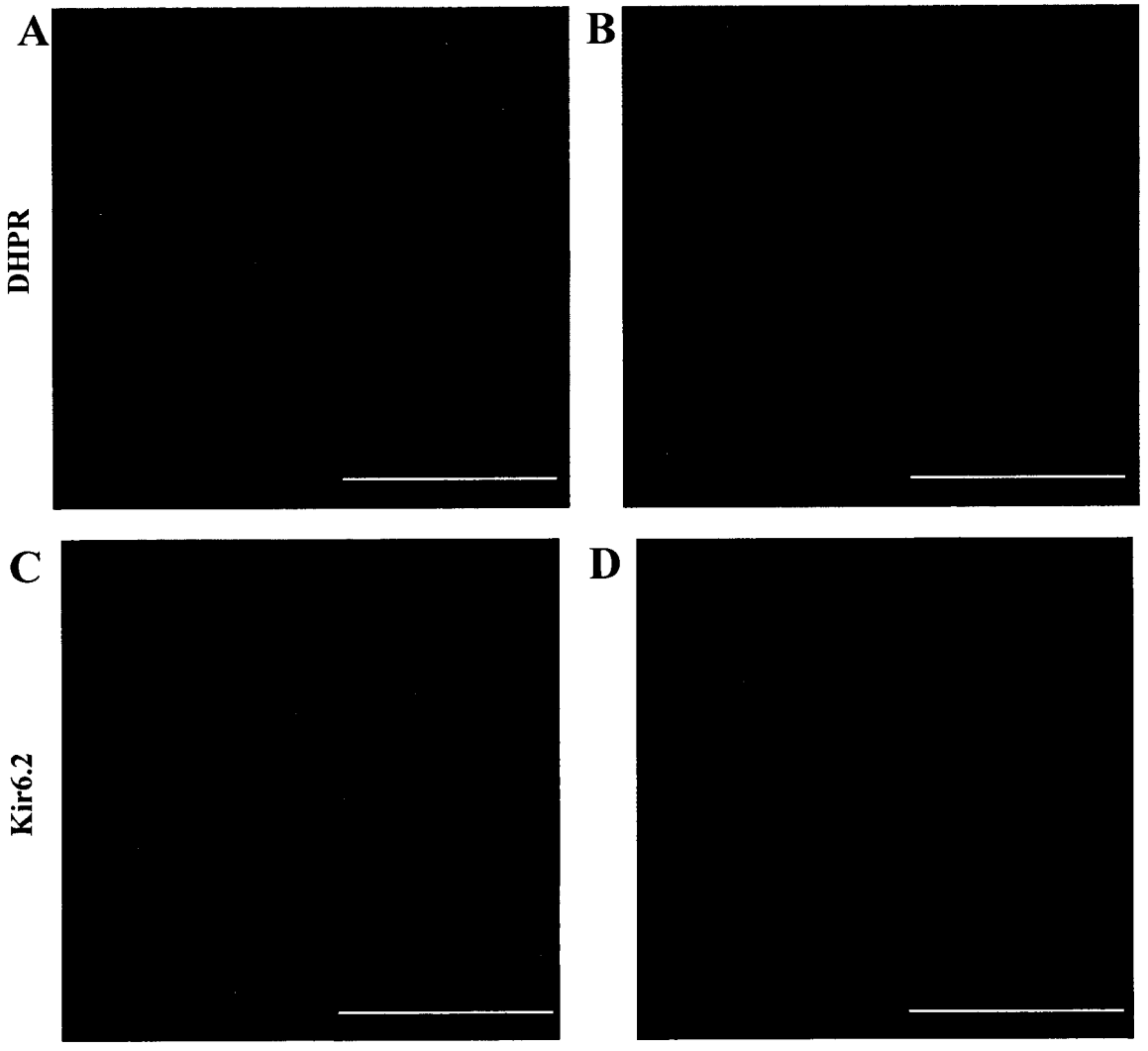

Figure 3-6: Complete antibody penetration into single FDB fibers is dependent on the antibody used. A/B: Staining pattern observed for Lana-fixed fibers stained with anti-DHPR antibody. C/D: Under the same fixation and staining conditions as in A/B, anti-Kir6.2 antibody binds the cell membrane at the fiber surface but staining does not diffuse throughout fiber. Images A/C were obtained from the outer surface of a fiber (top image from a 20-25 series of confocal images) while images B/D images were obtained from middle of the fiber (mid-stack image from a series of 20-25 confocal images). (Section = 0.5 μm; Bar = 25 μm)

It was also noted that antibody binding and penetration was inconsistent after Lana fixation, in particular for anti-MHC antibodies. Fibers fluoresced intensely at the cell surface but did not exhibit the expected banding pattern and in many cases staining occurred in an all or nothing fashion (all fibers fluoresced or no fibers were labeled) (data not shown). To test if the fixative employed was interfering with the binding of anti-MHC or anti-Kir6.2 antibodies, Lana-fixed and unfixed muscle cross sections of soleus, EDL, and FDB were double-labeled with anti-Kir6.2 and anti-type IIA antibodies. Indeed, Figure 3-7 illustrates that Lana fixation affects the staining pattern of both anti-myosin and anti-Kir6.2 antibodies. Instead of staining fibers in a pattern independent of one another, Lana fixation caused both antibodies to label the same regions of the muscle and to exaggerate staining at the cell membranes, thus suggesting that Lana's fixative may not be ideal for future single muscle fiber studies.

Overall, several technical problems needed to be resolved before a single fiber approach could be used to study Kir6.2 localization and distribution by immunofluorescence. Due to these limitations, a different approach was chosen to determine Kir6.2 protein content and distribution amongst different fiber types in mouse muscle. To understand how Kir6.2 subunit expression specifically varies in a muscle and across muscles, fiber typing, Kir6.2, and DHPR content was determined immunofluorescently on cross sections of SOL, EDL, and FDB.

FIGURE 3-7

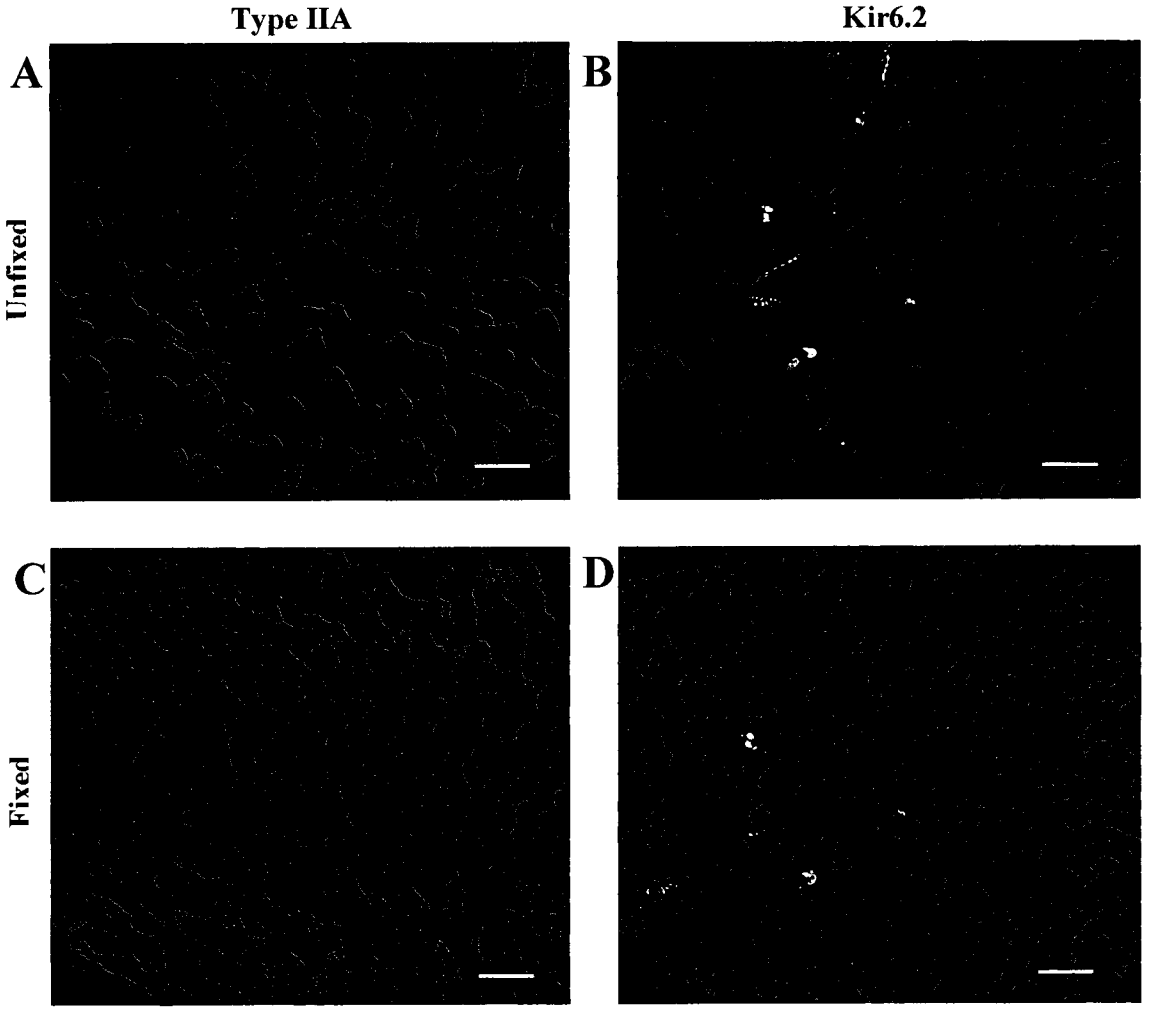

Figure 3-7: Fixation affects the nature of Kir6.2 and anti-MHC IIA binding in mouse skeletal muscles (bar=100 μm). Panels A and B illustrate the staining pattern observed for unfixed cross sections of the soleus with anti-type IIA (A) and anti-Kir6.2 (B) antibodies. Panels C and D illustrate that fixation prior to immunohistochemistry distorted the staining pattern of both anti-type IIA (C) and anti-Kir6.2 (B).

EXPRESSION OF KIR6.2 SUBUNIT AMONG FIBER TYPES IN DIFFERENT MUSCLES

Recent studies have shown that co-expression of multiple MHCs within individual muscle fibers occurs to a much greater extent than originally thought, with up to 70% of fibers expressing two or more MHCs [138]. To ascertain if fibers with multiple MHC expression form a significant proportion of all fibers in muscles of CD-1 mice used in this study and if these hybrid fibers may impact channel subunit content, fiber typing was performed using antibodies for the four MHCs. Thus, this section of the thesis is divided into two parts: a) the results of fiber typing of single and multiple MHCs in soleus, EDL, and FDB, and b) the results of the semi-quantitative measurement of Kir6.2 and DHPR across fiber types within soleus, EDL, and FDB. In the following section, "fluorescence intensity" refers to the amount of fluorescence measured from the fluorophore-conjugated secondary antibody that is bound to the primary antibody that is bound to the protein of interest (myosin, Kir6.2, or DHPR).

Fiber typing of Soleus, EDL, and FDB muscles

Soleus

Most fibers stained strongly for type I (Figure 3-8 A) while fewer stained strongly for type IIA MHC (Figure 3-8 B). In both cases, fluorescent staining was evenly distributed across the whole fiber. In comparison, very few fibers stained intensely and solely for type IIX MHC (Figure 3-8 C). A number of soleus fibers contained more than one myosin isoform. Some fibers stained strong for type I and weakly for type IIA or vice versa (Figure 3-9 A, B). Many fibers that stained strongly for type I or type IIA also stained weakly for type IIX (Figure 3-9 C, D; Figure 3-9 E, F). The majority of fibers that stained for type IIX in conjunction with type I or IIA exhibited less uniform and more granular type of staining. However, this staining pattern is consistent with the IIX isoform being expressed with a second, dominant myosin isoform.

The fibers expressing more than one myosin were defined as hybrid fibers based on reduced fluorescence intensity for one or more myosins compared to the average fluorescence intensity of fibers expressing a single myosin isoform. To illustrate how

FIGURE 3-8

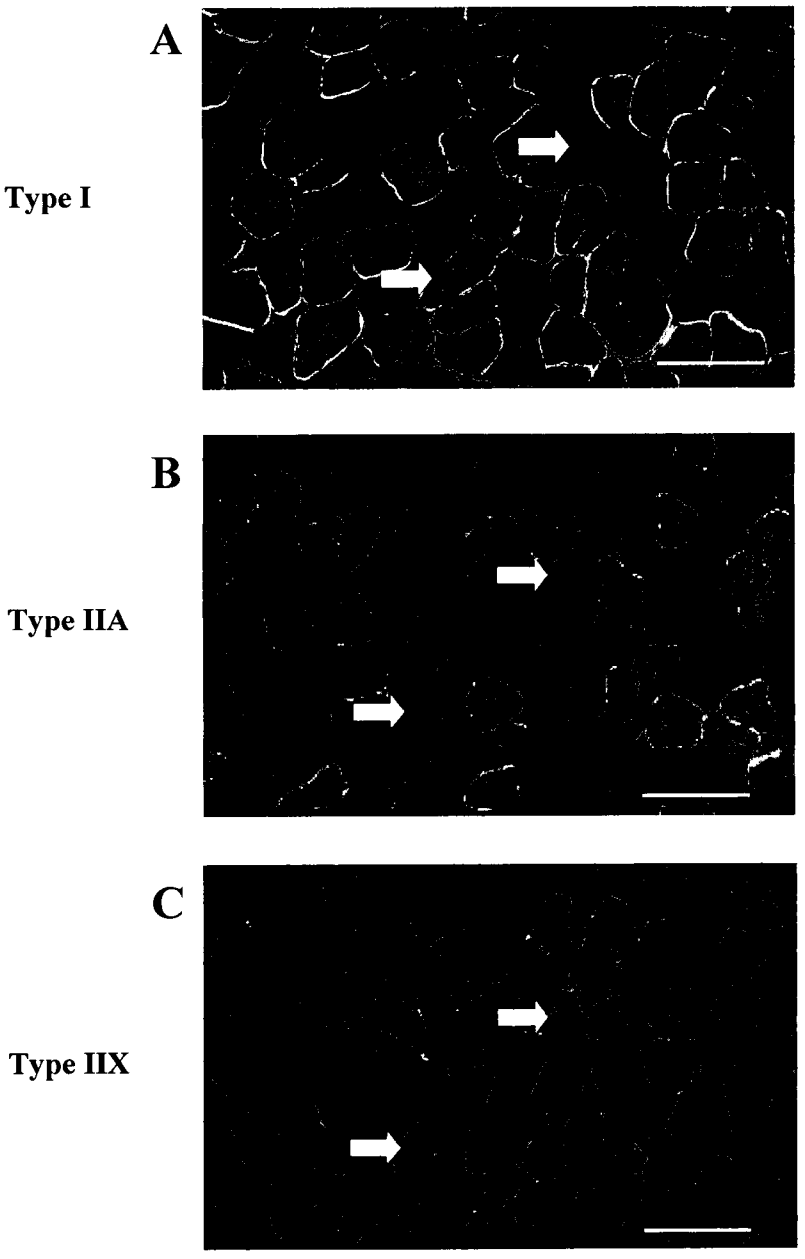

Figure 3-8: Examples of soleus fibers expressing only one myosin isoform. Cross sections were with either anti-type I (A), anti-type IIA (B), or anti-type IIX (C) MHC antibody (green) plus anti-laminin antibody (red). Coloured arrows indicate the same fiber across multiple cross sections. Bar=100 μm.

FIGURE 3-9

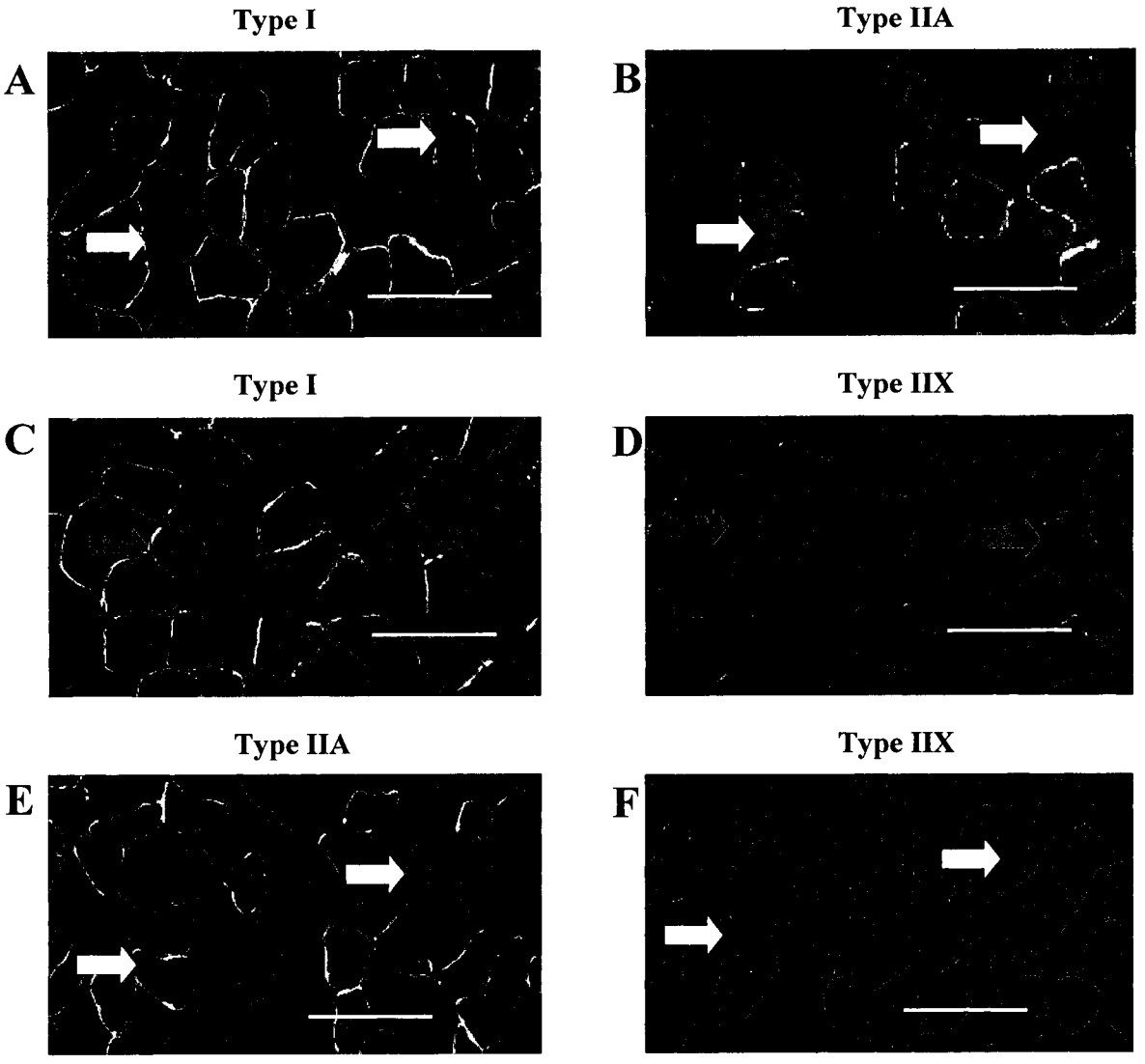

Figure 3-9: Examples of soleus fibers expressing two myosin isoforms. Cross sections were stained with either anti-type I (A, C), anti-type IIA (B, E) or anti-type IIX (D, F) MHC antibody (green) plus anti-laminin antibody (red). Arrows of the same colour indicate the same fiber in different cross sections. Hybrid fiber types present in soleus include type I-IIA (A, B), type I-IIX (C, D) and type IIA-IIX (E, F). Bar=100 μm.

hybrids can be differentiated from fibers expressing single myosins, the relative myosin intensities of the single and multiple myosin-expressing fibers detected in soleus are shown in Figure 3-10. The average myosin intensity of fibers expressing only type I or type IIA myosin showed little variability while fibers expressing solely type IIX in soleus had larger variability. Since only one of the five animals tested contained soleus fibers expressing type IIX alone, the high variability in type IIX is related to its small sample size (7 fibers). Similar to fibers expressing type I or type IIA alone, the relative myosin intensities in hybrid fibers expressing strong type I-weak type IIX or strong type IIA-weak type IIX showed little variability. These fibers had high relative intensities of type I (109%) or IIA (99%) with correspondingly low relative type IIX intensities (25% and 29% for type I-IIX and type IIA-IIX fibers respectively). In contrast, the type I-IIA hybrid fibers had notably lower relative myosin intensity for each myosin. However, higher variability was observed in the intensities of both myosins. The fibers pooled as type I-IIA appeared to demonstrate a continuum of myosin intensities, from strong type I-weak IIA to weak type I-strong type IIA, which likely explains the larger variability observed in their myosin intensity compared to other fiber types.

EDL

Contrary to the soleus that stained primarily for type I and IIA, most EDL fibers stained strongly for type IIX and IIB (Figure 3-11 A, B). However, like the soleus, EDL also contained fibers expressing multiple myosin isoforms. One major hybrid isoform found in both soleus and EDL was type IIA-IIX. In the EDL, some of the type IIA-IIX fibers showed strong staining for both isoforms while other fibers exhibited fairly strong type IIA or IIX staining combined with weaker intensity staining for type IIX or IIA respectively (Figure 3-11 C, D). The other major hybrid isoform expressed in EDL was type IIX/type IIB. Unlike the variations in staining seen in type IIA-IIX fibers, this combination consistently stained with greater intensity for type IIX and weakly for type IIB (Figure 3-11 E, F).

The relative myosin intensities of the multiple myosin-expressing fibers as compared to their single myosin-expressing counterparts found in EDL are shown in Figure 3-12. As

FIGURE 3-10

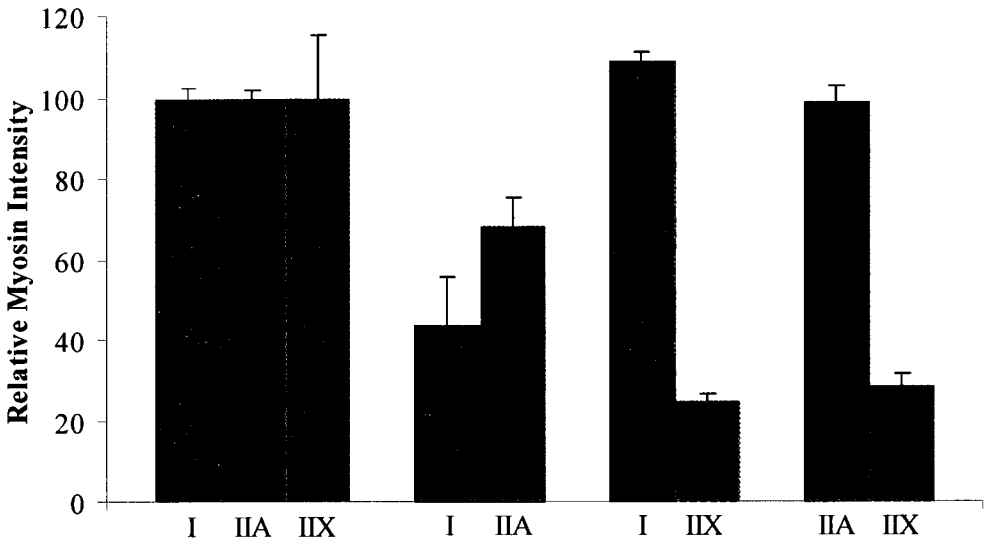

Figure 3-10: Variability of myosin content in different soleus muscle fibers. Fluorescence intensities of myosin staining in fibers expressing a single myosin (only type I, IIA, or IIX) were averaged and set as 100% for each fiber type. For hybrid fibers, or those fibers expressing multiple isoforms, average fluorescence intensities for each individual isoform were expressed in proportion to the value observed in fibers expressing only one myosin. Hybrid myosin expression can vary between fibers, with some fibers exhibiting lower fluorescence for both myosins (type I-IIA) or expressing one myosin more dominantly than another (type I-IIX, IIA-IIX).

FIGURE 3-11

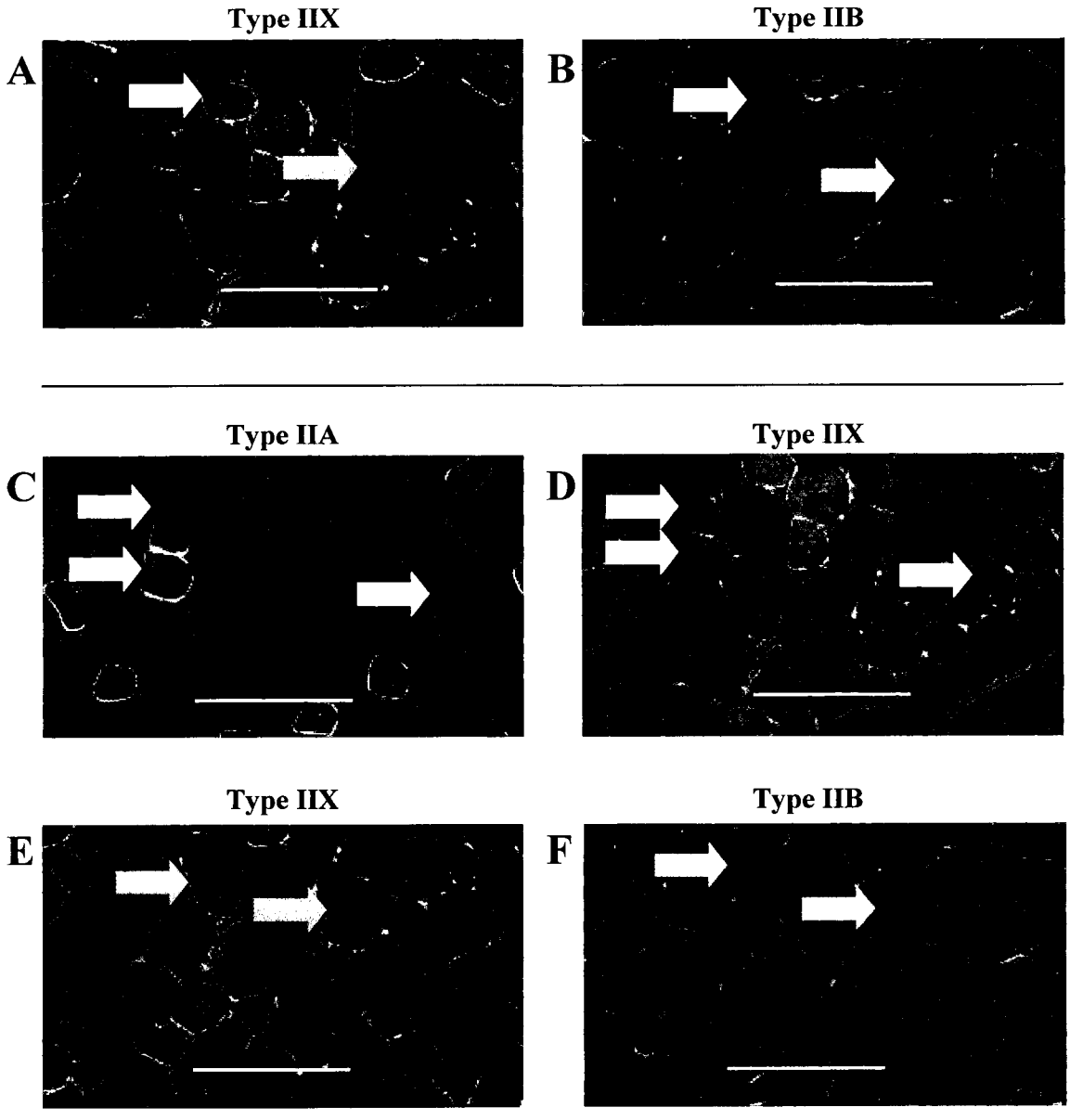

Figure 3-11: Examples of EDL fibers expressing one and two myosin isoforms. Cross sections were exposed to either anti-type IIA (C), anti-type IIX (A, D, E) or anti-type IIB (B, F) MHC antibody (green) plus anti-laminin antibody (red). Coloured arrows indicate the same fiber across multiple cross sections. Hybrid fiber types present in EDL include type IIA-IIX (C, D) and type IIX-IIB (E, F). Bar=100 μm.

FIGURE 3-12

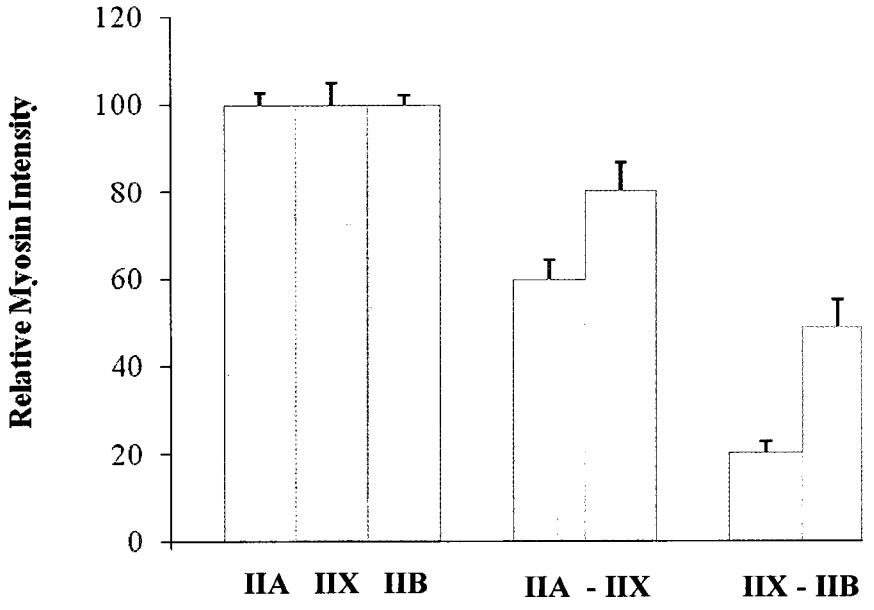

Figure 3-12: Variability of myosin content in different EDL muscle fibers. Fluorescence intensities of myosin staining in fibers expressing a single myosin (only type I, IIA, or IIX) were averaged and set as 100% for each fiber type. For hybrid fibers, average fluorescence intensities for each individual isoform were expressed in proportion to the value observed in fibers expressing only one myosin. Hybrid myosin expression can vary between fibers, with some fibers exhibiting lower fluorescence for both myosins (type IIA-IIX) or expressing one myosin more dominantly than another compared to the average single myosin intensity (type IIX-IIB).

seen in soleus, those fibers expressing a single myosin showed low variability amongst myosin intensity values. The type IIA-IIX hybrid showed slightly greater variability in average myosin intensities, which is consistent with the observation of some fibers exhibiting strong IIA staining were paired with weaker IIX staining, or vice versa. On average, the type IIA-IIX fibers had IIA fluorescence intensities which were 60% of that observed in fibers expressing only type IIA and IIX intensity equivalent to 80% of the myosin intensity seen in fibers expressing IIX only. For the strong type IIX-weak type IIB hybrid, there was little variability in the average IIX staining but greater variability in the type IIB staining within this hybrid isoform. The IIX fluorescence intensity here was 20% of that observed in singly-expressing type IIX fibers while IIB fibers on average had 49% the intensity seen in fibers expressing IIB alone. It must be noted that the intensities observed for each fiber type within a hybrid fiber are expressed in reference to the average myosin intensity of the corresponding non-hybrid myosin. Hence, although type IIX-IIB fibers appear to have a strong type IIX/weak type IIB staining appearance (Figure 3-11 E, F), their corresponding relative myosin intensities are 20% IIX and 49% IIB (expressed in relation to average type IIX and IIB myosin intensities respectively) (Figure 3-12). The intensities within one fiber type cannot be compared across fiber types, but can only be compared to the corresponding non-hybrid fiber type.

FDB

Similar to the soleus, fibers staining for either type I or type IIA stained intensely and evenly (Figure 3-13 A, B). In comparison, fibers staining solely for type IIX had uniform but slightly punctate staining compared to that observed in type I and type IIA FDB fibers (Figure 3-13 C). In addition, three major hybrid fiber type combinations were present in the FDB: type I-IIA, type I-IIX, and type IIA-IIX (Figure 3-14 A - F). In most cases, type I-IIA hybrid fibers stained strongly for both type I and IIA, but at intensities less than that of fibers expressing a single myosin (Figure 3-14 A, B). A few fibers expressed both type I and IIX, and as seen in soleus, type I staining was strong while type IIX staining appeared weaker (Figure 3-14 C, D). The fibers staining for both type IIA-IIX followed the same pattern as this fiber type in EDL, either coupling strong IIA staining with weak type IIX staining, or vice versa (Figure 3-14 E, F).

FIGURE 3-13

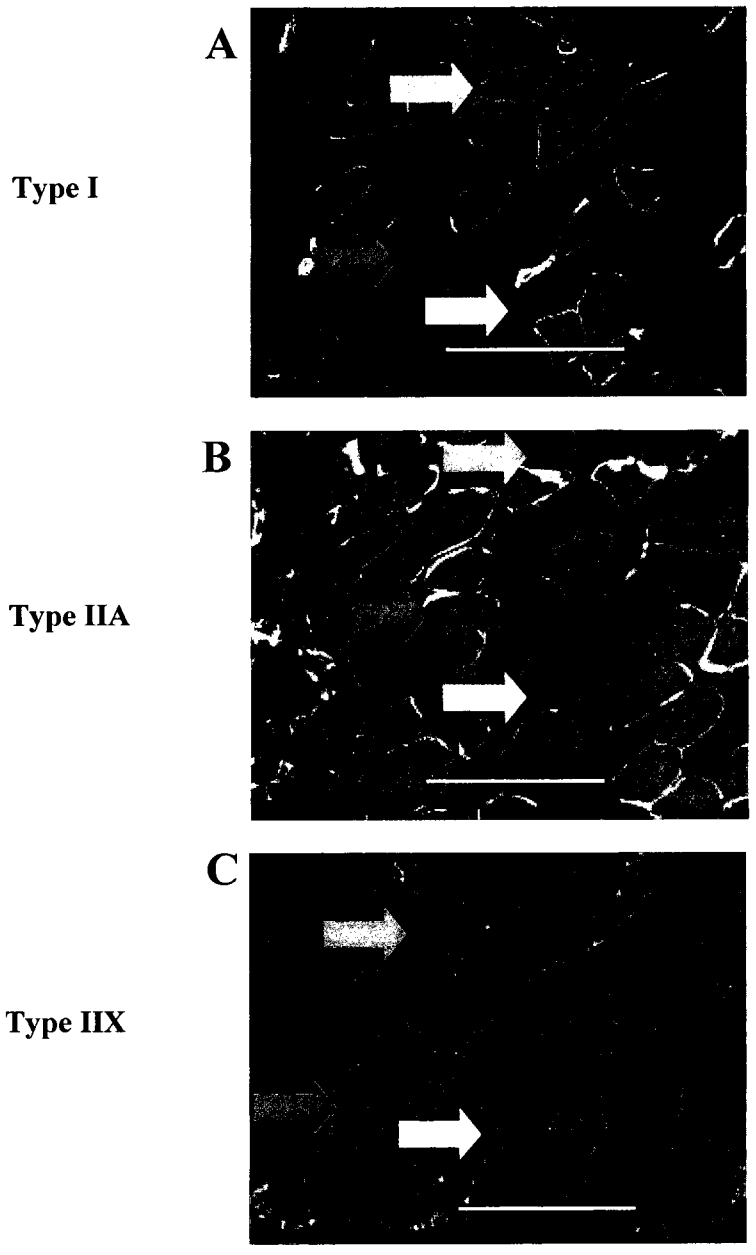

Figure 3-13: Examples of FDB fibers expressing only one myosin isoform. Cross sections were with either anti-type I (A), anti-type IIA (B), or anti-type IIX (C) MHC antibody (green) plus anti-laminin antibody (red). Coloured arrows indicate the same fiber across multiple cross sections. Bar=100 μm.

FIGURE 3-14

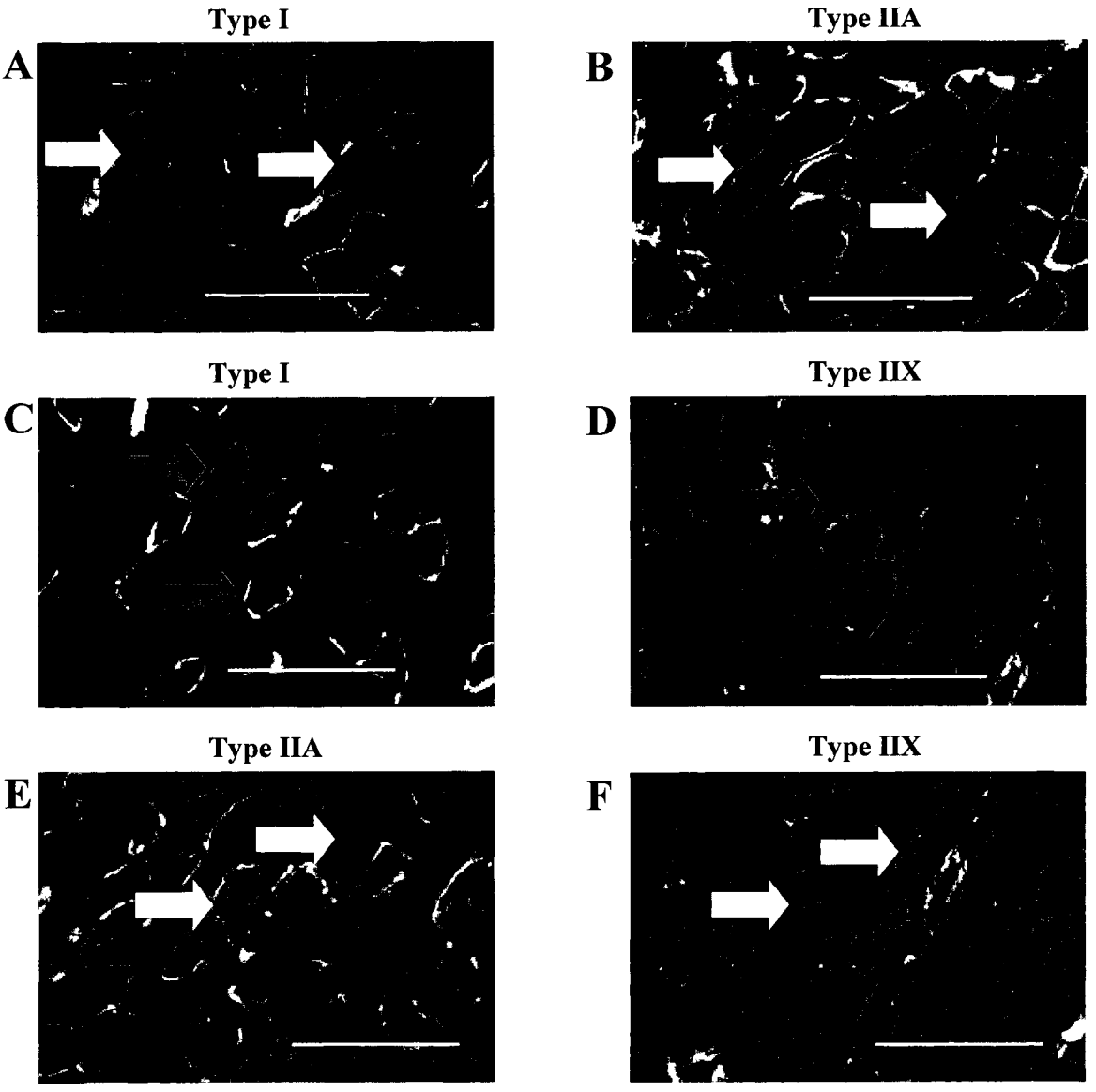

Figure 3-14: Examples of FDB fibers expressing two myosin isoforms. Cross sections were with either anti-type I (A, C), anti-type IIA (B, E) or anti-type IIX (D, F) MHC antibody (green) plus anti-laminin antibody (red). Arrows indicate the same fiber in different cross sections. Hybrid fiber types present in FDB include type I-IIA (A, B), type I-IIX (C, D) and type IIA-IIX (E, F). Bar=100 μm.

In comparison to soleus and EDL, the relative myosin intensities for both single and hybrid fiber types in the FDB showed greater variability, illustrating that some fibers had high intensity staining for one fiber type paired with low intensity staining for the other fiber type, or the other way around. For type I-IIA and type IIA-IIX fibers, the relative myosin intensities were between 60-70% of that observed in fibers expressing the corresponding single myosin (Figure 3-15). In comparison, the type I-IIX hybrid fibers had high intensity type I (105%) and slightly weaker type IIX myosin intensity (67%), which was consistent with very strong type I staining observed in this hybrid type.

Fiber type proportions observed in all muscles

On an average basis, the majority (69%) of soleus fibers expressed type I MHC. However, only 27% of the total fibers expressed solely type I (Figure 3-16). A larger portion (36%) expressed type I and IIX concurrently. Similarly, while 40% of fibers expressed type IIA MHC, just 26% of fibers expressed type IIA only. A little over 10% of total soleus fibers expressed type IIA in conjunction with either type IIX or type I.

In the EDL, type IIB was expressed in more than half its fibers (57%), with 42% of the total fibers expressing type IIB alone (Figure 3-16). Almost a quarter of the fibers expressed type IIX only. Other fibers expressing IIX were hybrids with type IIA (13%), IIB (15%), or type I/type IIA (3%). Many fibers also expressed type IIX (56%), but only a small portion of the EDL's fibers (24%) express type IIX only. About 25% of fibers in EDL stained for type I (6%) or type IIA (17%) but less than 2% of total EDL fibers expressed either type I or IIA myosin alone.

In contrast to soleus and EDL, the FDB consisted mostly of fibers expressing multiple MHCs (56%). Although this muscle demonstrated very high proportions of fibers expressing type IIX (72%), type IIA (67%) and type I (27%), none of these fiber types were present in large amounts on their own (Figure 3-16). Interestingly, 21% of FDB muscle fibers stained for type IIX, another 19% of fibers stained solely for type IIA, and less than 3% of fibers stained only for type I. The major hybrid fiber types observed were type IIA-IIX (32%), type I-IIA-IIX (9%), type I-IIA (8%) or type I-IIA (6%).

FIGURE 3-15

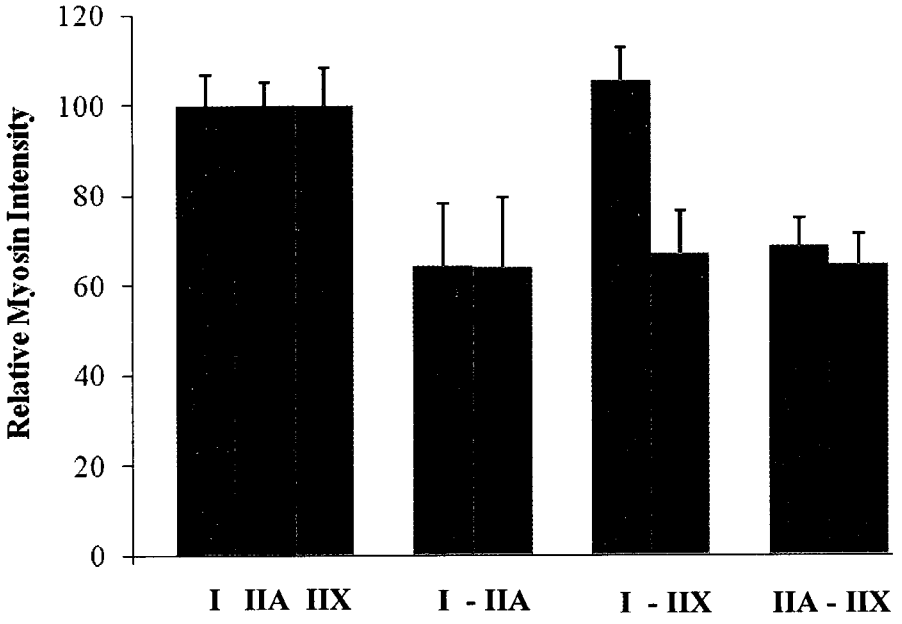

Figure 3-15: Variability of myosin content in different FDB muscle fibers. Fluorescence intensities of myosin staining in fibers expressing a single myosin (only type I, IIA, or IIX) were averaged and set as 100% for each fiber type. For hybrid fibers, average fluorescence intensities for each individual isoform were expressed in proportion to the value observed in fibers expressing only one myosin. Hybrid myosin expression can vary between fibers, with some fibers exhibiting lower fluorescence for both myosins (type I-IIA, type IIA-IIX) or expressing one myosin more dominantly than another compared to the average single myosin intensity (type I-IIX).

FIGURE 3-16

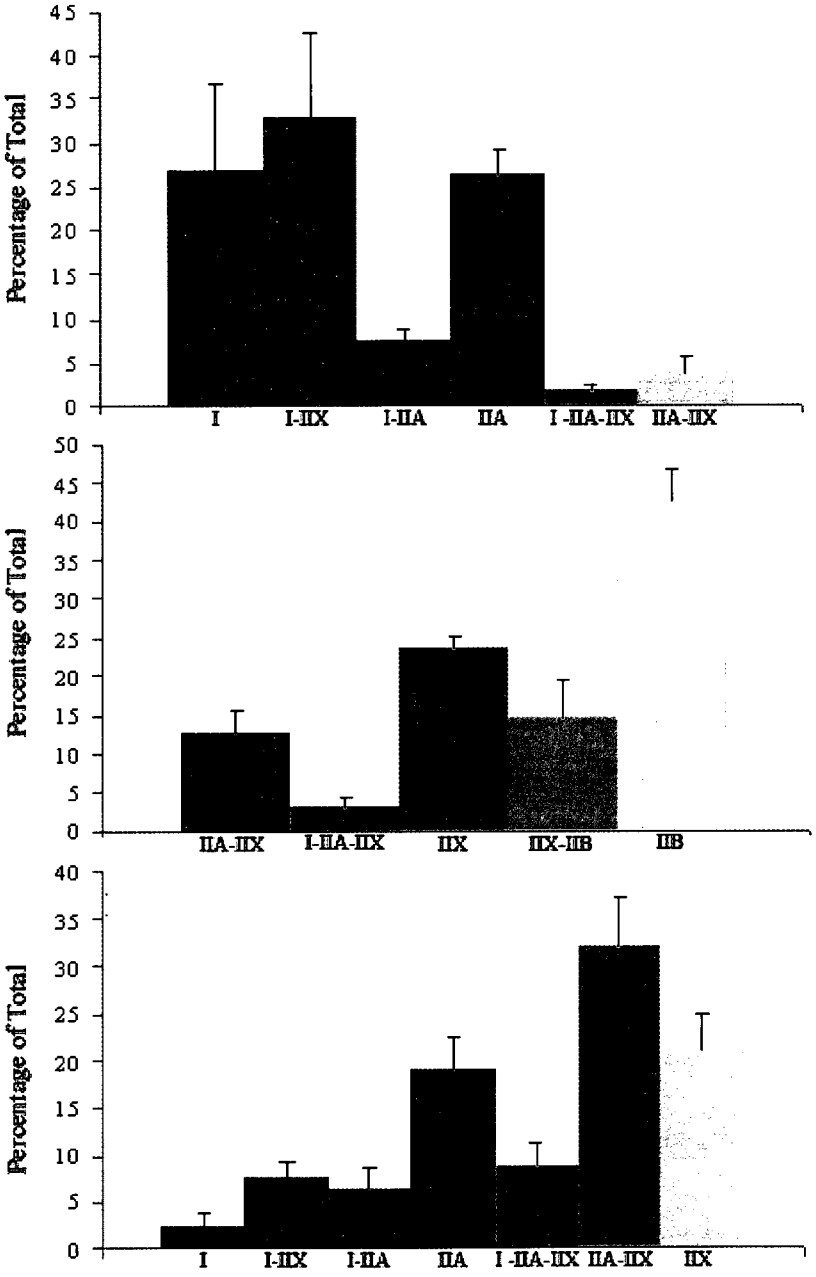

Soleus

Myosin	%
I	69
IIA	40
IIX	40
IIB	0.1
Total	149

EDL

Myosin	%
I	6
IIA	17
IIX	56
IIB	57
Total	136

FDB

Myosin	%
I	27
IIA	67
IIX	72
IIB	3
Total	169

Figure 3-16: Fiber type composition of soleus, EDL, and FDB muscles. Figures show proportion of fibers expressing each fiber type as a percent of total number of fibers within the muscle. Tables on the right represent percentage of fibers expressing each given myosin within a muscle, illustrating the large proportion of fibers that are hybrids. Bars represent S.E.M. n=5.

RT-PCR fiber typing

While it is well established that both EDL and FDB express type IIX myosin, this is the first study in which the presence of type IIX is detected in the soleus muscle. To further substantiate the fiber type composition of all muscles, RT-PCR was performed to determine the presence of the mRNA transcript of each MHC. All MHC types were detected in all three muscles studied (Figure 3-17). The soleus contained high levels of I and IIA myosin transcripts, with lesser amounts of IIX and IIB mRNA. The EDL had approximately equal relative amounts of each fiber type transcript while the FDB had the greatest amount of type IIA and type I transcripts, with less IIX and very low levels of IIB.

Kir6.2 and DHPR fluorescence intensities across muscle fiber types

Soleus

In soleus muscle, many fibers had anti-Kir6.2 staining in the cell membrane while very little or no staining was observed in the center of the fibers where t-tubules are located (Figure 3-18 A). Other fibers had some fluorescence in the center but with varying intensity. In contrast, DHPR staining was observed throughout every fiber, albeit with different intensities between fibers (Figure 3-18 B). After identifying the fiber types, the t-tubules of type I and type I-IIX fibers had the lowest fluorescence intensity of anti-Kir6.2 staining (0.1 and 0.17 respectively) (Figure 3-19). Compared to fibers expressing type I, fibers expressing IIA myosin all had significantly greater Kir6.2 fluorescence intensities (between 0.57 and 2.17) (Figure 3-19). Interestingly, Kir6.2 fluorescence intensity was greatest in type IIA-IIX (2.17) and type IIX fibers of the soleus (3.23) (Figure 3-19).

The differences in intensity of DHPR staining amongst the t-tubules of fibers in the soleus showed a similar trend to that observed for Kir6.2, except that the relative differences in DHPR intensities were much smaller between fiber types. DHPR fluorescence intensity was significantly lower in type I (0.44) and I-IIX (0.59) fibers as compared to the rest of the fiber types in soleus (0.89 to 1.33) (Figure 3-19). Intensities were higher in all the type IIA-containing fibers. Type I - IIA, IIA, and I - IIA - IIX fibers

FIGURE 3-17

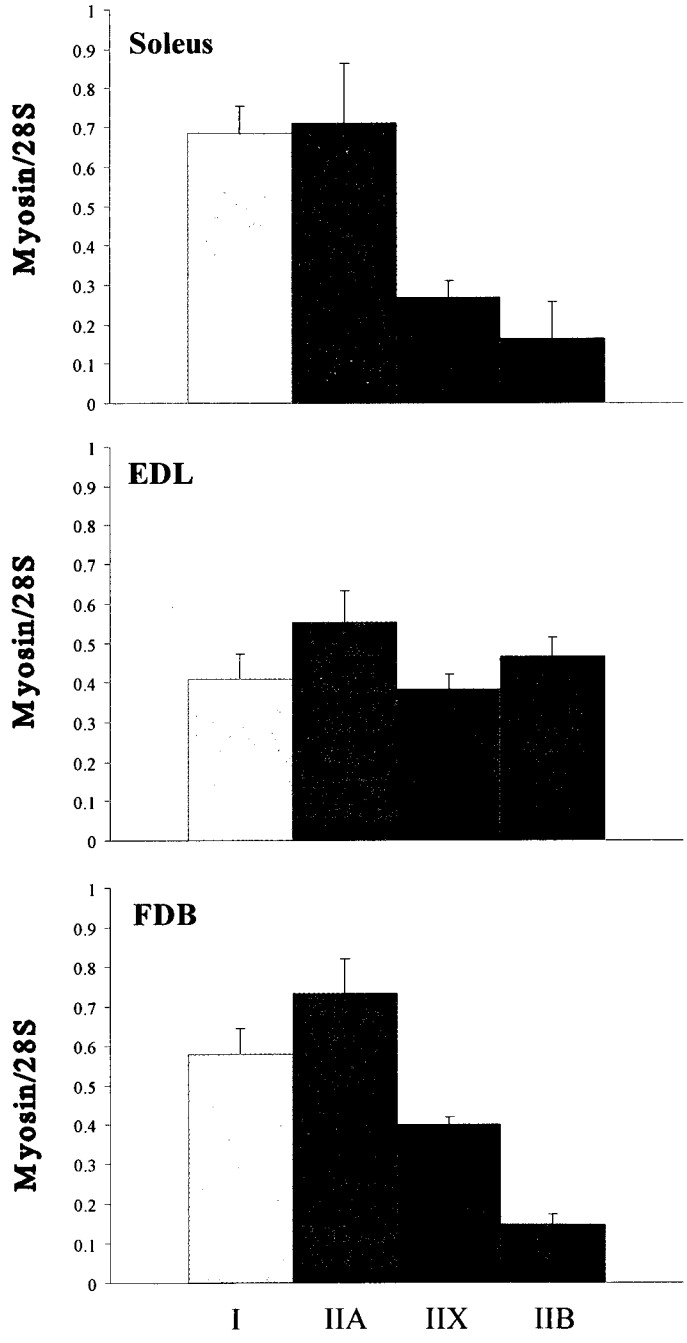

Figure 3-17: Soleus, EDL, and FDB express mRNA transcripts for all fiber types, confirming the presence of all four myosin isoforms in all three muscles. Data expressed as MHC intensity to 28S rRNA standard and represents the mean from 5 animals. Bars are S.E.M.

FIGURE 3-18

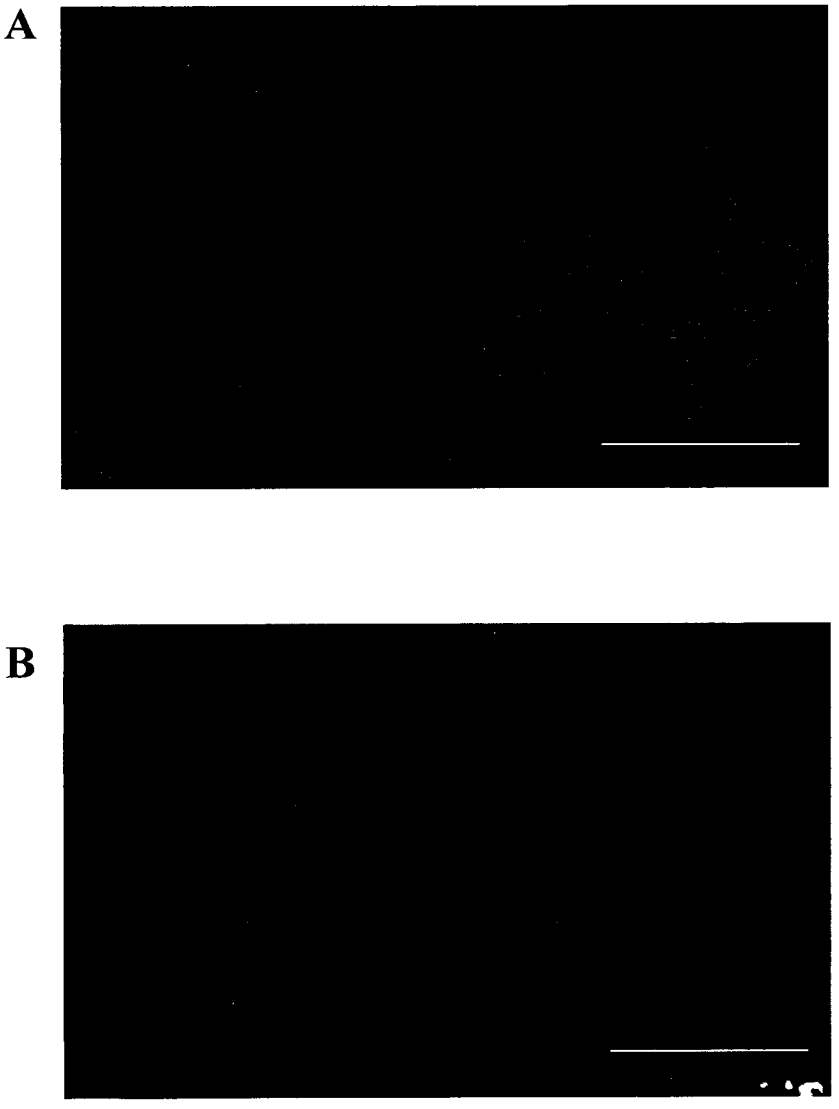

Figure 3-18: Immunofluorescence images of Kir6.2 and DHPR in mouse soleus. Low level Kir6.2 staining (panel A) is visible within a small population of fibers in the mouse soleus while in most fibers Kir6.2 is limited to fiber periphery. DHPR staining (panel B) occurs in numerous fibers, both within fibers and peripherally. Fibers that could not be identified across consecutive cross sections were disregarded for analysis, as were fibers where staining did not appear evenly distributed across the fiber. Bar=100 μm

FIGURE 3-19

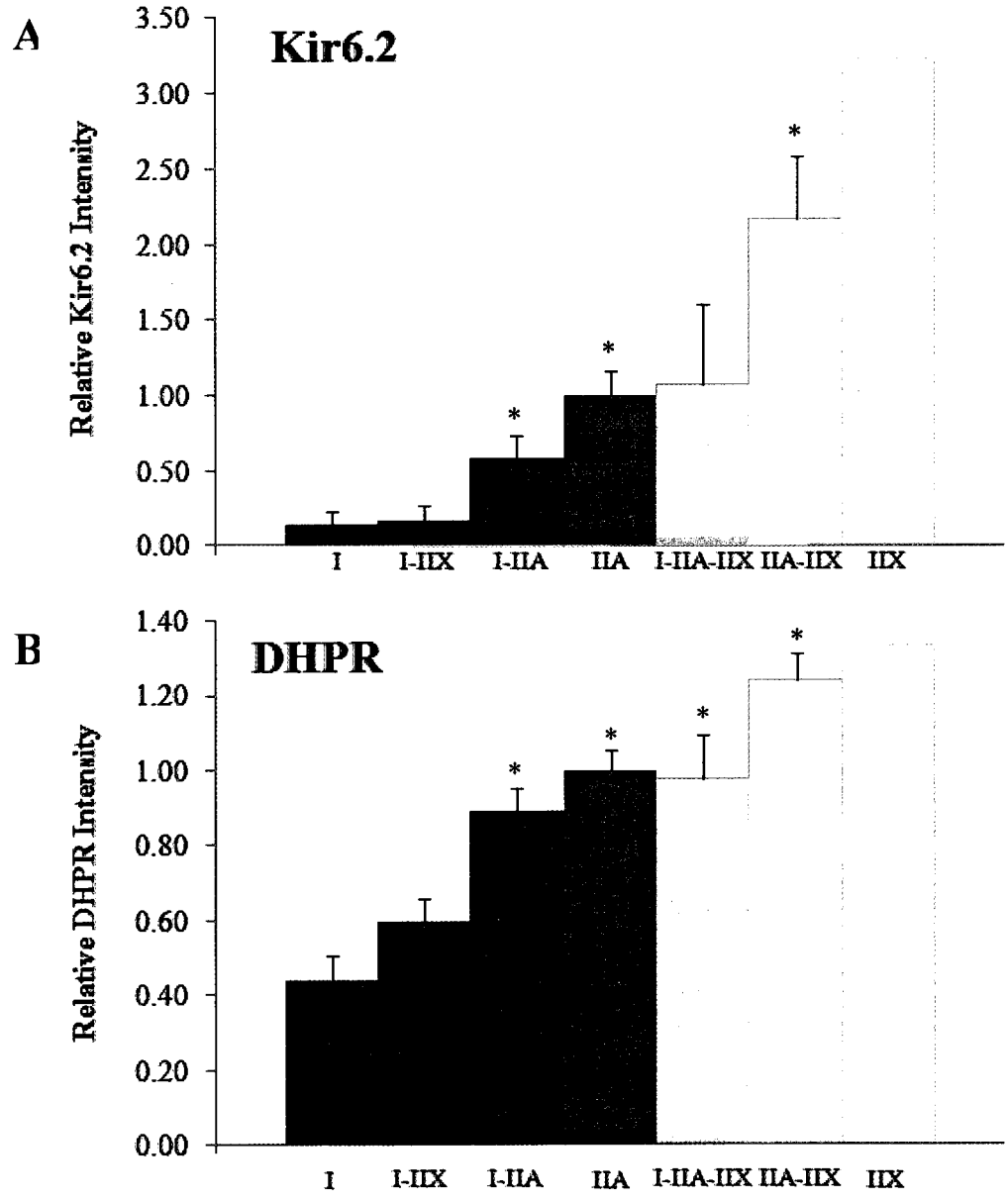

Figure 3-19: Relative intensity of A) Kir6.2 and B) DHPR fluorescence in major fiber types in mouse soleus. Results expressed as ratio of intensity of fluorescently labelled Kir6.2 or DHPR to average intensity of Kir6.2 or DHPR in fibers expressing only type IIA. Data shows mean from 5 animals except for type IIX (n=1). Bars represent S.E.M., * Significantly different from type I, ANOVA and M.C.T. $P < 0.05$

shared similar fluorescence intensities for DHPR staining (0.89 to 0.98), while it was notably greatest in the type IIA-IIX (1.24) and IIX (1.33) fibers of soleus (Figure 3-19).

EDL

Compared to the soleus, the Kir6.2 fluorescence intensity appears much more intensive across most fibers of the EDL (Figure 3-20 A). Very few fibers had almost no t-tubular staining. In terms of DHPR, the differences in fluorescence intensities between fibers in the EDL are again less than the differences in staining intensity between fibers seen for Kir6.2 in this muscle (Figure 3-20 B). Interestingly, those fibers with the weakest Kir6.2 staining were fibers that primarily expressed type IIA MHC, ranging from 1.0 to 1.82 (Figure 3-21). Similar to what was observed in soleus, Kir6.2 intensities varied based on fiber type, in the order of type IIA < IIX < IIB and this trend also extended to the hybrid fiber types present in the EDL (Figure 3-21). Type IIA-IIX fibers of the EDL had average Kir6.2 intensity of 1.37 which was intermediate between that of type IIA (1.0) and type IIX fibers (2.06); likewise, the average Kir6.2 intensity of type IIX-IIB fibers (3.71) was between that of type IIX and IIB fibers, being significantly greater than that observed in type IIX (2.06) but not type IIB (3.81) fibers (Figure 3-21).

As observed in the soleus, the variations in DHPR fluorescence intensity in the EDL between fiber types were much less than the variations observed for Kir6.2. Although no significant differences exist between the fiber types, there was a slight upward trend in DHPR intensities. Fibers identified as type IIA had the lowest DHPR fluorescence (1.00), type IIA hybrids and type IIX fibers had intermediate amounts of DHPR fluorescence (1.09 to 1.29), and type IIX-IIB and type IIB fibers exhibited the highest DHPR intensities in the EDL (1.55) (Figure 3-21 B).

FDB

Unlike the soleus and EDL, Kir6.2 staining in the FDB showed more homogeneity across most fiber types, and high intensity staining was observed within the t-tubules of the majority of fibers (Figure 3-22 A). In comparison, the DHPR staining in FDB showed some variation across fibers, with medium to high intensity fluorescence in most fibers

FIGURE 3-20

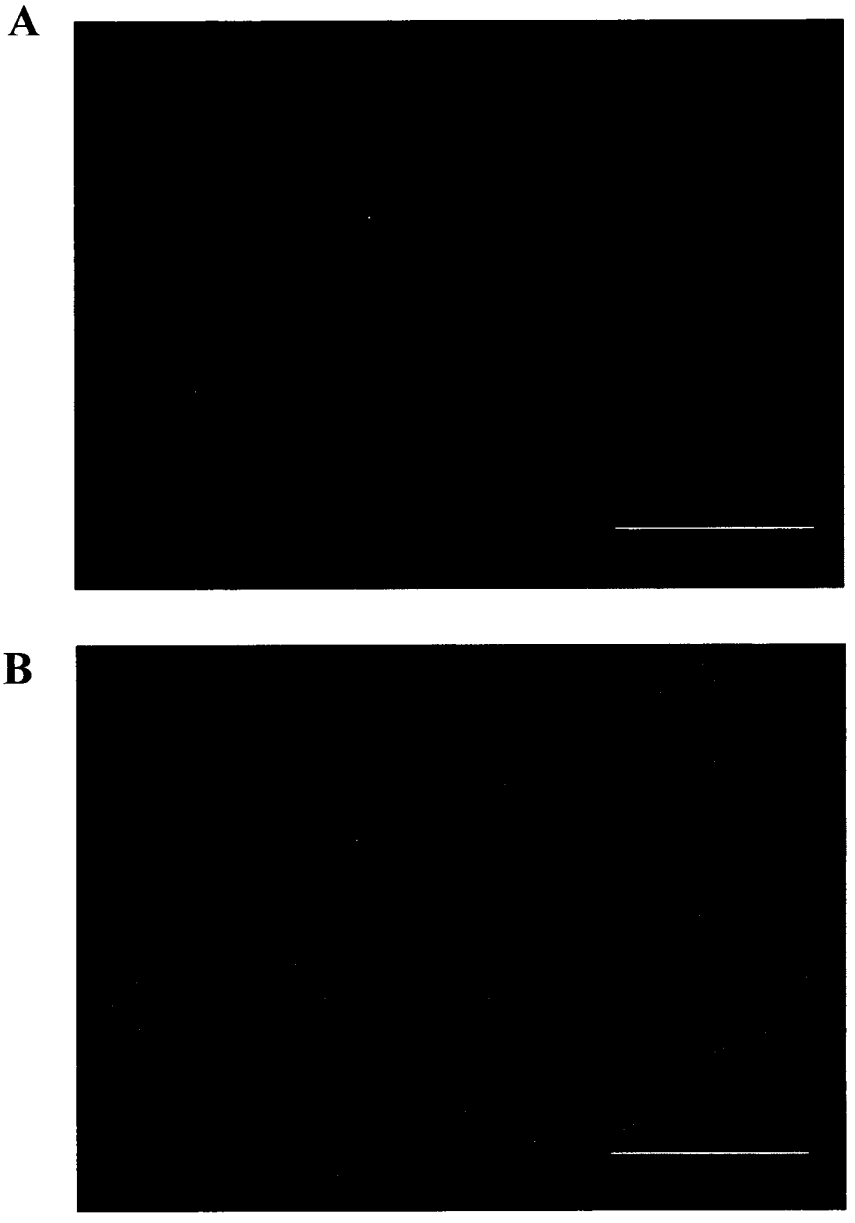

Figure 3-20: Immunofluorescence images of Kir6.2 and DHPR in mouse EDL. Kir6.2 (panel A) and DHPR (panel B) staining are both intense throughout most fibers in the mouse EDL. Fibers that could not be identified across consecutive cross sections were disregarded for analysis, as were fibers where staining did not appear evenly distributed across the fiber. Bar=100 μm.

FIGURE 3-21

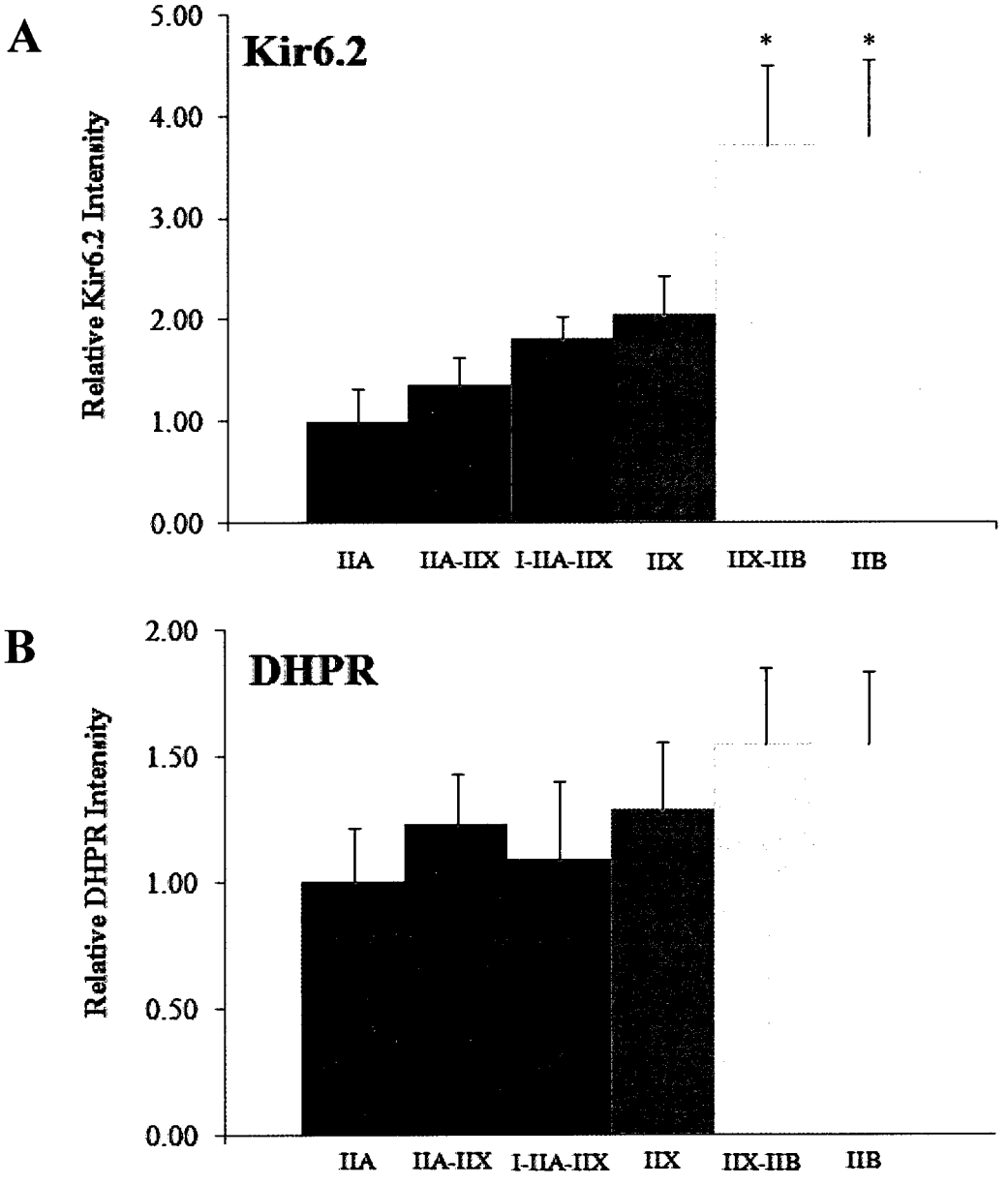

Figure 3-21: Relative intensity of A) Kir6.2 and B) DHPR fluorescence in major fiber types in mouse EDL. Results are expressed as ratio of intensity of fluorescently labelled Kir6.2 or DHPR to average intensity of Kir6.2 or DHPR in fibers expressing only type IIA. Data shows mean from 5 animals. Bars represent S.E.M., * Significantly different from type IIA, ANOVA and M.C.T. $P < 0.05$

FIGURE 3-22

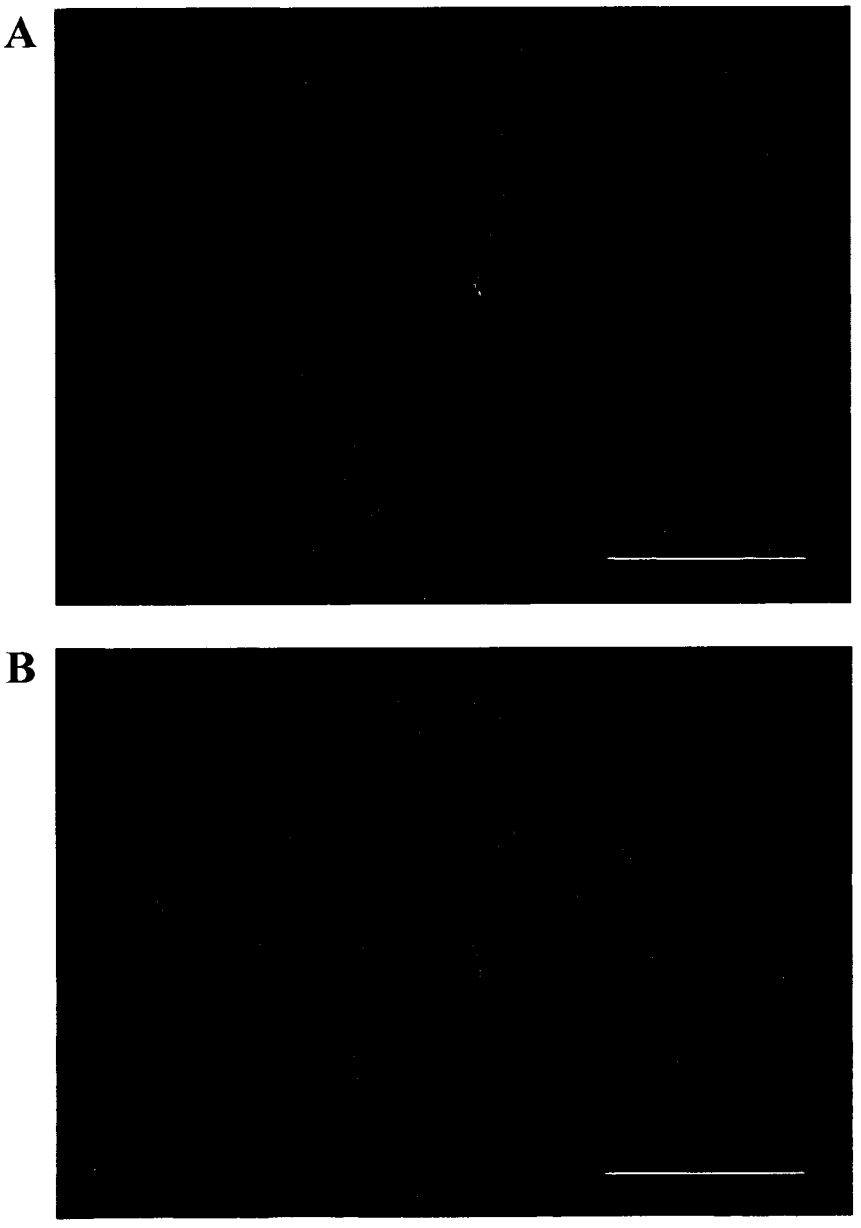

Figure 3-22: Immunofluorescence images of Kir6.2 and DHPR in mouse FDB. Kir6.2 staining (panel A) and DHPR staining (panel B) are visible in the majority of fibers in the mouse FDB. Fibers that could not be identified across consecutive cross sections were disregarded for analysis, as were fibers where staining did not appear evenly distributed across the fiber. Bar=100 μm

(Figure 3-22 B). Type I and type I-IIX fibers had noticeably lower Kir6.2 staining intensities (0.79 and 0.6) of all FDB fiber types, though there were no significant differences between the fiber types (Figure 3-23). As seen in the other muscles, an upward trend in Kir6.2 intensities existed. However, in the FDB there were smaller relative differences between fiber types, with intensities ranging from 0.6 to 1.5 for all fiber types (Figure 3-23). Kir6.2 fluorescence intensities were similar amongst type IIA, I-IIA, and I-IIA-IIX fibers (between 0.9 and 1.0), and again the highest Kir6.2 intensities were seen in type IIA-IIX (1.32) and IIX (1.5) fibers (Figure 3-23).

Interestingly, unlike the soleus and EDL, the upward trends across fiber types in the FDB are similar between Kir6.2 and DHPR (Figure 3-23). Fibers identified as type I and I-IIX had the lowest values (0.67 and 0.71), the type I-IIA, IIA, and I-IIA-IIX shared similar intermediate values (0.89 to 1.0), and type IIA-IIX and IIX fibers possessed the highest DHPR intensity values (1.38 and 1.51) (Figure 3-23). There were no significant differences between any DHPR intensities except between type I-IIX and type IIX.

Comparison of Kir6.2 and DHPR intensities in the same fiber type across different muscles

Overall Kir6.2 fluorescence intensity varied between muscles: staining of EDL and FDB whole muscle fluoresced intensely whereas staining in the soleus was much weaker (Figure 3-18A, 3-20A, 3-22 A). Upon comparison, it became apparent that in addition to the observed differences in Kir6.2 among fibers within a muscle that differences also existed for a specific fiber type across different muscles. For type I fibers, the Kir6.2 fluorescence intensity was approximately 15 times greater in FDB than in soleus (Figure 3-24 A). For type IIA fibers, the Kir6.2 fluorescence was highest in FDB and about half as high in soleus and EDL (Figure 3-24 A). Type IIX fibers in the FDB had twice as much Kir6.2 compared to the IIX fibers of the EDL (Figure 3-24 A).

For DHPR fluorescence intensity in overall muscle cross sections, DHPR staining was similar between EDL and FDB, while soleus fluorescence intensity was weaker and not comparable in intensity to the other two muscles (Figure 3-18 B, 3-20 B, 3-22 B).

FIGURE 3-23

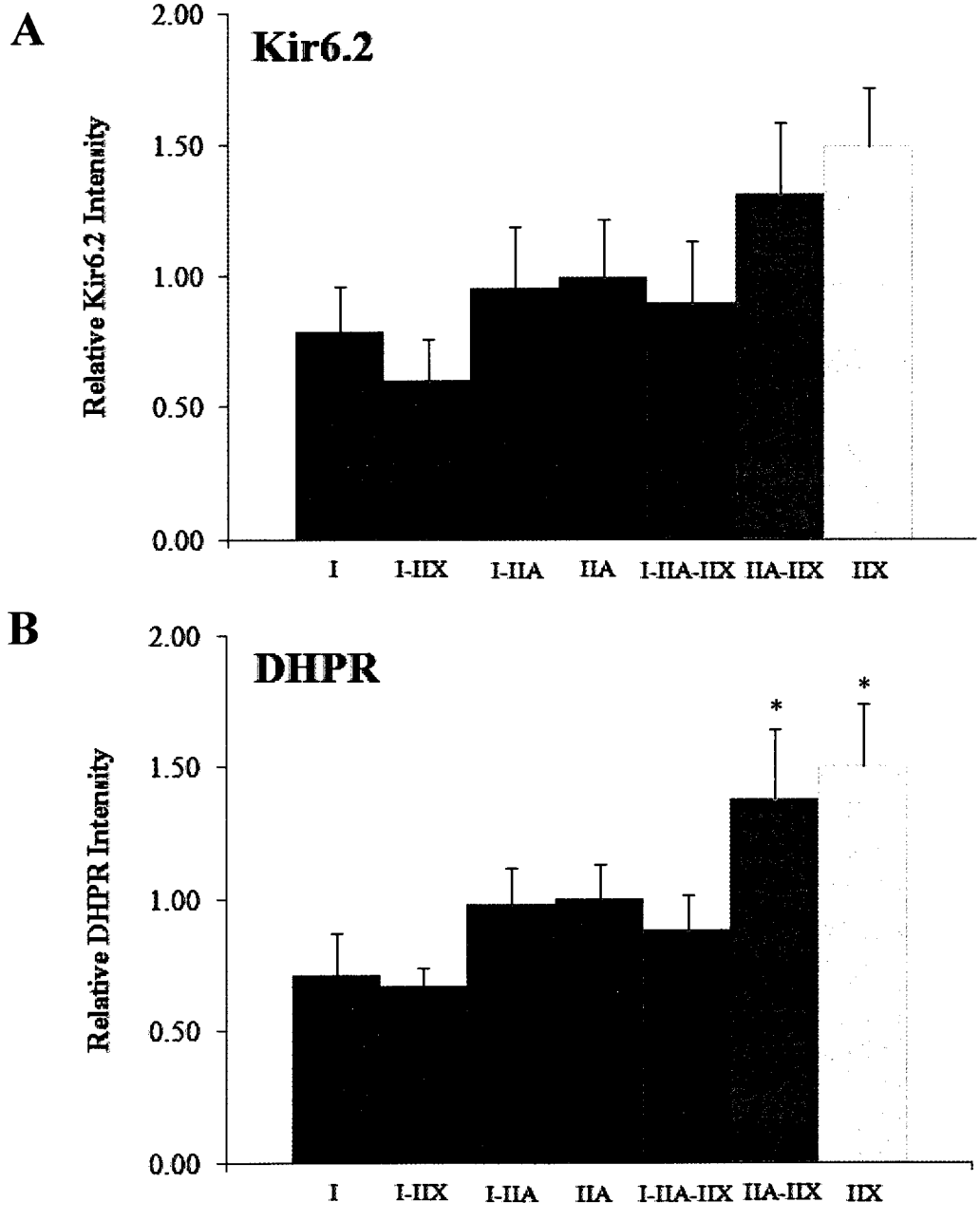

Figure 3-23: Relative intensity of A) Kir6.2 and B) DHPR fluorescence in major fiber types in mouse FDB. Results are expressed as ratio of intensity of fluorescently labelled Kir6.2 or DHPR to average intensity of Kir6.2 or DHPR in fibers expressing only type IIA. Data shows mean from 5 animals. Bars represent S.E.M., * Significantly different from type I, ANOVA and M.C.T. $P < 0.05$

FIGURE 3-24

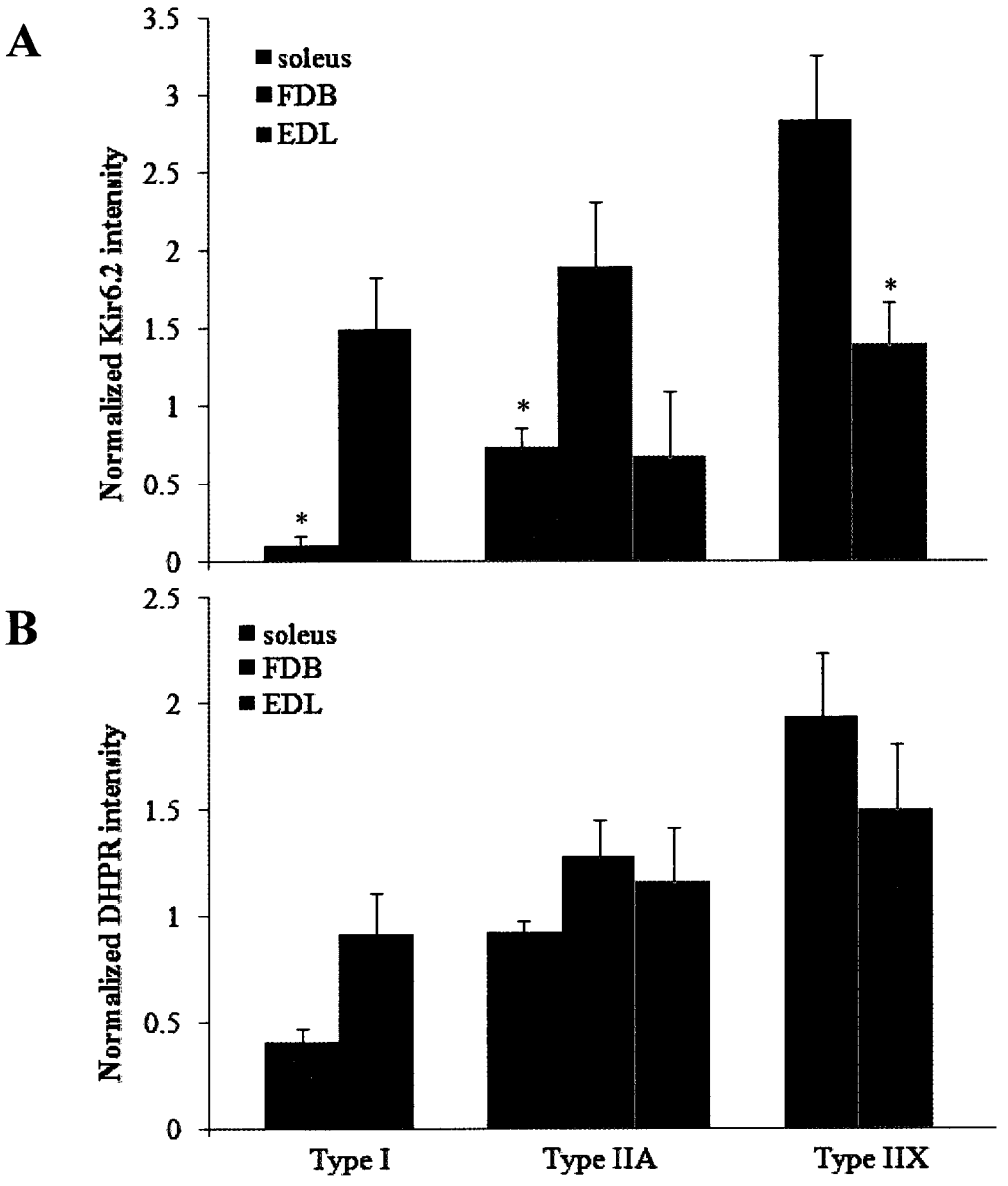

Figure 3-24: Relative intensity of A) Kir6.2 and B) DHPR fluorescence in pure fiber types of mouse soleus, EDL, and FDB. Results are expressed as ratio of intensity of fluorescently labelled Kir6.2 or DHPR to average intensity of Kir6.2 or DHPR in pure type IIA fibers. Data shows mean results from 5 animals. Bars represent S.E.M., * Significantly different from FDB within fiber type, ANOVA and M.C.T. $P < 0.05$

Differences in DHPR staining within the same fiber type across different muscles were also much less apparent than that observed for Kir6.2. FDB type I fibers had about twice as much DHPR fluorescence compared to that in soleus (Figure 3-24 B). There was no significant difference between DHPR intensities of the other fibers.

Relationship between Kir6.2 and DHPR intensities among muscles from the same animal

To establish if the measured Kir6.2 intensities vary with t-tubular content, muscles were labelled for DHPR to provide an index of t-tubular volume. For each mouse, the relative Kir6.2 fluorescence intensity was plotted versus relative DHPR fluorescence intensity (Figure 3-25).

In all mice, soleus consistently had lower Kir6.2:DHPR values compared to EDL and FDB ratios (Figure 3-25). With respect to EDL, four mice generally had higher Kir6.2:DHPR fluorescence ratios compared to soleus (Figure 3-25 B, C, D, E) while for the fifth mouse the Kir6.2 values were similar to that observed in soleus but the DHPR values consistently higher, resulting in an overall lower Kir6.2:DHPR ratio than that observed in soleus (Figure 3-25 A). Compared to soleus and EDL, the FDB Kir6.2:DHPR fluorescence ratios showed much more variability in all mice studied. The Kir6.2:DHPR values were often higher than those observed in soleus. In all mice, many of FDB's Kir6.2:DHPR values overlapped those observed for EDL (Figure 3-25). For one mouse, a large portion of the FDB Kir6.2:DHPR values were intermediate between soleus and EDL (Figure 3-25 C). In another mouse, the majority of the FDB Kir6.2:DHPR values were greater than that observed in EDL (Figure 3-25 A). In general, the ratios of relative Kir6.2:DHPR fluorescence intensities followed this trend: SOL < FDB < EDL.

For three of the five mice, the R^2 value was high, ranging from 0.623 to 0.791 (Figures 3-25 B, C, D), while for the other two mice, the R^2 value was much lower (0.331 and 0.356; Figures 3-25 A, E). In four cases, the slope of the regression lines was greater than 1; it ranged from 1.15 to 1.90 for data from three mice, while the fourth slope was 3.1 (Figure 3-25 B-E). The fifth mouse had a slope close to but less than 1 (Figure 3-25 A). Although the slopes of the regression lines varied among animals, the trend observed was that Kir6.2 intensity increased at a greater rate than DHPR intensity.

FIGURE 3-25

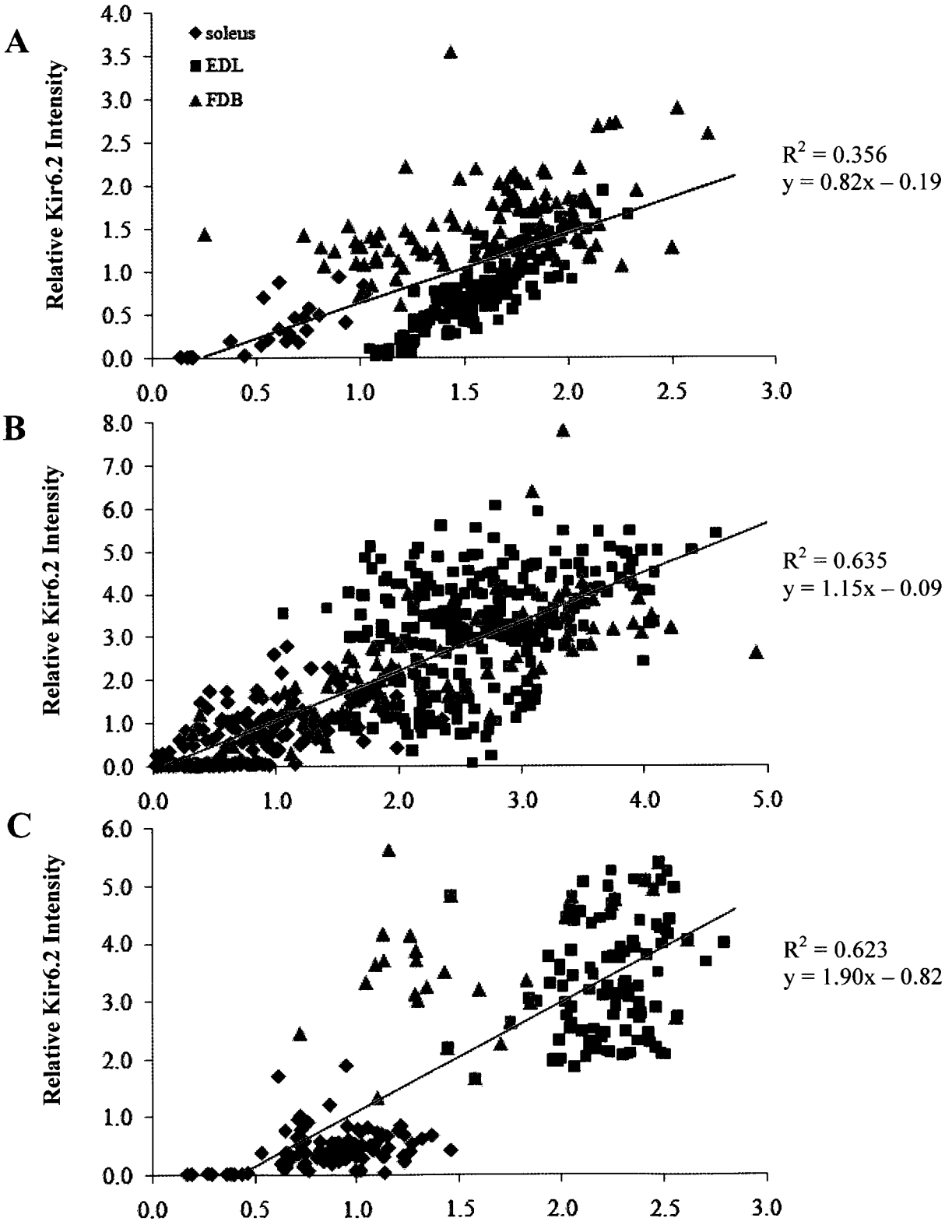
A
B
C
Relative Kir6.2 Intensity
soleus
EDL
FDB
$R^2 = 0.356$
$y = 0.82x - 0.19$
$R^2 = 0.635$
$y = 1.15x - 0.09$
$R^2 = 0.623$
$y = 1.90x - 0.82$

Figure3-25 (continued)

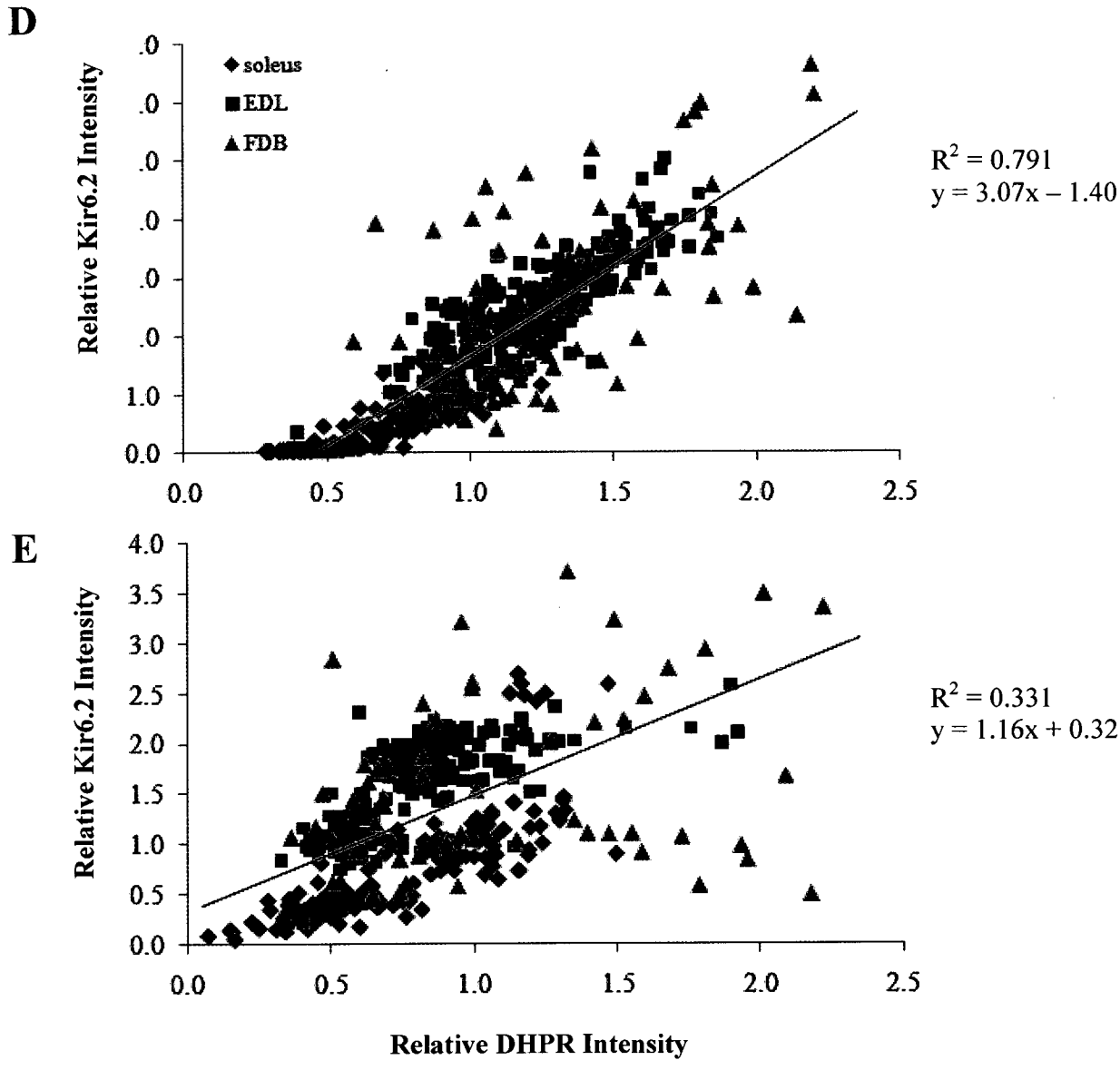

Figure 3-25: Correlation of relative Kir6.2 intensity to relative DHPR fluorescence intensity in soleus, EDL, and FDB within individual animals. Results are expressed as ratio of intensity of fluorescently labelled Kir6.2 or DHPR to mean intensity of Kir6.2 or DHPR in type IIA fibers for each mouse.

CHAPTER 4

DISCUSSION

DEVELOPMENT OF SINGLE SKELETAL MUSCLE FIBER PROTOCOL FOR IMMUNOHISTOCHEMISTRY

Originally, the goal of this study was to establish the localization and distribution of K_{ATP} channel subunits along the length of and within single muscle fibers. To achieve this goal, a common immunohistochemical protocol was to be employed on paraformaldehyde-fixed FDB fibers that had adhered to Matrigel-coated glass coverslips. However, this protocol proved to be inadequate for several reasons: multiple washes caused fiber loss, a large proportion of the remaining fibers were bent and/or supercontracted at one or multiple sites along their length, and in addition several of the antibodies tested did not penetrate fully through muscle fibers.

Immunohistochemical (IHC) and immunofluorescence (IF) channel subunit analysis have been performed on isolated cardiomyocytes [131, 139, 140] and fetal skeletal muscle fibers [141], though no established and definitive protocol is available preparing adult skeletal muscle fibers for IHC or IF analysis. Some of the limitations of previous protocols were that they were optimized only for single-labeling of tissues, employed fixatives that were not compatible to the antibodies for this study, used fixation that resulted in low level autofluorescent background staining, optimized to visualize proteins that localized subcellularly but very close to the cell surface (such that antibody penetration was not a large concern), and generally did not use the same antibodies or nature of antibodies as those required for this study (specifically mouse hybridoma-generated anti-myosin antibodies). Direct application of current cardiomyocyte protocols (such as Zimmer *et al.* [131]) did not suffice for FDB muscle fibers, thus it was apparent that a skeletal muscle fiber protocol would need to be established and optimized, by testing various components and aspects of other available protocols.

The protocol for single FDB muscle fibers was thus revisited from the fiber adhesion step onwards, to establish the best adhesion substrate, pre-fixation conditions, and fixative for

this study. The ideal substrate would maintain the greatest number of fibers on the coverslip and be able to withstand both fixation and the numerous washes inherent in the immunofluorescence procedure. Laminin and Matrigel coatings were tested and neither proved to be superior to the other in terms of fiber adhesion. The secondary consideration, however, was maintenance of fiber morphology. As mentioned in the results, during the post-adherence incubation period most fibers appear straight, had a clear appearance, and no disturbances to the cell membrane. Originally, after fibers had settled and become affixed to the glass coverslips, they were rinsed with 1X PBS prior to 4% PFA fixation, but this resulted in fiber loss as well as partial or complete fiber supercontraction. A common reason for fiber contraction is increased intracellular calcium. In cardiomyocyte preparations, caffeine is often employed to empty SR stores. Application of BAPTA-AM or an ionomycin/EGTA solution prior to fixation was tested as it could buffer any intracellular calcium release which may occur over time or during fixation that may lead to contraction. Interestingly, while developing this skeletal muscle fiber protocol it appeared that use of a calcium-free buffer solution permitted maintenance of fiber morphology comparable to application of either calcium-buffering treatment. Thus, the buffer application step was eliminated and replaced with a zero calcium solution.

The choice of fixative for this protocol had to meet three main criteria. It must: maintain good structural morphology through all immunofluorescence processing steps, permit full penetration of antibodies into muscle fibers, and ensure that the antigenic sites remained unhindered by fixation. Fixation was the step that differed the most between the various protocols. Zinc-paraformaldehyde-alcohol fixation (ZnPF), Lana's (picric acid-paraformaldehyde) fixation, and paraformaldehyde fixation alone were tested based on their success in multiple tissue types as well as in muscle [131-134]. While more straight fibers remained after ZnPF fixation under all calcium buffering conditions, it caused fibers to have a streaked appearance. Since alcohol is known to denature proteins when used in a fixative, it is possible that this component of the ZnPF fixative caused the streaked appearance by denaturing proteins within the fibers. Based on the loss of visibility of the A-I banding and the importance of its visibility in channel subunit

localization, ZnPF was excluded as a possible fixative for use with single skeletal muscle fibers. Paraformaldehyde alone was tested briefly but since few to no suitable fibers remain after its application, it was eliminated as well. Since Lana's fixative did not affect visualization of A-I banding and provided a number of suitable fibers, it was chosen as the best fixative for single FDB fibers.

Although adhesion, buffering, and fixation appeared to be optimized, immunofluorescence staining efficacy and efficiency required optimization because it appeared that not all antibodies were adequately penetrating the fibers. By confocal microscopy it became obvious that some but not all antibodies could diffuse through an entire muscle fiber of 50 μm thickness. In particular, when visualized with confocal microscopy the anti-Kir6.2 antibody (vital to this study) primarily showed cell membrane expression only. Morrissey and colleagues [94] had also observed streaked and uneven staining of cardiomyocytes with methanol fixation alone, but by using a two step fixation/permeabilization protocol (4% paraformaldehyde + methanol) they obtained an excellent preparation for immunofluorescence. Both -20°C methanol treatment after fixation, and a 10% sucrose incubation followed by freeze cracking were briefly tested (data not shown) but did not improve penetration of the antibodies required for this study. A secondary issue arose while addressing the antibody penetration issue. It became apparent that the binding of some antibodies was affected by fixation, in particular both the anti-Kir6.2 and anti-MHC antibodies. Negative controls stained with goat anti-mouse IgG demonstrated autofluorescence, possibly due to the secondary antibody binding non-specifically to the mouse tissue, but since autofluorescence was not an issue before, it is more likely binding of secondary antibody to cell regions structurally altered by the fixative.

Further testing of more antibody/fixative combinations with initial testing of anti-MHC antibody/fixative combinations attempted on muscle cross sections will assist in narrowing down the ideal parameters for an immunofluorescence and fixation protocol for single FDB fibers plated on laminin-coated coverslips.

DISTRIBUTION OF KIR6.2 SUBUNIT IN THE T-TUBULES AMONG FIBER TYPES IN DIFFERENT MOUSE SKELETAL MUSCLES

The major findings of this study were: (a) a large number of fibers in mouse skeletal muscle express more than one myosin; (b) the K_{ATP} channel's Kir6.2 subunit is present in the t-tubules of most fiber types but its protein content varies both between muscle type and fiber type; and (c) the relative Kir6.2 content in the t-tubules shows some correlation with DHPR content, but Kir6.2 tends to vary and increase more across fiber types than DHPR content.

Fiber type distribution among Soleus, EDL, and FDB muscles

Fiber typing has been used regularly in muscle studies to detect and understand changes in muscle phenotype based on changes in its contractile proteins [142, 143]. Generally, fiber type composition has been determined using SDS-PAGE (which detects the presence or absence of each of the four fiber types) or immunohistochemical methods using the three available anti-myosin antibodies (type I, IIA, and IIB) and determining the type IIX fiber population by subtracting those fibers that are labelled from the total number of fibers present.

A few studies have reported up to 70% of hybrid fibers (fibers expressing two or more MHCs) in rodent hind limb muscles as detected by SDS-PAGE [138] and up to 50% hybrid fibers through immunohistochemistry [144]. In the present study, fiber typing was performed to ascertain if fibers expressing more than one MHC constitute a large enough population of total fibers such that it should be taken into consideration when later investigating channel subunit distribution. It became apparent that a large proportion and variety of hybrid fiber types exist in normal, unexercised muscle of CD-1 mice. Indeed, the muscles investigated in this study demonstrate similar levels of hybrid fibers: 46% in soleus, 33% in EDL, and 58% in FDB (Table 4-1). With the recent availability of the anti-type IIX MHC antibody [145], the proportions of all four fibers types could be determined unequivocally, making this study one of the first to determine both pure and

TABLE 4-1

Muscle	Myosin Expression	# of Fibers	Mean % of Total Muscle
Soleus	Single	717	54
	Hybrid	545	46
EDL	Single	1032	67
	Hybrid	495	33
FDB	Single	357	42
	Hybrid	515	58

Table 4-1: Proportions of fibers expressing single and hybrid myosin fiber types in soleus, EDL, and FDB.

hybrid fiber type populations in mouse soleus, EDL and FDB using four anti-MHC specific antibodies instead of determining the type IIX fiber population by subtraction. The fiber type distribution determined by immunohistochemistry using four antibodies showed slightly different fiber type proportions than those determined in other studies. Data derived using whole muscle SDS-PAGE can only be compared to data from this study in which percentages of each myosin are expressed as a fraction of the total fibers enumerated (insets in Figure 3-16). A study using single fiber SDS-PAGE for soleus showed 64% type I, 30% type IIA, and 5% type I/IIA hybrid fibers [146]. If the 5% hybrid fibers are added to each of the pure fiber groups, these results reflect data similar to this study, where 69% type I and 40% type IIA were observed (inset, Figure 3-16). Surprisingly, their study did not detect any pure type IIX or IIX-containing hybrids, but this may be a function of random sampling of single fibers used in their study rather than a lack of this fiber type in soleus. However, another study investigating MHC using whole muscle indicated slightly less than 30% IIX in soleus [147], similar to the detection of 40% IIX in this study (Figure 3-16). Thabet *et al.* [3] also used immunohistochemistry to determine soleus fiber type, but compared to the data from this study their findings showed greater number of type I and lower number of type IIA fibers.

In contrast to soleus, EDL fiber type determination showed less agreement with prior SDS-PAGE data and greater agreement with immunohistochemical data. In EDL in this study, 57% of fibers expressed type IIB, 56% type IIX, 17% type IIA and 6% type I, while whole muscle gel electrophoresis showed 87% type IIB, 9% type IIX, 4% IIA and no type I expression [148]. Other immunohistochemically derived fiber typing was more consistent with this study, as it found 61% type IIB, 29% type IIX, 10% type IIA, but detected <1% type I [3]. Thus, the current findings are supported, particularly with respect to the presence of type IIA myosin in EDL.

Some of the fiber type proportions seen in this study reflect those reported by others for the FDB. Similar amounts of type IIA and IIB were observed both by whole muscle SDS-PAGE (67% IIA and 2% IIB) [149] and in this study by immunohistochemistry (60% IIA and 3% IIB, Figure 3-16). Some discrepancy exists for type I and IIX detected

in the FDB between the various studies, with our study indicating higher amounts of type I (27%) and type IIX (72%) compared to the amounts detected by gel electrophoresis (3.6% type I, 34% type IIX) [149]. A separate study which employed immunofluorescence (without anti-IIX antibody) also illustrated comparable proportions of type IIX (71%) and IIB (0%) fibers [150] versus this study, which found 72% type IIX and 3% type IIB (Figure 3-16).

Differences in the methodology used to determine fiber types may explain, in part, the discrepancies observed in fiber type distribution amongst studies. In the current study, it is possible that positive immunofluorescence staining on a black background made detection of positive fibers easier. As seen in the example images of each of the fiber types in Chapter 3, myosin staining in hybrid myosin-expressing fibers can be very weak compared to the expression of the same myosin in a fiber expressing only that myosin. Other detection methods, such as the use of DAB, a chromogen that produces a brown precipitate when it reacts with a HRP-conjugated secondary antibody, for visualizing anti-MHC binding, may not have been as sensitive as immunofluorescent detection for low level staining of any of the fiber types [3]. This methodological difference may explain, for instance, the lower IIA expression in soleus and of type I fibers in EDL seen by Thabet *et al.* [3]. Another reason for variability in fiber types detected, particularly between gel electrophoresis and immunofluorescence, may be dependent on the localization of certain MHCs within a muscle fiber. Immunohistochemistry effectively bases fiber type on those MHCs expressed within a cross-sectional snapshot of the muscle mid-belly. Thus, if some MHCs are either underrepresented or absent in the cross section examined but expressed to a greater extent elsewhere along the length of a muscle fiber (as has been observed histochemically in untrained rabbit hind leg muscles), the expression of some fiber types may be underestimated [158].

The inconsistencies between proportions of IIX fibers observed, however, is most likely due to underestimation since an anti-type IIX antibody was previously unavailable. In the past, type IIX fibers were enumerated by subtraction instead of being enumerated by positive staining with a MHC-specific antibody. The combination of

immunohistochemical fiber typing using DAB and only three anti-MHC antibodies likely underestimated type IIX in the EDL and may not have been sensitive enough to detect weak type I staining since this MHC appears to primarily express together with type IIA in EDL in a hybrid form. RT-PCR analysis of all myosins (Figure 3-17) confirms the detection of type IIX (and the three other myosins) as real rather than artifact. This evidence is particularly valuable for the soleus since, based on fiber typing of earlier studies, it is not commonly considered to express type IIX protein [146, 147]. Though the presence of an mRNA transcript does not confer with absolute certainty that its corresponding protein product will be present in a tissue, its absence or only baseline expression of mRNA for a given protein would negate the possibility of the protein in mature tissue. Type IIX MHC mRNA expression is not as high in our soleus as in our EDL or FDB samples, but its relative mRNA expression is greater than the baseline expression observed for type IIB mRNA, which is barely detected in the soleus (Figure 3-17).

Functional role for single and hybrid fiber types

The data presented in this study also illustrates the preponderance of hybrids present in all muscles studied and the nature of these hybrids. Based on the role of a muscle, it should possess a specific composition of MHC isoforms that allow it to perform its function most efficiently. For instance, muscles involved in maintaining posture are generally composed of slow twitch, more oxidative fiber types. In contrast, muscles involved in quick movements are composed of fast twitch, more glycolytic fiber types. Fibers are typed according to the myosin isoforms(s) they express: types I, IIA, IIX, and IIB. These fiber types effectively differ in their maximal shortening velocity, oxidative capacity, and fatigue resistance. For fibers composed of a single MHC isoform, the maximum velocity of contraction increases from slowest to fastest, or from type I <IIA<IIX<IIB [151] [152]. Metabolically, type I and type IIA fibers are primarily oxidative and have the lowest glycolytic activity; conversely, type IIB fibers have the greatest glycolytic capacity and lowest oxidative activity, while IIX fibers are intermediate between type I and IIB. The more oxidative a fiber is, the greater its fatigue resistance. Consequently, type I and IIA fibers are most fatigue resistant, type IIB are the

least fatigue resistant, and type IIX fibers have intermediate fatigability [153]. Fatigue resistant fibers possess higher mitochondrial content compared to more fatigable fibers [153]. Considering all the factors discussed above, the specific properties of every muscle result from the individual properties and proportions of the fiber types present within the muscle [154].

The majority of hybrids observed in muscle in this study are double MHC hybrids. The relevance of hybrid fibers, thus, becomes clear if all functional differences that are associated with the expression of certain MHC types are taken into consideration. The expression of more than one myosin in a single fiber provides that fiber increased flexibility in how it responds to certain functional demands it may face within the fiber, or as part of the whole muscle. Combining multiple MHC expression with heterogeneity of other contractile proteins found in muscle (for example, tropomyosin isoforms or myosin light chains) results in a spectrum of fiber types that can better adapt to changes or stress at both the fiber and whole muscle level.

Kir6.2 subunit distribution among Soleus, EDL and FDB muscles

Apart from MHC expression demonstrating heterogeneity within the fibers of a muscle, this thesis provides evidence that non-contractile proteins such as Kir6.2 of the K_{ATP} channel also appear to vary in content and representation across muscles in a variety of ways.

Differences in localization of Kir6.2 subunit in skeletal muscle

Electrophysiological, mRNA, and immunofluorescence studies have previously confirmed the presence of Kir6.2 in skeletal muscle [29, 98, 106]. Previous work with Kir6.2 antibodies in skeletal muscle also showed this subunit localizing to the muscle sarcolemma, both in membrane fractionation studies and via immunohistochemistry [29]. In agreement with these findings, soleus, EDL, and FDB muscle cross sections labelled with anti-Kir6.2 in this study demonstrated the presence of this subunit in the cell membrane, as seen in immunofluorescence at the periphery of muscle fibers. The K_{ATP}

channel in skeletal muscle sarcolemma is most evident in the soleus, as intra-fiber intensities are weakest in this muscle (Figure 3-18 A). The strong Kir6.2 peripheral staining pattern observed at the sarcolemmal boundaries is similar to that seen previously in the primarily type I, IIA, and IIX composed human vastus lateralis muscle [29, 155]. However, K_{ATP} channel Kir6.2 staining was also present within muscle fibers (Figure 3-18, 20, 22).

Kir6.2 expression also appeared to localize to the t-tubules, as illustrated by immunofluorescence inside many muscle fibers in addition to that in the cell membrane. The intra-fiber and sub-surface Kir6.2 fluorescence labeling observed in the current study stained in a similar fashion to anti-DHPR, a t-tubular marker antibody (Figures 3-6 A, C; 3-18; 3-20; 3-22). A cardiomyocyte immunofluorescence study employing several different antibodies against Kir6.2 revealed sarcolemmal Kir6.2 expression in a sarcomeric striated pattern [94]. The same study co-localized SUR2 and Kir6.2 staining and showed by confocal microscopy that K_{ATP} channels may not only be sarcolemmally expressed but also expressed in the t-tubules. This observation concurs with other immunohistochemical findings that show K_{ATP} channel SUR2 subunits localize both to the sarcolemma and to t-tubules of cardiomyocytes [102], and also agrees with the observation made via scanning ion conductance microscopy of K_{ATP} channels localizing in the Z-grooves of the sarcolemma [156]. Taken together, cardiomyocyte data lends support to the t-tubular localization of Kir6.2, and thus K_{ATP} channel presence, in addition to the channel's confirmed presence in the cell membrane.

Although based on their data Nielsen and colleagues [29] concluded that Kir6.2 subunits are present in all skeletal muscle fiber types of vastus lateralis, their study did not describe the variations in Kir6.2 fluorescence within each fiber type, nor did it elucidate which fiber types possessed greater or lesser Kir6.2 staining intensity and consequently, channel content. The data in this thesis goes further, by demonstrating similar differences in Kir6.2 fluorescence intensity within different fibers in a single muscle type, and shows that this variation occurs consistently in three different mouse muscles. Differences in localization, but more importantly differences in K_{ATP} channel content within different

muscles suggest that dependence of a muscle on the channel function could vary in a muscle-specific and fiber type-specific fashion.

Kir6.2 Content across Muscle Types as related to K_{ATP} channel functions

As mentioned in the Introduction, differences are evident for the importance of the K_{ATP} channel function in various types of muscle to perform some of its physiological functions. Previous experimental evidence in skeletal muscle underscores that K_{ATP} channels are especially important in maintaining contractility and minimizing contractile impairments to protect muscle from fiber damage when faced with physiological stress such as fatigue. Now, this thesis provides evidence that variation in channel content in the t-tubules of these muscles may impact the importance of the channel in certain muscles and not in others.

The α_1DHPR calcium channel subunit was used as an index of t-tubular content in this study. Because the role of this channel is primarily contractility, this limits its localization to the t-tubules to be in close proximity to the SR. It was expected that K_{ATP} channel content would increase as t-tubular volume increased, thus using this channel subunit provided a standard for semi-quantitatively measuring Kir6.2 content across muscles. Indeed, in the soleus which experiences lower frequency stimulation and lower Ca^{2+} currents, the DHPR content was much lower, while the highly active and glycolytic FDB and EDL muscles experiencing high Ca^{2+} currents had increased DHPR content (Figure 3-19 B; 3-21 B; 3-23 B). Similarly, the most oxidative fiber types, all fiber types containing type I MHC, consistently had the lowest DHPR content. In comparison, there were no significant differences in DHPR content amongst any of the type IIA/IIX/IB fiber types in any of the muscles, underscoring the primary importance of this channel in mediating the high contractility in fast twitch muscles. Since the K_{ATP} channel has multiple functions outside of contractility, it is not surprising that Kir6.2 content does not follow a 1:1 ratio with DHPR content and that DHPR content shows much less variability amongst fiber types or within specific fiber types as compared to Kir6.2 content (Figure 3-24 B).

Muscles which face fatigue exhibit differences in the amount of force generated during fatigue, unstimulated force, and force recovery. Both FDB and EDL have faster rates of fatigue compared to the soleus and reach lower amounts of force generation at the end of fatiguing stimulation. While soleus still maintains more than 50% pre-fatigue force at 60 s into fatigue, at only 30 s into fatigue FDB exerts 34% and EDL 25% of the pre-fatigue force and force drops as low as 19% and 8% respectively at the end of fatiguing stimulation [4, 121, 126]. Administering a channel opener increases the rate of fatigue and lowers the force exerted by both soleus and EDL, but this occurs to a greater rate and a much larger extent for EDL [121, 126]. This difference when K_{ATP} channel are activated can be directly related to a difference in Kir6.2 content, as soleus Kir6.2:DHPR ratios are on the whole consistently lower than those of EDL (Figure 3-25).

The extent of contractile dysfunction due to exercise in the absence of K_{ATP} channel activity also varies amongst different muscles. In wild type mice, unstimulated force is highest in soleus and barely detectable in EDL and FDB. In contrast, unstimulated force generated by fatigued Kir6.2$^{-/-}$ muscle is almost 20 times greater than wild type for FDB and about 5 times greater in EDL, while in soleus no significant difference exists [4, 121, 126]. Activation of K_{ATP} channels by pinacidil, however, abolishes unstimulated force for both soleus and EDL [126]. Again, both muscles with consistently higher Kir6.2:DHPR ratios, FDB and EDL, develop higher unstimulated forces when no K_{ATP} channel is present while are least affected under normal conditions. The soleus' loss of unstimulated force during pinacidil treatment shows that this muscle reacts to enhanced K_{ATP} activity but does not rely as heavily on this channel when faced with fatiguing stimulation, which again can be related to lower Kir6.2 protein content in this muscle.

Force recovery after fatigue is also muscle dependent. No significant decreases or improvements in force recovery are observed in the soleus based on (genetic and pharmacological) loss of K_{ATP} channel activity or enhanced K_{ATP} channel activity [121, 126]. However, both EDL and FDB show reduced force recovery in Kir6.2$^{-/-}$ muscles, with 25% and 10% increases respectively in post-fatigue force of wild type muscles [4, 126]. Further, activation of K_{ATP} channels with pinacidil increased post-fatigue force in

EDL by more than 30% of that observed in wild type [121, 126]. The considerable effects on both EDL and FDB force recovery when K_{ATP} channels are present and functional again underscores the channels importance in preserving contractility in this muscle type and can be related to higher Kir6.2 content within these muscles. Further, a greater magnitude of effect on EDL's force recovery compared to FDB is consistent with the Kir6.2:DHPR ratios illustrating higher Kir6.2 content in the EDL versus FDB (Figure 3-25).

Studies have shown permanent fiber damage, indicated by signs of fiber regeneration, are present in plantaris, TA, and EDL muscles of treadmill-exercised Kir6.2$^{-/-}$ mice but are absent in treadmill-exercised Kir6.2$^{-/-}$ soleus and in all aforementioned muscles of exercised wild type mice [3]. Again, EDL muscle lacking functional Kir6.2 subunits are affected while soleus is not. This is consistent with the pattern observed that muscles that typically express greater Kir6.2 content (EDL) are more dependent on the channel to preserve normal contractile function in the face of repeated stress made above and furthermore, provides *in vivo* evidence of the importance of this channel.

In respect to other roles of the K_{ATP} channel, volume regulation is mediated in part by K_{ATP} channels in the slow twitch soleus muscle, but not in the fast twitch plantaris or EDL muscles, since only soleus had reduced ability to counter osmotic changes when K_{ATP} channels were pharmacologically blocked [1]. This function of the channel does not appear to depend on t-tubular channel content since a muscle with higher Kir6.2 content (EDL) was unaffected by loss of the channel. However, as observed in this study, absence of t-tubular K_{ATP} channels in soleus does not mean that there is reduced channel content in the cell membrane; perhaps the population of K_{ATP} channels important in volume regulation are those located in the cell membrane. A second, well established role of the channel in skeletal muscle is glucose uptake. Basal and insulin-stimulated glucose uptake both vary between EDL and soleus in different ways, based on presence and absence of K_{ATP} channel function. Basal insulin uptake is enhanced *in vivo* and *in vitro* for Kir6.2$^{-/-}$ EDL muscles compared to wild type EDL muscles, while soleus muscles show no significant differences in basal uptake in the presence or absence of the

channel [2]. However, insulin-stimulated glucose uptake in soleus is higher than basal uptake in vivo, and uptake significantly increases in Kir6.2$^{-/-}$ soleus both *in vivo* and *in vitro* compared to wild type muscles [2]. Since these two types of glucose uptake are enhanced differently between soleus and EDL while t-tubular Kir6.2 content is very dissimilar between the two types of muscles, it suggests that channel content does not directly affect the performance of glucose uptake in muscle, although this role is probably dependent on both the cell membrane and t-tubular K_{ATP} channel populations.

Based on the above, the K_{ATP} channel's role in both volume regulation and insulin-stimulated glucose uptake appears to be less dependent on the presence and function of the channel. Consequently, differences in Kir6.2 content do not align with the different responses observed in different muscles in the presence or absence of the channel. In comparison, rate of fatigue, unstimulated force, force recovery, and evidence of fiber damage can clearly be related to (lack of) both cell membrane but also t-tubule-localized K_{ATP} channels. These dysfunctions also tend to occur in muscles that are composed of primarily glycolytic fiber types. Both the FDB and EDL are muscles containing many glycolytic fibers that face short, intense, high frequency stimulation of contractile activity: the EDL of the mouse hind limb is important in locomotion (and was affected during the treadmill running regimen) and the FDB is responsible for controlling the mouse's hind foot digits, which are used to grasp and manipulate objects. In contrast, the soleus is mainly composed of oxidative fibers and acts in the mouse hind limb as a postural muscle which would experience lower frequency but continuous stimulation. The importance of greater K_{ATP} channel content in the t-tubules of FDB and EDL as opposed to soleus appear to be related to the type of activities and hence, metabolic demands faced by each type of muscle. The soleus does not face the aerobic stress which is seen by FDB or EDL. Thus, the findings of this thesis confirm the hypothesis that "t-tubular Kir6.2 channel subunit content varies between muscles in the order of EDL,FDB>>>SOL". The differences in t-tubular Kir6.2 content are not limited to differences across muscles, however, but also vary across fiber types within muscles and may explain variances in responses of specific groups of fibers within a muscle type when exposed to fatigue.

Kir6.2 Content across Fiber Types as related to K_{ATP} channel function

The importance of the K_{ATP} channel with respect to fiber type specific differences was first observed *in vivo*. Only selected hind limb muscles from treadmill-run Kir6.2$^{-/-}$ mice showed fiber damage, but the only fiber type demonstrating any damage in these muscles was the most glycolytic type IIB fibers [3]. More interestingly, the diaphragm muscles from Kir6.2$^{-/-}$ mice that were run on an uphill incline showed evidence of mild to severe damage (mononucleated cells and infiltration of connective tissue) despite this muscle composed mainly of IIA and IIX fibers and few IIB fibers [3]. This is consistent with the findings in this study, which illustrated that the most glycolytic fibers within a specific muscle exhibit the highest Kir6.2 content.

Differences in membrane excitability and fatigue kinetics of K_{ATP}-deficient FDB fibers were observed *in vitro*, and although fiber types were not distinguished, fibers segregated into groupings that suggest differentiation by fiber type.

Membrane excitability varied when tested on glibenclamide-treated FDB fibers. Two groups arose: fibers that exhibited a fast and large membrane depolarization and supercontracted; and fibers that had a slower, smaller membrane depolarization which did not supercontract [125]. By blocking both calcium influx and the K_{ATP} channel increases in membrane potential of FDB fibers again segregated into two groups: those with a large and fast membrane depolarization and those with a smaller membrane depolarization [125]. It is possible that these differential responses reflect groupings of the fibers into more glycolytic MHC-expressing and more oxidative-MHC expressing fibers, which could then be related to the differences observed in Kir6.2 content in type I-containing fiber types versus type IIA- and IIX-containing fiber types (Figure 3-23 A).

In the examination of fatigue kinetics of single FDB fibers treated with glibenclamide, out of 19 fibers: 21% did not supercontract, had small increases in unstimulated Ca^{2+} and recovered after fatigue; 16% partially supercontracted, had larger increases in unstimulated Ca^{2+} and partially recovered; and 63% partially or completely supercontracted, had the largest increase in unstimulated Ca^{2+} and did not recover after fatigue [4]. Increases in unstimulated Ca^{2+} can be equated to what would be referred to

as unstimulated force in fatigued muscle bundles [125]. The group percentages observed in the single fibers roughly match several pooled groupings of the fiber types seen in the FDB in this study: 21% type I-containing fibers (types I, I-IIX, I-IIA); 20% single myosin-expressing type IIA fibers, and 65% type IIX expressing fibers (types IIX, IIA-IIX, I-IIA-IIX) respectively (Figure 3-16). There was no significant difference detected between the Kir6.2 content amongst FDB fiber types in this study, but a definite trend existed in the data with type I fibers having lower Kir6.2 content, type IIA-containing fibers having intermediate content, and type IIA-IIX and IIX fibers possessing the highest level of Kir6.2 (Figure 3-23 A). Again, those fibers containing the greatest Kir6.2 content are the most severely affected by lack of K_{ATP} channel activity (type IIX) while those fibers with the lowest Kir6.2 content (type I-containing fibers) showed little effects during and post-fatigue. Though no single fiber data is available for soleus or EDL, the same fiber type-specific pattern exists in Kir6.2 content between fiber types. In both soleus and EDL, the least oxidative and most glycolytic fibers within that muscle have significantly greater Kir6.2 content compared to the most oxidative fiber type expressed in the given muscle (Figure 3-19 A; 3-21 A). Thus, it can be suggested strongly that variations in Kir6.2 content between different fiber types can affect individual fiber responses to fatiguing stimulation.

Comparison of Kir6.2 content in same fiber type amongst muscles

By comparing type IIA fibers (the only pure fiber type consistently expressed in all three muscles) it is apparent that Kir6.2 content is significantly greater in the FDB compared to EDL and soleus (Figure 3-24). Kir6.2 content in soleus type I fibers is also significantly less than that in FDB type I fibers, while Kir6.2 content in EDL type IIX fibers is significantly less than that seen in FDB type IIX fibers. RT-PCR has illustrated that relative Kir6.2 mRNA expression differs amongst muscles in the order of highest Kir6.2 content in FDB >> EDL > soleus, with no statistically significant difference between EDL and soleus [106]. This finding follows a pattern similar to that observed in this study for Kir6.2 content across type IIA fibers (Figure 3-24 A). Taken together, this lends evidence to the finding that muscle specific variation in K_{ATP} channel content exists, but is apparent at both the mRNA and protein level.

The data from the literature gathered after the initial *in vivo* treadmill study, in conjunction with the data presented in this thesis indicate that the K_{ATP} channel's myoprotective effects are not limited to IIB fibers, as was suggested by *in vivo* data. It is still unclear why a discrepancy exists between which types of fibers become damaged during fatigue *in vivo* and *in vitro*. Type IIB fibers may experience greater metabolic stress as they are highly glycolytic. However, the FDB muscle used in both single fiber and muscle bundle studies is primarily composed of type IIA and IIX fibers with almost no type IIB fibers and still demonstrated significant contractile dysfunctions and fiber damage with loss of K_{ATP} channel activity. It is possible that fibers *in vitro* were forced to face greater stress than they would experience *in vivo* because of the imposed fatigue protocol, while treadmill running leads to recruitment of the most glycolytic, primarily IIB fibers *in vivo* while type I, IIA, or IIX fibers are better able to cope with metabolic stress since they are more oxidative fibers. Similar to what was observed across muscles, the findings of this thesis suggest that the most glycolytic fiber types within a muscle have the greatest dependence on K_{ATP} channel function and the most oxidative fiber types have the least dependence on the K_{ATP} channel to maintain control of membrane excitability and avoid contractile dysfunction during fatigue.

CONCLUSION

K_{ATP} channels appear to play varied roles in a number of physiological functions in skeletal muscle. The effect of enhanced K_{ATP} channel activity or impact of loss of K_{ATP} affecting the FDB and EDL to a greater extent than soleus is recapitulated repeatedly in this thesis. The Kir6.2 content varies across muscles, being highest in the order of EDL>FDB>soleus and within a muscle across fiber types, being highest in the order of IIB>IIX>IIA>I.

Based on what is understood about the channel's function and the fact that the data generated in this study considers specifically the t-tubular content of the channel, it appears that differences in Kir6.2 content between fiber type and muscle type are most relevant to the K_{ATP} channel's role in preventing contractile dysfunctions when faced by

the metabolic stress of fatigue. However, the presence of a channel through the determination of channel content does not indicate to what extent the channels are actually activated in the face of metabolic stress. Further studies investigating the level of channel activity within different muscle types or amongst fiber types during fatigue would provide further insight into the importance of the channel and in the extent of its protective role. Nevertheless, it appears that the increased K_{ATP} channel content in some muscle types partly explains why the glycolytic FDB and EDL muscles generally suffer greater contractile dysfunctions in the absence of the channel and show greater dependence on the t-tubular presence of the K_{ATP} channel than the highly oxidative soleus for cytoprotection.

CHAPTER 5

REFERENCES

1. Gosmanov, A.R., et al., *ATP-sensitive potassium channels mediate hyperosmotic stimulation of NKCC in slow-twitch muscle.* Am J Physiol Cell Physiol, 2004. **286**(3): p. C586-95.
2. Miki, T., et al., *ATP-sensitive potassium channels participate in glucose uptake in skeletal muscle and adipose tissue.* Am J Physiol Endocrinol Metab, 2002. **283**(6): p. E1178-84.
3. Thabet, M., et al., *Treadmill running causes significant fiber damage in skeletal muscle of KATP channel-deficient mice.* Physiol Genomics, 2005. **22**(2): p. 204-12.
4. Cifelli, C., et al., *KATP channel deficiency in mouse flexor digitorum brevis causes fibre damage and impairs Ca2+ release and force development during fatigue in vitro.* J Physiol, 2007. **582**(Pt 2): p. 843-57.
5. Berg, J., J. Tymoczko, and L. Stryer, *Biochemistry.* 2002: WH Freeman San Francisco CA:.
6. Bezanilla, F., et al., *Sodium dependence of the inward spread of activation in isolated twitch muscle fibres of the frog.* J Physiol, 1972. **223**(2): p. 507-23.
7. Lehmann-Horn, F. and K. Jurkat-Rott, *Voltage-gated ion channels and hereditary disease.* Physiol Rev, 1999. **79**(4): p. 1317-72.
8. Marban, E., T. Yamagishi, and G.F. Tomaselli, *Structure and function of voltage-gated sodium channels.* J Physiol, 1998. **508 (Pt 3)**: p. 647-57.
9. Torres, Y.P., et al., *A marriage of convenience: beta-subunits and voltage-dependent K+ channels.* J Biol Chem, 2007. **282**(34): p. 24485-9.
10. Dulhunty, A.F., *Heterogeneity of T-tubule geometry in vertebrate skeletal muscle fibres.* J Muscle Res Cell Motil, 1984. **5**(3): p. 333-47.
11. Ahlijanian, M.K., R.E. Westenbroek, and W.A. Catterall, *Subunit structure and localization of dihydropyridine-sensitive calcium channels in mammalian brain, spinal cord, and retina.* Neuron, 1990. **4**(6): p. 819-32.

12. Lacerda, A.E., et al., *Normalization of current kinetics by interaction between the alpha 1 and beta subunits of the skeletal muscle dihydropyridine-sensitive Ca2+ channel.* Nature, 1991. **352**(6335): p. 527-30.

13. Birnbaumer, L., et al., *Structures and functions of calcium channel beta subunits.* J Bioenerg Biomembr, 1998. **30**(4): p. 357-75.

14. Ursu, D., et al., *Altered inactivation of Ca2+ current and Ca2+ release in mouse muscle fibers deficient in the DHP receptor gamma1 subunit.* J Gen Physiol, 2004. **124**(5): p. 605-18.

15. Alden, K.J. and J. Garcia, *Dissociation of charge movement from calcium release and calcium current in skeletal myotubes by gabapentin.* Am J Physiol Cell Physiol, 2002. **283**(3): p. C941-9.

16. Melzer, W., A. Herrmann-Frank, and H.C. Luttgau, *The role of Ca2+ ions in excitation-contraction coupling of skeletal muscle fibres.* Biochim Biophys Acta, 1995. **1241**(1): p. 59-116.

17. Fabiato, A. and F. Fabiato, *Calcium release from the sarcoplasmic reticulum.* Circ Res, 1977. **40**(2): p. 119-29.

18. Ferguson, D.G., H.W. Schwartz, and C. Franzini-Armstrong, *Subunit structure of junctional feet in triads of skeletal muscle: a freeze-drying, rotary-shadowing study.* J Cell Biol, 1984. **99**(5): p. 1735-42.

19. Zalk, R., S.E. Lehnart, and A.R. Marks, *Modulation of the ryanodine receptor and intracellular calcium.* Annu Rev Biochem, 2007. **76**: p. 367-85.

20. Tanabe, T., et al., *Regions of the skeletal muscle dihydropyridine receptor critical for excitation-contraction coupling.* Nature, 1990. **346**(6284): p. 567-9.

21. Rossi, A.E. and R.T. Dirksen, *Sarcoplasmic reticulum: the dynamic calcium governor of muscle.* Muscle Nerve, 2006. **33**(6): p. 715-31.

22. Brandl, C.J., et al., *Adult forms of the Ca2+ATPase of sarcoplasmic reticulum. Expression in developing skeletal muscle.* J Biol Chem, 1987. **262**(8): p. 3768-74.

23. Hundal, H.S., et al., *Insulin induces translocation of the alpha 2 and beta 1 subunits of the Na+/K(+)-ATPase from intracellular compartments to the plasma membrane in mammalian skeletal muscle.* J Biol Chem, 1992. **267**(8): p. 5040-3.

24. Clausen, T., *Na+-K+ pump regulation and skeletal muscle contractility.* Physiol Rev, 2003. **83**(4): p. 1269-324.

25. Clausen, T., *The Na+, K+ pump in skeletal muscle: quantification, regulation and functional significance.* Acta Physiol Scand, 1996. **156**(3): p. 227-35.

26. Delpire, E., et al., *Molecular cloning and chromosome localization of a putative basolateral Na(+)-K(+)-2Cl- cotransporter from mouse inner medullary collecting duct (mIMCD-3) cells.* J Biol Chem, 1994. **269**(41): p. 25677-83.

27. Wong, J.A., et al., *Insulin-independent, MAPK-dependent stimulation of NKCC activity in skeletal muscle.* Am J Physiol Regul Integr Comp Physiol, 2001. **281**(2): p. R561-71.

28. Ferenczi, E.A., et al., *Membrane potential stabilization in amphibian skeletal muscle fibres in hypertonic solutions.* J Physiol, 2004. **555**(Pt 2): p. 423-38.

29. Nielsen, J.J., et al., *Localization and function of ATP-sensitive potassium channels in human skeletal muscle.* Am J Physiol Regul Integr Comp Physiol, 2003. **284**(2): p. R558-63.

30. Garcia-Calvo, M., et al., *Purification and reconstitution of the high-conductance, calcium-activated potassium channel from tracheal smooth muscle.* J Biol Chem, 1994. **269**(1): p. 676-82.

31. Jacquemond, V. and B. Allard, *Activation of Ca2+-activated K+ channels by an increase in intracellular Ca2+ induced by depolarization of mouse skeletal muscle fibres.* J Physiol, 1998. **509 (Pt 1)**: p. 93-102.

32. Gessner, G., et al., *BKCa channels activating at resting potential without calcium in LNCaP prostate cancer cells.* J Membr Biol, 2005. **208**(3): p. 229-40.

33. Fahlke, C., *Ion permeation and selectivity in ClC-type chloride channels.* Am J Physiol Renal Physiol, 2001. **280**(5): p. F748-57.

34. Middleton, R.E., D.J. Pheasant, and C. Miller, *Homodimeric architecture of a ClC-type chloride ion channel.* Nature, 1996. **383**(6598): p. 337-40.

35. Dulhunty, A.F., *Distribution of potassium and chloride permeability over the surface and T-tubule membranes of mammalian skeletal muscle.* J Membr Biol, 1979. **45**(3-4): p. 293-310.

36. Jurkat-Rott, K., M. Fauler, and F. Lehmann-Horn, *Ion channels and ion transporters of the transverse tubular system of skeletal muscle.* J Muscle Res Cell Motil, 2006. **27**(5-7): p. 275-90.

37. Aromataris, E.C. and G.Y. Rychkov, *ClC-1 chloride channel: Matching its properties to a role in skeletal muscle.* Clin Exp Pharmacol Physiol, 2006. **33**(11): p. 1118-23.

38. Kristensen, M., T. Hansen, and C. Juel, *Membrane proteins involved in potassium shifts during muscle activity and fatigue.* Am J Physiol Regul Integr Comp Physiol, 2006. **290**(3): p. R766-72.

39. Hille, B., *Ionic channels of excitable membranes.* 2nd ed. 1992, Sunderland, Mass.: Sinauer Associates. xiii, 607 p.

40. Noma, A., *ATP-regulated K+ channels in cardiac muscle.* Nature, 1983. **305**(5930): p. 147-8.

41. Ashcroft, F.M. and F.M. Gribble, *Correlating structure and function in ATP-sensitive K+ channels.* Trends Neurosci, 1998. **21**(7): p. 288-94.

42. Inagaki, N., et al., *Reconstitution of IKATP: an inward rectifier subunit plus the sulfonylurea receptor.* Science, 1995. **270**(5239): p. 1166-70.

43. Higgins, C.F., *ABC transporters: from microorganisms to man.* Annu Rev Cell Biol, 1992. **8**: p. 67-113.

44. Lorenz, E., et al., *Evidence for direct physical association between a K+ channel (Kir6.2) and an ATP-binding cassette protein (SUR1) which affects cellular distribution and kinetic behavior of an ATP-sensitive K+ channel.* Mol Cell Biol, 1998. **18**(3): p. 1652-9.

45. Guo, D., et al., *Mechanism of rectification in inward-rectifier K+ channels.* J Gen Physiol, 2003. **121**(4): p. 261-75.

46. Ashcroft, F.M., *ATP-sensitive potassium channelopathies: focus on insulin secretion.* J Clin Invest, 2005. **115**(8): p. 2047-58.

47. Zhang, C., et al., *Identification and characterization of a novel member of the ATP-sensitive K+ channel subunit family, Kir6.3, in zebrafish.* Physiol Genomics, 2006. **24**(3): p. 290-7.

48. Sakura, H., et al., *Cloning and functional expression of the cDNA encoding a novel ATP-sensitive potassium channel subunit expressed in pancreatic beta-cells, brain, heart and skeletal muscle.* FEBS Lett, 1995. **377**(3): p. 338-44.

49. Inagaki, N., et al., *Cloning and functional characterization of a novel ATP-sensitive potassium channel ubiquitously expressed in rat tissues, including pancreatic islets, pituitary, skeletal muscle, and heart.* J Biol Chem, 1995. **270**(11): p. 5691-4.

50. Isomoto, S., et al., *A novel sulfonylurea receptor forms with BIR (Kir6.2) a smooth muscle type ATP-sensitive K+ channel.* J Biol Chem, 1996. **271**(40): p. 24321-4.

51. Doupnik, C.A., N. Davidson, and H.A. Lester, *The inward rectifier potassium channel family.* Curr Opin Neurobiol, 1995. **5**(3): p. 268-77.

52. Heginbotham, L., T. Abramson, and R. MacKinnon, *A functional connection between the pores of distantly related ion channels as revealed by mutant K+ channels.* Science, 1992. **258**(5085): p. 1152-5.

53. Tanabe, K., et al., *Direct photoaffinity labeling of the Kir6.2 subunit of the ATP-sensitive K+ channel by 8-azido-ATP.* J Biol Chem, 1999. **274**(7): p. 3931-3.

54. Chutkow, W.A., et al., *Cloning, tissue expression, and chromosomal localization of SUR2, the putative drug-binding subunit of cardiac, skeletal muscle, and vascular KATP channels.* Diabetes, 1996. **45**(10): p. 1439-45.

55. Inagaki, N., et al., *A family of sulfonylurea receptors determines the pharmacological properties of ATP-sensitive K+ channels.* Neuron, 1996. **16**(5): p. 1011-7.

56. Shi, N.Q., B. Ye, and J.C. Makielski, *Function and distribution of the SUR isoforms and splice variants.* J Mol Cell Cardiol, 2005. **39**(1): p. 51-60.

57. Nichols, C.G., *KATP channels as molecular sensors of cellular metabolism.* Nature, 2006. **440**(7083): p. 470-6.

58. Tusnady, G.E., et al., *Membrane topology distinguishes a subfamily of the ATP-binding cassette (ABC) transporters.* FEBS Lett, 1997. **402**(1): p. 1-3.

59. Schneider, E. and S. Hunke, *ATP-binding-cassette (ABC) transport systems: functional and structural aspects of the ATP-hydrolyzing subunits/domains.* FEMS Microbiol Rev, 1998. **22**(1): p. 1-20.

60. Burke, M.A., R.K. Mutharasan, and H. Ardehali, *The sulfonylurea receptor, an atypical ATP-binding cassette protein, and its regulation of the KATP channel.* Circ Res, 2008. **102**(2): p. 164-76.

61. Dean, M., A. Rzhetsky, and R. Allikmets, *The human ATP-binding cassette (ABC) transporter superfamily.* Genome Res, 2001. **11**(7): p. 1156-66.

62. Zerangue, N., et al., *A new ER trafficking signal regulates the subunit stoichiometry of plasma membrane K(ATP) channels.* Neuron, 1999. **22**(3): p. 537-48.

63. Sharma, N., et al., *The C terminus of SUR1 is required for trafficking of KATP channels.* J Biol Chem, 1999. **274**(29): p. 20628-32.

64. Antcliff, J.F., et al., *Functional analysis of a structural model of the ATP-binding site of the KATP channel Kir6.2 subunit.* Embo J, 2005. **24**(2): p. 229-39.

65. John, S.A., J.N. Weiss, and B. Ribalet, *ATP sensitivity of ATP-sensitive K+ channels: role of the gamma phosphate group of ATP and the R50 residue of mouse Kir6.2.* J Physiol, 2005. **568**(Pt 3): p. 931-40.

66. Wang, R., et al., *Subunit-stoichiometric evidence for kir6.2 channel gating, ATP binding, and binding-gating coupling.* Mol Pharmacol, 2007. **71**(6): p. 1646-56.

67. Craig, T.J., F.M. Ashcroft, and P. Proks, *How ATP inhibits the open K(ATP) channel.* J Gen Physiol, 2008. **132**(1): p. 131-44.

68. Ashcroft, F.M. and M. Kakei, *ATP-sensitive K+ channels in rat pancreatic beta-cells: modulation by ATP and Mg2+ ions.* J Physiol, 1989. **416**: p. 349-67.

69. Markworth, E., C. Schwanstecher, and M. Schwanstecher, *ATP4- mediates closure of pancreatic beta-cell ATP-sensitive potassium channels by interaction with 1 of 4 identical sites.* Diabetes, 2000. **49**(9): p. 1413-8.

70. Forestier, C. and M. Vivaudou, *Modulation by Mg2+ and ADP of ATP-sensitive potassium channels in frog skeletal muscle.* J Membr Biol, 1993. **132**(1): p. 87-94.

71. Davies, N.W., N.B. Standen, and P.R. Stanfield, *The effect of intracellular pH on ATP-dependent potassium channels of frog skeletal muscle.* J Physiol, 1992. **445**: p. 549-68.

72. Xu, H., et al., *Direct activation of cloned K(atp) channels by intracellular acidosis.* J Biol Chem, 2001. **276**(16): p. 12898-902.

73. Xu, H., et al., *Distinct histidine residues control the acid-induced activation and inhibition of the cloned K(ATP) channel.* J Biol Chem, 2001. **276**(42): p. 38690-6.

74. Piao, H., et al., *Requirement of multiple protein domains and residues for gating K(ATP) channels by intracellular pH.* J Biol Chem, 2001. **276**(39): p. 36673-80.

75. Shyng, S.L. and C.G. Nichols, *Membrane phospholipid control of nucleotide sensitivity of KATP channels.* Science, 1998. **282**(5391): p. 1138-41.

76. Haider, S., et al., *Identification of the PIP2-binding site on Kir6.2 by molecular modelling and functional analysis.* Embo J, 2007. **26**(16): p. 3749-59.

77. Tucker, S.J., et al., *Truncation of Kir6.2 produces ATP-sensitive K+ channels in the absence of the sulphonylurea receptor.* Nature, 1997. **387**(6629): p. 179-83.

78. Gribble, F.M., et al., *MgATP activates the beta cell KATP channel by interaction with its SUR1 subunit.* Proc Natl Acad Sci U S A, 1998. **95**(12): p. 7185-90.

79. Ueda, K., N. Inagaki, and S. Seino, *MgADP antagonism to Mg2+-independent ATP binding of the sulfonylurea receptor SUR1.* J Biol Chem, 1997. **272**(37): p. 22983-6.

80. Matsuo, M., et al., *Functional analysis of a mutant sulfonylurea receptor, SUR1-R1420C, that is responsible for persistent hyperinsulinemic hypoglycemia of infancy.* J Biol Chem, 2000. **275**(52): p. 41184-91.

81. Matsuo, M., Y. Kimura, and K. Ueda, *KATP channel interaction with adenine nucleotides.* J Mol Cell Cardiol, 2005. **38**(6): p. 907-16.

82. Gribble, F.M., S.J. Tucker, and F.M. Ashcroft, *The essential role of the Walker A motifs of SUR1 in K-ATP channel activation by Mg-ADP and diazoxide.* Embo J, 1997. **16**(6): p. 1145-52.

83. Shyng, S., T. Ferrigni, and C.G. Nichols, *Regulation of KATP channel activity by diazoxide and MgADP. Distinct functions of the two nucleotide binding folds of the sulfonylurea receptor.* J Gen Physiol, 1997. **110**(6): p. 643-54.

84. Ueda, K., et al., *Cooperative binding of ATP and MgADP in the sulfonylurea receptor is modulated by glibenclamide.* Proc Natl Acad Sci U S A, 1999. **96**(4): p. 1268-72.

85. Miki, T., et al., *ATP-sensitive K+ channels in the hypothalamus are essential for the maintenance of glucose homeostasis.* Nat Neurosci, 2001. **4**(5): p. 507-12.

86. Ashford, M.L., P.R. Boden, and J.M. Treherne, *Tolbutamide excites rat glucoreceptive ventromedial hypothalamic neurones by indirect inhibition of ATP-K+ channels.* Br J Pharmacol, 1990. **101**(3): p. 531-40.

87. Ashford, M.L., P.R. Boden, and J.M. Treherne, *Glucose-induced excitation of hypothalamic neurones is mediated by ATP-sensitive K+ channels.* Pflugers Arch, 1990. **415**(4): p. 479-83.

88. Karschin, C., et al., *Overlapping distribution of K(ATP) channel-forming Kir6.2 subunit and the sulfonylurea receptor SUR1 in rodent brain.* FEBS Lett, 1997. **401**(1): p. 59-64.

89. Liss, B., R. Bruns, and J. Roeper, *Alternative sulfonylurea receptor expression defines metabolic sensitivity of K-ATP channels in dopaminergic midbrain neurons.* Embo J, 1999. **18**(4): p. 833-46.

90. Lee, K., et al., *Identification of an ATP-sensitive potassium channel current in rat striatal cholinergic interneurones.* J Physiol, 1998. **510 (Pt 2)**: p. 441-53.

91. Bokvist, K., et al., *Characterisation of sulphonylurea and ATP-regulated K+ channels in rat pancreatic A-cells.* Pflugers Arch, 1999. **438**(4): p. 428-36.

92. Yamada, M., et al., *Sulphonylurea receptor 2B and Kir6.1 form a sulphonylurea-sensitive but ATP-insensitive K+ channel.* J Physiol, 1997. **499 (Pt 3)**: p. 715-20.

93. Li, L., J. Wu, and C. Jiang, *Differential expression of Kir6.1 and SUR2B mRNAs in the vasculature of various tissues in rats.* J Membr Biol, 2003. **196**(1): p. 61-9.

94. Morrissey, A., et al., *Immunolocalization of KATP channel subunits in mouse and rat cardiac myocytes and the coronary vasculature.* BMC Physiol, 2005. **5**(1): p. 1.

95. Ravel, D., et al., *Differential effects of sulphonylureas on the vasodilatory response evoked by K(ATP) channel openers.* Fundam Clin Pharmacol, 2003. **17**(1): p. 61-9.

96. Sim, J.H., et al., *ATP-sensitive K(+) channels composed of Kir6.1 and SUR2B subunits in guinea pig gastric myocytes.* Am J Physiol Gastrointest Liver Physiol, 2002. **282**(1): p. G137-44.

97. Koh, S.D., et al., *Basal activation of ATP-sensitive potassium channels in murine colonic smooth muscle cell.* Biophys J, 1998. **75**(4): p. 1793-800.

98. Inagaki, N., J. Inazawa, and S. Seino, *cDNA sequence, gene structure, and chromosomal localization of the human ATP-sensitive potassium channel, uKATP-1, gene (KCNJ8).* Genomics, 1995. **30**(1): p. 102-4.

99. O'Rourke, B., *Mitochondrial ion channels.* Annu Rev Physiol, 2007. **69**: p. 19-49.

100. O'Rourke, B., *Evidence for mitochondrial K+ channels and their role in cardioprotection.* Circ Res, 2004. **94**(4): p. 420-32.

101. Inagaki, N. and S. Seino, *ATP-sensitive potassium channels: structures, functions, and pathophysiology.* Jpn J Physiol, 1998. **48**(6): p. 397-412.

102. Singh, H., et al., *Distribution of Kir6.0 and SUR2 ATP-sensitive potassium channel subunits in isolated ventricular myocytes.* J Mol Cell Cardiol, 2003. **35**(5): p. 445-59.

103. van Bever, L., et al., *Pore loop-mutated rat KIR6.1 and KIR6.2 suppress KATP current in rat cardiomyocytes.* Am J Physiol Heart Circ Physiol, 2004. **287**(2): p. H850-9.

104. Flagg, T.P., et al., *Differential structure of atrial and ventricular KATP: atrial KATP channels require SUR1.* Circ Res, 2008. **103**(12): p. 1458-65.

105. Zhou, M., et al., *Localization of sulfonylurea receptor subunits, SUR2A and SUR2B, in rat heart.* J Histochem Cytochem, 2007. **55**(8): p. 795-804.

106. Tricarico, D., et al., *Hybrid assemblies of ATP-sensitive K+ channels determine their muscle-type-dependent biophysical and pharmacological properties.* Proc Natl Acad Sci U S A, 2006. **103**(4): p. 1118-23.

107. Henquin, J.C., *Triggering and amplifying pathways of regulation of insulin secretion by glucose.* Diabetes, 2000. **49**(11): p. 1751-60.

108. Ashcroft, F.M., *K(ATP) channels and insulin secretion: a key role in health and disease.* Biochem Soc Trans, 2006. **34**(Pt 2): p. 243-6.

109. Miki, T., et al., *Defective insulin secretion and enhanced insulin action in KATP channel-deficient mice.* Proc Natl Acad Sci U S A, 1998. **95**(18): p. 10402-6.

110. Gromada, J., et al., *ATP-sensitive K+ channel-dependent regulation of glucagon release and electrical activity by glucose in wild-type and SUR1-/- mouse alpha-cells.* Diabetes, 2004. **53 Suppl 3**: p. S181-9.

111. Newgard, C.B. and J.D. McGarry, *Metabolic coupling factors in pancreatic beta-cell signal transduction.* Annu Rev Biochem, 1995. **64**: p. 689-719.

112. Bergen, H.T., N. Monkman, and C.V. Mobbs, *Injection with gold thioglucose impairs sensitivity to glucose: evidence that glucose-responsive neurons are important for long-term regulation of body weight.* Brain Res, 1996. **734**(1-2): p. 332-6.

113. Chutkow, W.A., et al., *Disruption of Sur2-containing K(ATP) channels enhances insulin-stimulated glucose uptake in skeletal muscle.* Proc Natl Acad Sci U S A, 2001. **98**(20): p. 11760-4.

114. James, J.H., et al., *Stimulation of both aerobic glycolysis and Na(+)-K(+)-ATPase activity in skeletal muscle by epinephrine or amylin.* Am J Physiol, 1999. **277**(1 Pt 1): p. E176-86.

115. Lohmann, S.M., U. Walter, and P. Greengard, *Identification of endogenous substrate proteins for cAMP-dependent protein kinase in bovine brain.* J Biol Chem, 1980. **255**(20): p. 9985-92.

116. Gong, B., et al., *A K(ATP) channel deficiency affects resting tension, not contractile force, during fatigue in skeletal muscle.* Am J Physiol Cell Physiol, 2000. **279**(5): p. C1351-8.

117. Farouque, H.M. and I.T. Meredith, *Inhibition of vascular ATP-sensitive K+ channels does not affect reactive hyperemia in human forearm.* Am J Physiol Heart Circ Physiol, 2003. **284**(2): p. H711-8.

118. Johnson, L.R. and J.H. Byrne, *Essential medical physiology.* 3rd ed. 2003, Amsterdam ; San Diego, Calif.: Academic Press. xvi, 1008 p.

119. Vallet, B., et al., *ATP-sensitive K+ channel blockade impairs O2 extraction during progressive ischemia in pig hindlimb.* J Appl Physiol, 1995. **79**(6): p. 2035-42.

120. Banitt, P.F., et al., *Activation of ATP-sensitive potassium channels contributes to reactive hyperemia in humans.* Am J Physiol, 1996. **271**(4 Pt 2): p. H1594-8.

121. Matar, W., et al., *Pinacidil suppresses contractility and preserves energy but glibenclamide has no effect during muscle fatigue.* Am J Physiol Cell Physiol, 2000. **278**(2): p. C404-16.

122. Gramolini, A. and J.M. Renaud, *Blocking ATP-sensitive K+ channel during metabolic inhibition impairs muscle contractility.* Am J Physiol, 1997. **272**(6 Pt 1): p. C1936-46.

123. Kane, G.C., et al., *ATP-sensitive K+ channel knockout compromises the metabolic benefit of exercise training, resulting in cardiac deficits.* Diabetes, 2004. **53 Suppl 3**: p. S169-75.

124. Carnwath, J.W. and D.M. Shotton, *Muscular dystrophy in the mdx mouse: histopathology of the soleus and extensor digitorum longus muscles.* J Neurol Sci, 1987. **80**(1): p. 39-54.

125. Cifelli, C., et al., *Contractile dysfunctions in ATP-dependent K+ channel-deficient mouse muscle during fatigue involve excessive depolarization and Ca2+ influx through L-type Ca2+ channels.* Exp Physiol, 2008. **93**(10): p. 1126-38.

126. Gong, B., et al., *KATP channels depress force by reducing action potential amplitude in mouse EDL and soleus muscle.* Am J Physiol Cell Physiol, 2003. **285**(6): p. C1464-74.

127. Ruff, R.L., *Insulin acts in hypokalemic periodic paralysis by reducing inward rectifier K+ current.* Neurology, 1999. **53**(7): p. 1556-63.

128. Belcastro, A.N., *Skeletal muscle calcium-activated neutral protease (calpain) with exercise.* J Appl Physiol, 1993. **74**(3): p. 1381-6.

129. Jackson, M.J., D.A. Jones, and R.H. Edwards, *Experimental skeletal muscle damage: the nature of the calcium-activated degenerative processes.* Eur J Clin Invest, 1984. **14**(5): p. 369-74.

130. Marty, I., et al., *Cloning and characterization of a new isoform of skeletal muscle triadin.* J Biol Chem, 2000. **275**(11): p. 8206-12.

131. Zimmer, T., et al., *Functional expression of GFP-linked human heart sodium channel (hH1) and subcellular localization of the a subunit in HEK293 cells and dog cardiac myocytes.* J Membr Biol, 2002. **186**(1): p. 1-12.

132. Staines, W.A., et al., *Three-color immunofluorescence histochemistry allowing triple labeling within a single section.* J Histochem Cytochem, 1988. **36**(2): p. 145-51.

133. Storbeck, C.J., et al., *Ste20-like kinase SLK displays myofiber type specificity and is involved in C2C12 myoblast differentiation.* Muscle Nerve, 2004. **29**(4): p. 553-64.

134. Eghbali, M., et al., *Molecular and functional signature of heart hypertrophy during pregnancy.* Circ Res, 2005. **96**(11): p. 1208-16.

135. Kleinman, H.K., et al., *Isolation and characterization of type IV procollagen, laminin, and heparan sulfate proteoglycan from the EHS sarcoma.* Biochemistry, 1982. **21**(24): p. 6188-93.

136. Swift, F., et al., *Altered Na+/Ca2+-exchanger activity due to downregulation of Na+/K+-ATPase alpha2-isoform in heart failure.* Cardiovasc Res, 2008. **78**(1): p. 71-8.

137. Chakkalakal, J.V., et al., *Modulation of utrophin A mRNA stability in fast versus slow muscles via an AU-rich element and calcineurin signaling.* Nucleic Acids Res, 2008. **36**(3): p. 826-38.

138. Bortolotto, S.K., et al., *MHC isoform composition and Ca(2+)- or Sr(2+)-activation properties of rat skeletal muscle fibers.* Am J Physiol Cell Physiol, 2000. **279**(5): p. C1564-77.

139. Maier, S.K., et al., *Distinct subcellular localization of different sodium channel alpha and beta subunits in single ventricular myocytes from mouse heart.* Circulation, 2004. **109**(11): p. 1421-7.

140. Qu, Y., et al., *Expression of skeletal muscle Na(V)1.4 Na channel isoform in canine cardiac Purkinje myocytes.* Biochem Biophys Res Commun, 2007. **355**(1): p. 28-33.

141. Couchoux, H., et al., *Loss of caveolin-3 induced by the dystrophy-associated P104L mutation impairs L-type calcium channel function in mouse skeletal muscle cells.* J Physiol, 2007. **580**(Pt.3): p. 745-54.

142. Chakkalakal, J.V., et al., *Targeted inhibition of Ca2+ /calmodulin signaling exacerbates the dystrophic phenotype in mdx mouse muscle.* Hum Mol Genet, 2006. **15**(9): p. 1423-35.

143. Hayward, L.J., et al., *Targeted mutation of mouse skeletal muscle sodium channel produces myotonia and potassium-sensitive weakness.* J Clin Invest, 2008. **118**(4): p. 1437-49.

144. Bottinelli, R., et al., *Maximum shortening velocity and coexistence of myosin heavy chain isoforms in single skinned fast fibres of rat skeletal muscle.* J Muscle Res Cell Motil, 1994. **15**(4): p. 413-9.

145. Lucas, C.A., L.H. Kang, and J.F. Hoh, *Monospecific antibodies against the three mammalian fast limb myosin heavy chains.* Biochem Biophys Res Commun, 2000. **272**(1): p. 303-8.

146. Suzuki, I., et al., *Fiber Type Specificity,Size,Myonuclear Number and Domain in Slow and Fast Muscles in Adult Mice.* Advances in exercise and sports physiology, 2006. **12**(2): p. 35-43.

147. Pellegrino, M.A., et al., *Clenbuterol antagonizes glucocorticoid-induced atrophy and fibre type transformation in mice.* Exp Physiol, 2004. **89**(1): p. 89-100.

148. Agbulut, O., et al., *Myosin heavy chain isoforms in postnatal muscle development of mice.* Biol Cell, 2003. **95**(6): p. 399-406.

149. Raymackers, J.M., et al., *Tetanus relaxation of fast skeletal muscles of the mouse made parvalbumin deficient by gene inactivation.* J Physiol, 2000. **527 Pt 2**: p. 355-64.

150. Gonzalez, E., et al., *Insulin-like growth factor-1 prevents age-related decrease in specific force and intracellular Ca2+ in single intact muscle fibres from transgenic mice.* J Physiol, 2003. **552**(Pt 3): p. 833-44.

151. Bottinelli, R., S. Schiaffino, and C. Reggiani, *Force-velocity relations and myosin heavy chain isoform compositions of skinned fibres from rat skeletal muscle.* J Physiol, 1991. **437**: p. 655-72.

152. Galler, S., *Stretch activation of skeletal muscle fibre types.* Pflugers Arch, 1994. **427**(3-4): p. 384-6.

153. Fitts, R.H., *Cellular mechanisms of muscle fatigue.* Physiol Rev, 1994. **74**(1): p. 49-94.

154. Pette, D., H. Peuker, and R.S. Staron, *The impact of biochemical methods for single muscle fibre analysis.* Acta Physiol Scand, 1999. **166**(4): p. 261-77.

155. Staron, R.S., et al., *Fiber type composition of the vastus lateralis muscle of young men and women.* J Histochem Cytochem, 2000. **48**(5): p. 623-9.

156. Korchev, Y.E., et al., *Functional localization of single active ion channels on the surface of a living cell.* Nat Cell Biol, 2000. **2**(9): p. 616-9.

157. Stefanini, M., DeMartino C., and L. Zamboni. *Fixation of ejaculated spermatozoa for electron microscopy.* Nature, 1967. **216**(5111): p. 173-174.

158. Peuker, H. and D. Pette. *Quantitative analyses of myosin heavy-chain mRNA and protein isoforms in single fibers reveal a pronounced fiber heterogeneity in normal rabbit muscles.* Eur J Biochem, 1997. **247**(1): p. 30-36.

159. Nichols, C.G. and W.J. Lederer. *The regulation of ATP-sensitive K+ channel activity in intact and permeabilized rat ventricular myocytes.* J Physiol, 1990. **423**: p. 91-110.

160. Matsuo, T, et al., *Quantification of immunohistochemistry using an image analyser: correltation with hormone concentrations in pituitary adenomas.* Histochemical J, 1995. **27**: p. 989-996.

161. Haddad, I.Y, et al. *Quantitation of Nitrotyrosine levels in lung sections of patients and animals with actue lung injury.* J Clin Invest, 1994. **94**(6): p. 2407-2413.

162. Hayashi, Y.K., et al. *Abnormal localization of laminin subunits in muscular dystrophies.* J Neurol Sci, 1993. **119**(1): p. 53-64.

163. Grube, D. *Constants and variables in immunohistochemistry.* Arch Histol Cytol, 2004. **67**(2): p. 115-134.

164. Mosedale, D.E., Metcalfe J.C., and D.J. Grainger. *Optimization of immunofluorescence methods by quantitative image analysis.* J Histochem Cytochem, 1996. **44**(9): p. 1043-1050.

APPENDIX 1

Chemicals used in experimental protocols.

Materials	Concentration	Diluent	Source
Collagenase I	0.3% (w/v)	DMEM	Worthington, USA
DMEM (Ca2+ free)	-	-	Gibco (Invitrogen), Canada
Fetal Bovine Serum (heat inactivated)	-	-	Gibco (Invitrogen), Canada
Matrigel	-	-	BD Biosciences, Canada
Mouse laminin	-	-	Sigma-Aldrich, Canada
OCT compound	-	-	Sakura, Japan
Isopentane	100%	-	Sigma-Aldrich, Canada
Acetone	30%	Tyrode	Fisher Scientific, Canada
Ethanol	10%	Tyrode	Fisher Scientific, Canada
Zinc Chloride	8 mM	Tyrode	Sigma-Aldrich, Canada
Bovine Serum Albumin	0.5% (w/v)	1X PBS	Sigma-Aldrich, Canada
10X Phosphate Buffered Saline	1X	water	Fisher Scientific, Canada
Triton-X 100	0.3% (v/v)	1X PBS	J.T. Baker Chemical, USA
EGTA	10 mM	water	Fisher Scientific, Canada
Ionomycin	5 µM	water	Sigma-Aldrich, Canada
BAPTA-AM	10 µM	water	Sigma-Aldrich, Canada
DNAse I (1 u/µl activity)	1:13	DEPC water, RNAse & DNAse inhibitor	Promega, USA